NASA Technical Paper 1078

Supersonic Aerodynamic Characteristics of a Sparrow III Type Missile Model With Wing Controls and Comparison With Existing Tail-Control Results

William J. Monta

NOVEMBER 1977

NASA

NASA Technical Paper 1078

Supersonic Aerodynamic Characteristics of a Sparrow III Type Missile Model With Wing Controls and Comparison With Existing Tail-Control Results

William J. Monta
Langley Research Center
Hampton, Virginia

National Aeronautics
and Space Administration

Scientific and Technical Information Office

1977

SUMMARY

An experimental investigation has been conducted on a model of a wing-control version of the Sparrow III type missile to determine the static aerodynamic characteristics over an angle-of-attack range of 0° to 40° for Mach numbers from 1.50 to 4.60. Comparisons were made of the characteristics of the wing-control configuration with those of the previously reported tail-control configuration of NASA TM X-2666.

The results indicate that the pitch-control effectiveness of the wings is less than that of the tails and is very nonlinear over the angle-of-attack range. The resultant trimmed-lift coefficient is correspondingly reduced. Wing pitch-control deflections at angles of attack above about 30° have reversed effectiveness in producing increases in the lift coefficient. The configuration at an asymmetric roll orientation of 26.6° exhibited large induced yawing and rolling moments at high angles of attack, which were accompanied by a complex pattern of vortices as indicated by vapor-screen photographs at a nominal Mach number of 2.35. Roll-control effectiveness was greater for the wing than for the tail at the tested model roll orientation of 45°. The yaw-control effectiveness of the wings at the model roll orientation of 45° was smaller than that of the tails, becoming reversed at angles of attack above about 14°, which is well below the maximum angles for which the configuration has longitudinal trim capability.

INTRODUCTION

Throughout the history of the development of air-to-air missile systems considerable debate has existed as to the type of aerodynamic-control configuration most suited to that role: canard, wing, or tail. (See ref. 1, for example.) Systems of each type have been built and are currently in the inventory; but generally as time progresses, there is a need to increase the missile operating envelope, including operation to higher altitudes, which often requires either enlarged aerodynamic surfaces or higher operating angles of attack. The wing-control Sparrow III has experienced several such increases in capability. Recent supersonic tests were made on a model of a Sparrow III type configuration utilizing the tails for control (ref. 2), but the model did not simulate wiring tunnels, or wing and tail stiffeners, as modeled in previous wing-control Sparrow III tests (refs. 3 and 4). In order to provide a direct comparison of wing-control and tail-control characteristics, an investigation has been made by using a new wing-control model, which is essentially the configuration of the tail-control model of reference 2.

The tests were conducted in the Langley Unitary Plan wind tunnel at Mach numbers from 1.50 to 4.60 and unit Reynolds numbers ranging between 8.20×10^6 and 4.92×10^6 per meter. The model was tested over an angle-of-attack range of 0° to 40° for model roll orientation angles of 0°, 26.6°, and 45°. The static aerodynamic characteristics of the model were investigated and included

the use of wing deflections to provide control in pitch, roll, and yaw. Direct comparisons were made of the aerodynamic characteristics of the wing-control configuration of this study and the tail-control configuration of reference 2.

SYMBOLS

The aerodynamic coefficients are referred to the body-axis system except for lift and drag, which are referred to the stability-axis system. The moment reference was located at 52.63 percent body length aft of the nose tip.

A maximum cross-sectional area of body, 0.000730 m^2

A_c chamber area, 0.000591 m^2

a_n instantaneous normal acceleration (perpendicular to flight path), $\frac{\text{Lift}}{\text{Weight}}$, g units (1g = 9.81 m/s^2)

C_A axial-force coefficient, $\frac{\text{Axial force}}{qA}$

$C_{A,c}$ balance-chamber axial-force coefficient, $\frac{(p - p_c)A_c}{qA}$

C_D drag coefficient, $\frac{\text{Drag}}{qA}$

$C_{D,c}$ balance-chamber drag coefficient, $C_{A,c} \cos \alpha$

$C_{D,o}$ drag coefficient at $\alpha = 0^o$

C_L lift coefficient, $\frac{\text{Lift}}{qA}$

C_{L_α} slope of lift curve measured at $\alpha = 0^o$, per deg

$C_{L,trim}$ trimmed-lift coefficient

C_l rolling-moment coefficient, $\frac{\text{Rolling moment}}{qAd}$

C_{l_δ} roll-control effectiveness at $\alpha = 0^o$, $\frac{\Delta C_l}{\delta_{roll}}$, per deg

C_m pitching-moment coefficient, $\frac{\text{Pitching moment}}{qAl}$

C_{m_α} slope of pitching-moment curve measured at $\alpha = 0^o$, per deg

C_{m_δ} pitch-control effectiveness at $\alpha = 0^o$, $\frac{\Delta C_m}{\delta_{pitch}}$, per deg

C_N normal-force coefficient, $\frac{\text{Normal force}}{qA}$

C_n yawing-moment coefficient, $\frac{\text{Yawing moment}}{qAd}$

C_{n_δ} yaw-control effectiveness at $\alpha = 0^o$, $\frac{\Delta C_n}{\delta_{yaw}}$, per deg

C_Y side-force coefficient, $\frac{\text{Side force}}{qA}$

d maximum body diameter, 3.048 cm

l model length, 54.86 cm

M Mach number

p free-stream static pressure, kPa

p_c balance-chamber pressure, kPa

q dynamic pressure, kPa

W weight, kN

x distance measured along model center line from nose apex, cm

x_{ac}/l aerodynamic-center position as fraction of model length, measured from nose apex

x_{cg}/l center-of-gravity position as fraction of model length, measured from nose apex

$\left(\frac{x_{cp}}{l}\right)_{\delta_{pitch}}$ effective center-of-pressure position due to pitch-control deflection as fraction of model length, measured from model nose apex, $\frac{x_{cg}}{l} - \frac{\Delta C_m}{\Delta C_N}$

$\left(\frac{x_{cp}}{l}\right)_{\delta_{yaw}}$ effective center-of-pressure position due to yaw-control deflection as fraction of model length, measured from model nose apex, $\frac{x_{cg}}{l} - \frac{\Delta C_n}{\Delta C_Y}\frac{d}{l}$

α angle of attack, deg

δ control-panel deflection, deg

δ_{pitch} control-panel deflection to provide pitching moment (negative for leading edge down; two panels deflected for $\phi = 0^o$; four deflected otherwise), deg

δ_{roll} control-panel deflection to provide rolling moment (positive for positive rolling moment; two panels deflected), deg

δ_{yaw} control-panel deflection to provide yawing moment (negative for leading edge left, viewed from the rear; two panels deflected for $\phi = 0^o$; four deflected for $\phi = 45^o$, deg

ϕ roll orientation of model (positive for clockwise roll angle when viewed from rear; $\phi = 0^o$ for wings in horizontal and vertical reference planes), deg

The panels are numbered 1, 2, 3, and 4 clockwise from top panel of $\phi = 0^o$ model position as viewed from rear.

APPARATUS AND TESTS

Tunnel

The investigation was conducted in the Langley Unitary Plan wind tunnel, which is a variable-pressure, continuous-flow facility having two test sections. Both test sections are approximately 1.22 m square in cross section and 2.13 m in length. The nozzles leading to the test sections are of the asymmetric sliding-block type, which permits a continuous variation in Mach number from about 1.5 to 2.9 in the low Mach number test section and 2.3 to 4.7 in the high Mach number test section.

Model

Details of the model are shown in figure 1, and a photograph of the model is given as figure 2. The configuration consisted of an ogive-cylinder body with a fineness ratio of 18, cruciform wings, and in-line tails. The wings had a trapezoidal planform with a leading-edge sweep of 45° and a diamond airfoil section. (See fig. 1(b).) The tails had a delta planform with a leading-edge sweep of 57° and a modified diamond airfoil section. (See fig. 1(c).) Both the wings and tails could be set at deflections within a ±20° range by 5° increments, although only wing-control tests were made on the present model. The present configuration differs from that of reference 2 in that the wing has a sharp trailing edge instead of 0.13 cm bluntness.

Tests

The tests were conducted under the following conditions:

Mach Number	Stagnation pressure, kPa	Stagnation temperature, K	Unit Reynolds number, per meter
1.50	66.5	339	[a]8.20×10^6
2.00	79.4	339	[a]8.20
2.35	94.1	339	[a]8.20
2.87	123.8	339	[a]8.20
3.95	231.1	353	8.20
4.60	311.7	353	8.20

[a]Unit Reynolds number was decreased to as low as 4.92×10^6 per meter to prevent balance overload for high angles of attack or for $\delta_{pitch} = 10°$ or more.

The dewpoint was maintained below about 239 K to insure negligible condensation effects for all force tests. Vapor-screen runs were made with the dewpoint raised to about 275 K to provide an optimum density of fog in the test section. At this condition it is estimated that the true free-stream Mach number is decreased by about 0.10 from the nominal value (ref. 5). Transition strips on the wings and fins were located 1.0 cm streamwise from the leading edges; on the nose, 3.0 cm from the model apex. The transition strips were composed of individual grains of No. 40 sand (0.046-cm nominal height) spaced about 0.184 cm between centers measured perpendicular to the airstream. The model was tested over an angle-of-attack range from 0° to 41° for roll angles of 0° and 45° primarily, although limited tests were made at 26.56°.

Measurements

Aerodynamic forces and moments were measured by means of a six-component electrical strain-gage balance which was housed within the body of the model. The balance was attached to a sting which, in turn, was rigidly fastened to the tunnel support system. Balance-chamber pressure was measured by means of a pressure orifice located in the balance chamber.

Corrections

The angles of attack have been corrected for deflection of the balance and sting due to aerodynamic load and for airflow misalinement. The drag and axial-force coefficients have been adjusted to correspond to free-stream static pressure acting over the base of the model. Typical chamber axial-force and drag coefficients are presented in figure 3.

PRESENTATION OF RESULTS

The results are presented in the following figures:

RESULTS AND DISCUSSION

Longitudinal Aerodynamic Characteristics

Wing control.- The longitudinal aerodynamic characteristics of the wing-control configuration are presented in figures 4 and 5 for $\phi = 0^\circ$ and 45°, respectively. The variation of normal-force coefficient with angle of attack is reasonably linear for all test conditions, but the increment produced by wing deflection diminishes significantly at the higher angles of attack. The axial-force coefficient increases with angle of attack for positive pitch-control deflections and contributes to a reversed lift-control effectiveness for angles of attack above about 30°. Pitch-control effectiveness varies greatly with both angle of attack and Mach number and can be seen directly in figure 6. At low Mach numbers the effectiveness decreases with increasing angles of attack, whereas at the highest Mach numbers it increases significantly.

A comparison of the longitudinal characteristics for $\phi = 0^\circ$ and 45° are presented in figure 7 for $M = 1.50$ and 4.60. At both Mach numbers the stability near zero angle of attack is about the same for the two roll orientations, but for the higher angles of attack at $M = 4.60$, there is considerably less stability at $\phi = 45^\circ$ than at 0°. As a result of the stability change combined with greater increases in the pitch-control effectiveness for $\phi = 45^\circ$ at $M = 4.60$, a great difference in the trim angle of attack between the orientation of $\phi = 0^\circ$ and 45° occurs (8° and 37°, respectively).

Comparison of wing- and tail-control configurations.- A comparison of the results for the wing-control configuration with those for the tail-control configuration (from ref. 2) is presented in figure 8 for $M = 1.50$, 2.87, and 4.60. The tail-control configuration produces a much larger pitching-moment increment which is nearly constant over the angle-of-attack range, yielding trimmed-angle-of-attack values which are correspondingly higher. The tail deflection, however, produces a negative C_N increment compared with the positive increment for the wing deflection. Consequently, the tail control requires a significantly greater angle of attack than the wing control to achieve the same C_N or C_L with an equal control deflection angle.

The effect of center-of-gravity position x_{cg}/l on the trimmed lift is shown in figure 9 for several Mach numbers. With the exception of $M = 1.50$, wing control provides significantly lower values of the trimmed lift than the tail control. Generally the tails can provide the same $C_{L,trim}$ as the wings with a center-of-gravity position about $0.05l$ more forward. At $\phi = 45^\circ$, the $C_{L,trim}$ for the wing control at $M = 4.60$ is very sensitive to small changes in the center of gravity near a value of $0.52l$.

The steady-state aerodynamic normal-acceleration capability of a configuration can be evaluated by examining the quantity $M^2C_{L,trim}$ (fig. 10) for a given value of W/A. The acceleration values (a_n) at three altitudes are shown for an assumed value of W/A = 47.9 kPa. The equation is

$a_n = \frac{\text{Lift}}{\text{Weight}} = \frac{C_L q}{W/A} = \frac{0.7pM^2C_L}{W/A}$. Both configurations display the usual increase in a_n with Mach number. The wing-control configuration shows the large difference in capability between the 0° and 45° roll orientations, which was mentioned previously. At $M = 4.60$, the difference is maximum with $\phi = 0^\circ$ exhibiting only about one-third of the capability of $\phi = 45^\circ$. For the 18.3-km altitude and $\phi = 45^\circ$, the wing-control configuration has a 12g capability at $M = 2.87$, whereas the tail control has greater than 17g capability.

Summary.- Longitudinal results for $\alpha = 0^\circ$ are summarized in figure 11. For zero control deflection the results are essentially the same as for the tail control of reference 2, as would be expected. The pitch-control effectiveness C_{m_δ} of the wings (fig. 11(a)) is about two-thirds of that for the tails at $M = 1.50$, but only about one-tenth at the highest Mach numbers. At $\phi = 45^\circ$, the pitch-control effectiveness for the wings is about 40 percent greater than at $\phi = 0^\circ$, just as for the tails. This result would indicate negligible interference between the pairs of panels, allowing each pair to contribute $\sin 45^\circ = 0.707$ of the two-panel C_m for a total of 1.41.

The effective center of pressure due to wing-control deflection at an angle of attack of 0° (fig. 11(b)) is seen to lie well forward of the wings at $M = 1.50$ and to move rearward rapidly with increase in Mach number. This condition is probably due to large induced body and tail loads at low Mach numbers acting to increase the positive pitching moment on the vehicle, whereas the reduced tail loads occurring at the higher Mach numbers would allow the center of pressure to move aft toward the wing hinge line.

Lateral Aerodynamic Characteristics

Effect of ϕ.- The lateral aerodynamic characteristics for the asymmetric roll orientation angle of 26.6° (fig. 12) indicate large values of C_l and C_n at the higher angles of attack. The highest induced rolling moments occur at the low Mach numbers, and increasing of the Mach number delays the peak values to higher angles of attack and decreases their magnitude.

A vapor-screen survey was made at $\phi = 26.6^\circ$ for a nominal $M = 2.35$. An early developmental photographic setup at the wind tunnel was used, with the camera located outside the test section and pointed toward the illuminated vapor "screen" at an angle of approximately 45°, similar to that of reference 6. The results presented in figure 13 indicate that a complex pattern of asymmetric vortices develop as the angle of attack increases. The large number of vortices present seems to preclude the possibility of an elementary analysis of their contribution to the induced rolling moments.

Roll control.- The effectiveness of two wings deflected for roll control at $\phi = 45^\circ$ was investigated at all six test Mach numbers (fig. 14), and the corresponding results from reference 2 are shown as dashed-line curves. The wings are effective for roll control throughout the test range of angle of

attack and Mach number, producing approximately twice that of the tails. At $M = 1.50$ and 2.00, both the wings and tails have a noticeable decrease in control moment at angles of attack above about 16°. At $M = 1.50$ and 2.00, the 10° roll-control deflection of the tails is sufficient to null the induced C_l ($\phi = 26.6^\circ$, fig. 12) up to only about $\alpha = 20^\circ$ and 24°, respectively, which is significantly less than the maximum α_{trim} of over 40°. Wing roll control causes a significant induced yawing moment, which peaks at approximately $\alpha = 10^\circ$; whereas the tail roll control causes very little at the low angles of attack, but the amount increases to a significant value at the high angles.

Although there is positive roll-control effectiveness at $\alpha = 45^\circ$ for the present test conditions, the results of reference 4 indicate that conditions exist at transonic Mach numbers up to 1.3 where wing roll control yields either small or reversed effectiveness, especially when roll control is superimposed on a pitch-control deflection.

Yaw control.- The deflection of four wings for yaw control at $\phi = 45^\circ$ (fig. 15) produced a constant effectiveness up to an angle of attack of only about 4° for $M = 1.50$ to 2.87. Beyond $\alpha = 4^\circ$, the effectiveness dropped off, becoming negative near $\alpha = 14^\circ$. As Mach number increased, the effectiveness at low angles of attack decreases rapidly to almost zero at $M = 3.95$ and 4.60. The loss in directional control at the higher angles of attack would tend to limit the missile capability to angles well below those for which the configuration has longitudinal trim capability. For angles of attack above about 2° the yaw-control deflection generated induced rolling moments which became very large as angle of attack increased.

The tails (fig. 15 also) are effective for yaw control throughout the test angle-of-attack range, although at $M = 1.50$ to 2.35 the effectiveness decreases with increasing angle of attack. The tails are more effective than the wings throughout the range of test Mach number. The tail control also induces rolling moments, but the magnitude is no more than about one-half of that due to wing control, although it is of opposite sign.

The position of the effective center of pressure x_{cp}/l due to yaw-control deflection of the wings is presented in figure 16 along with yaw-control effectiveness C_{n_δ}. The center of pressure varies widely with both angle of attack and Mach number and moves from well forward of the center-of-gravity location at $\alpha = 0^\circ$ to well behind it at the maximum test angle of attack. As Mach number increases, the center of pressure for $\alpha = 0^\circ$ moves aft toward the center of gravity; this is the same effect observed earlier for the case of pitch-control deflection. For high angles of attack the center of pressure lies behind the wing trailing edge, thereby indicating that the loads induced on the body and tail have become opposite to those at the low angles of attack.

Lateral directional summary.- A summary of the lateral- and directional-control characteristics for an angle of attack of 0° are presented in figure 17. The roll-control effectiveness of the wings is greater than that of the tails by about 80 percent at $M = 1.50$ and only by about 50 percent at $M = 4.60$. The yaw-control effectiveness of the wings is only about 60 percent of that of the tails at $M = 1.50$ and about 15 percent at $M = 4.60$.

CONCLUSIONS

An experimental investigation has been conducted on a wing-control version of the Sparrow III type missile to determine the static aerodynamic characteristics over an angle-of-attack range from 0° to 40° for Mach numbers from 1.50 to 4.60. Comparisons were made of the characteristics of the wing-control configuration with those of the previously reported tail-control configuration of NASA TM X-2666. The results led to the following conclusions:

1. The pitch-control effectiveness for the wings is less than for the tails and is very nonlinear over the angle-of-attack range. Above a Mach number of 1.50 the trimmed-lift coefficient for wing control is significantly less than for tail control, especially at the model roll orientation of 0°.

2. Wing pitch-control deflections at angles of attack above about 30° have reversed effectiveness for generating lift coefficient.

3. The configuration at an asymmetric roll orientation of 26.6° exhibited large induced values of yawing and rolling moments at high angles of attack, which were accompanied by a complex pattern of vortices, as indicated by vapor-screen photographs at a nominal Mach number of 2.35.

4. Roll-control effectiveness was greater for the wing than for the tail at the tested model roll orientation of 45°.

5. The yaw-control effectiveness of the wings at the tested model roll orientation of 45° was less than that of the tails and became reversed at angles of attack above about 14°, which is well below the maximum angles for which the configuration has longitudinal trim capability.

Langley Research Center
National Aeronautics and Space Administration
Hampton, VA 23665
October 19, 1977

REFERENCES

1. Chin, S. S.: Missile Configuration Design. McGraw-Hill Book Co., Inc., c.1961.

2. Monta, William J.: Supersonic Aerodynamic Characteristics of an Air-to-Air Missile Configuration With Cruciform Wings and In-Line Tail Controls. NASA TM X-2666, 1972.

3. McKinney, Royce L.: Longitudinal Stability and Control Characteristics of an Air-to-Air Missile Configuration at Mach Numbers of 2.30 and 4.60 and Angles of Attack From -45° to 90°. NASA TM X-846, 1963.

4. Friedman, R. F.: Aerodynamic Stability and Control Report for the Sparrow III Model XAAM-N-6b and YAAM-N-6b Missile. BR-1018 (Contract No. NOas-59-0317), Missile & Space Div., Raytheon Co., Nov. 1962. (Available from DDC as AD 511 006.)

5. Hill, J. A. F.; Baron, J. R.; Schindel, L. H.; and Markham, J. R.: Mach Number Measurements in High-Speed Wind Tunnels. AGARDograph 22, North Atlantic Treaty Organization (Paris), Oct. 1956.

6. Gapcynski, John P.: An Experimental Investigation of the Flow Phenomena Over Bodies at High Angles of Attack at a Mach Number of 2.01. NACA RM L55H29, 1955.

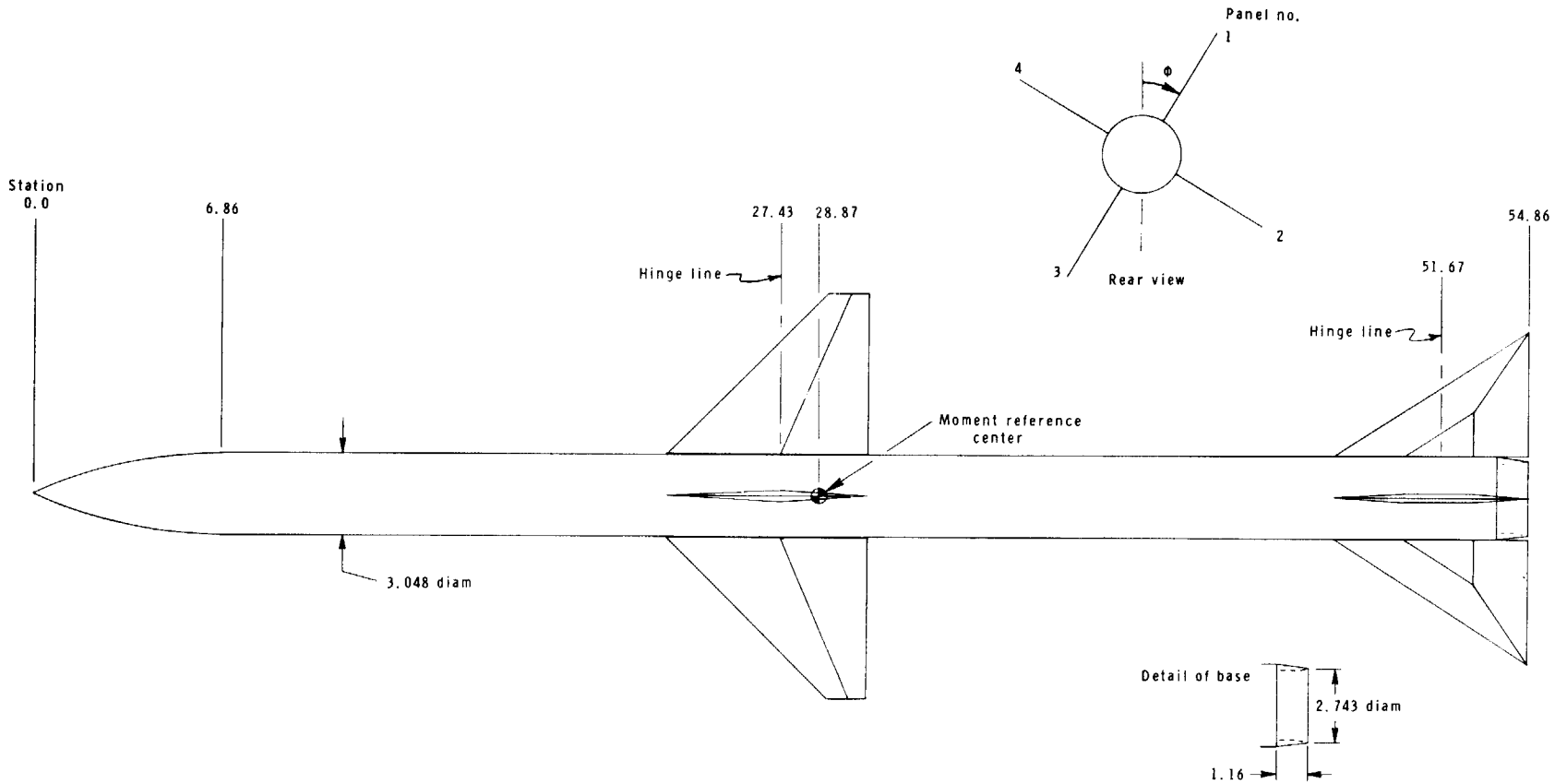

(a) Complete model.

Figure 1.- Drawing of model. All dimensions are given in cm unless otherwise noted.

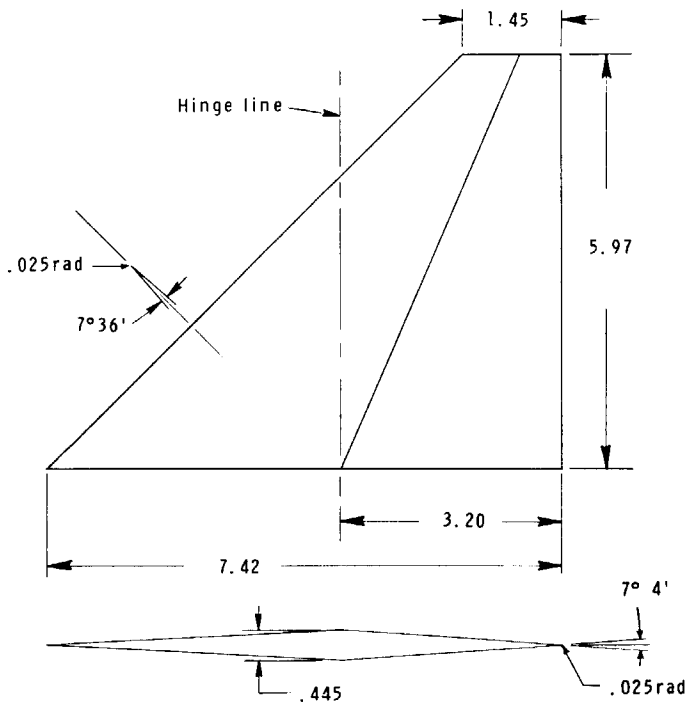

(b) Wing.

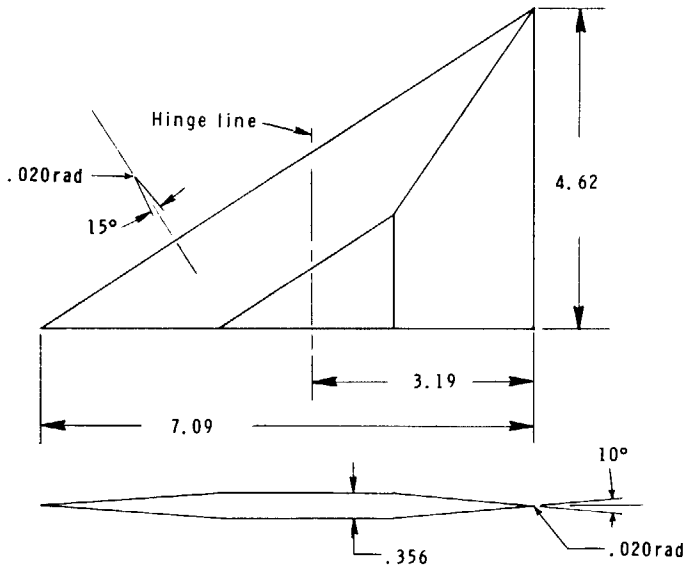

(c) Tail.

Figure 1.- Concluded.

L-73-8772

Figure 2.- Model in high Mach number test section. $\phi = 45^{\circ}$; $\delta_{pitch} = 20^{\circ}$.

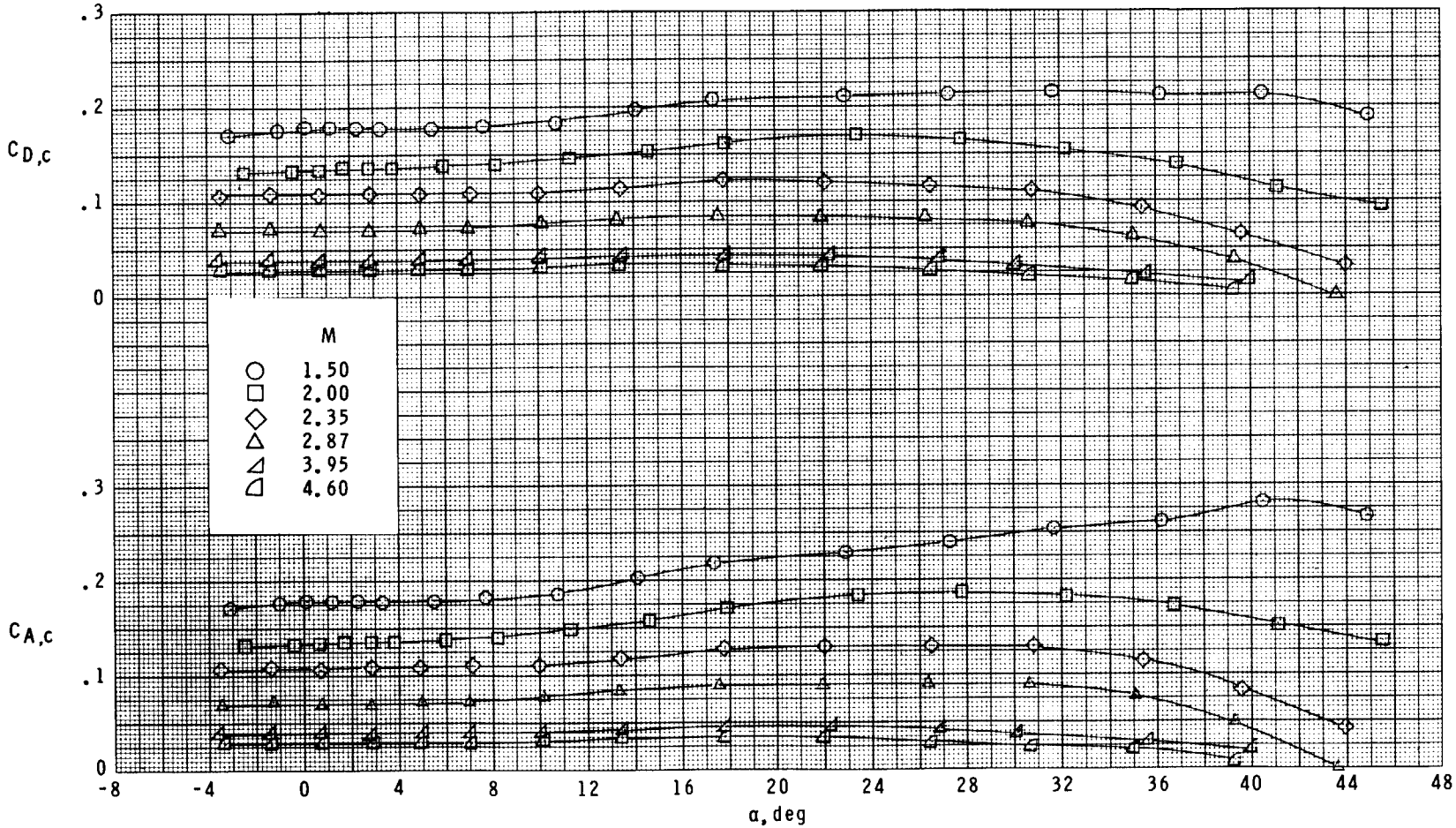

Figure 3.- Typical variation of balance-chamber axial-force and drag coefficients with angle of attack. $\phi = 0^{o}$; zero control deflection.

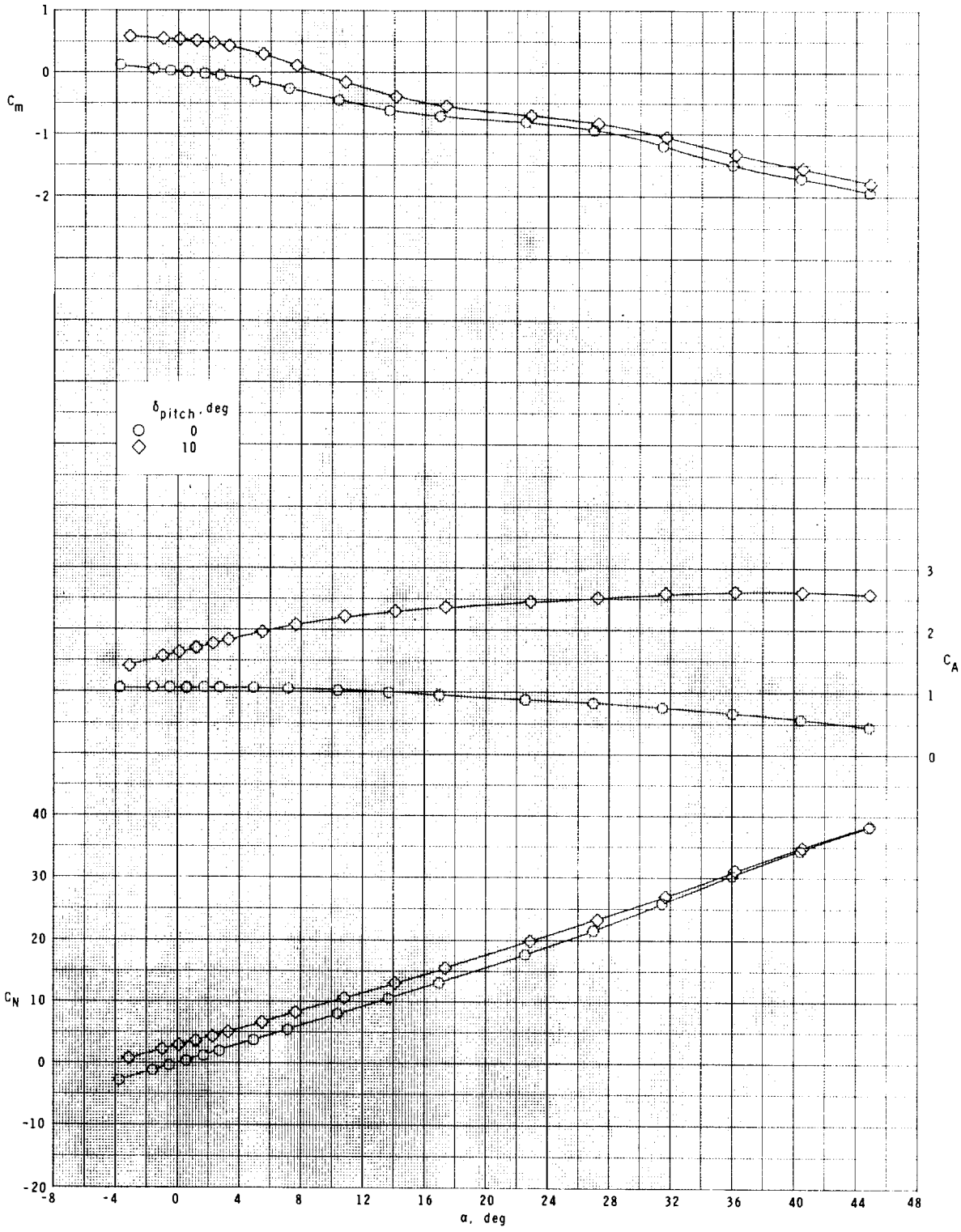

(a) M = 1.50.

Figure 4.- Pitch-control characteristics of wing-control configuration at $\phi = 0^o$.

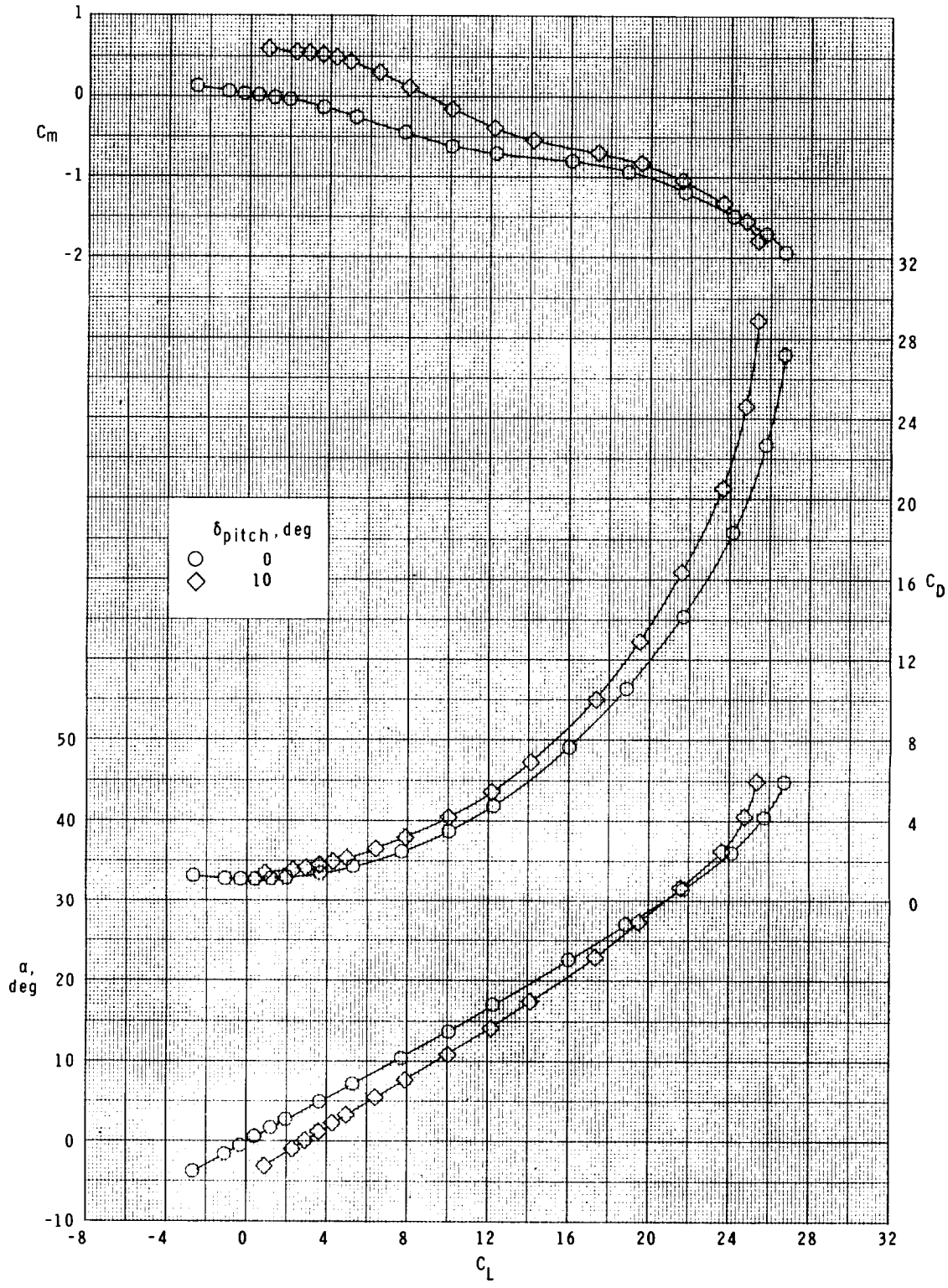

(a) Concluded.

Figure 4.- Continued.

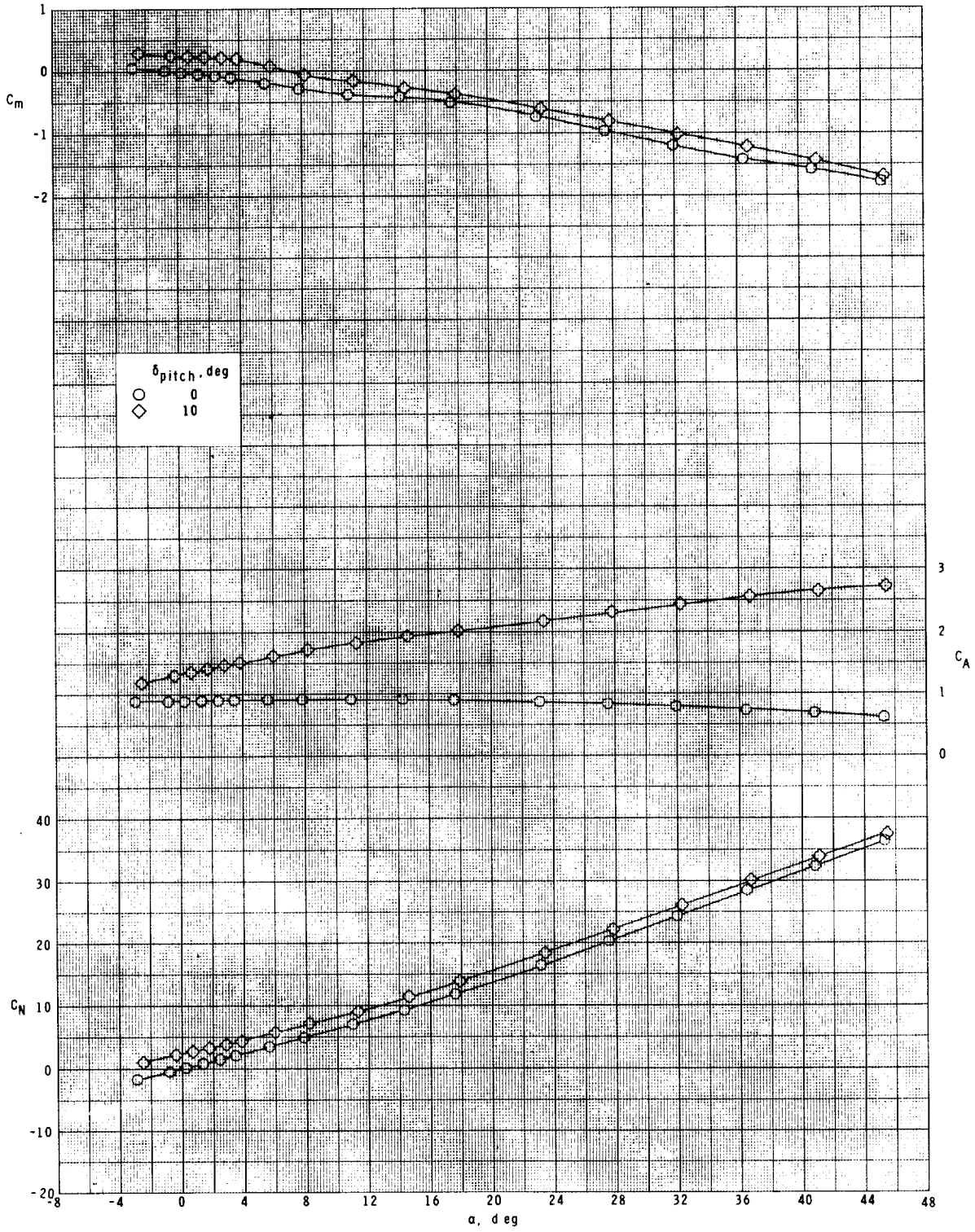

(b) M = 2.00.

Figure 4.- Continued.

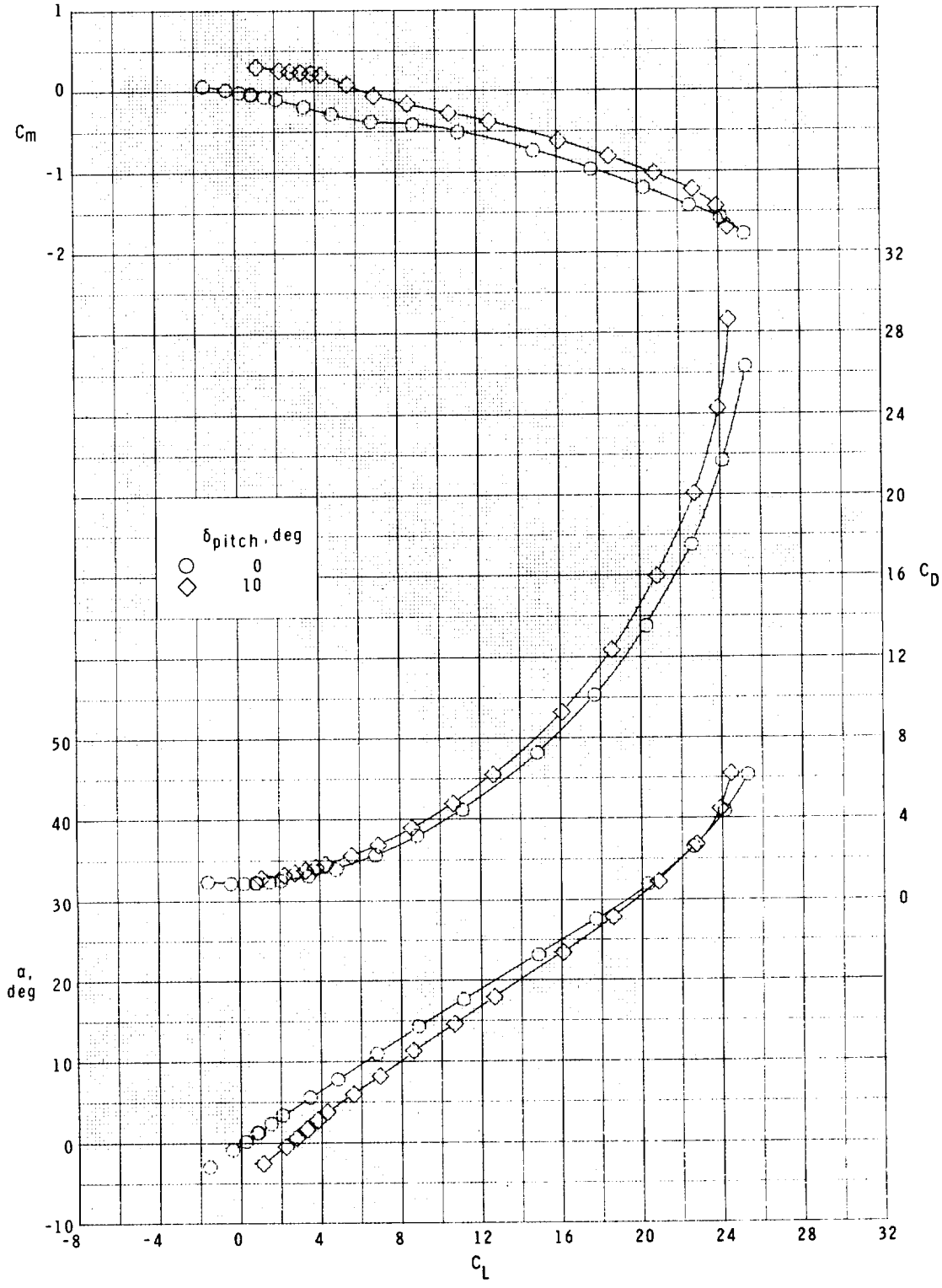

(b) Concluded.

Figure 4.- Continued.

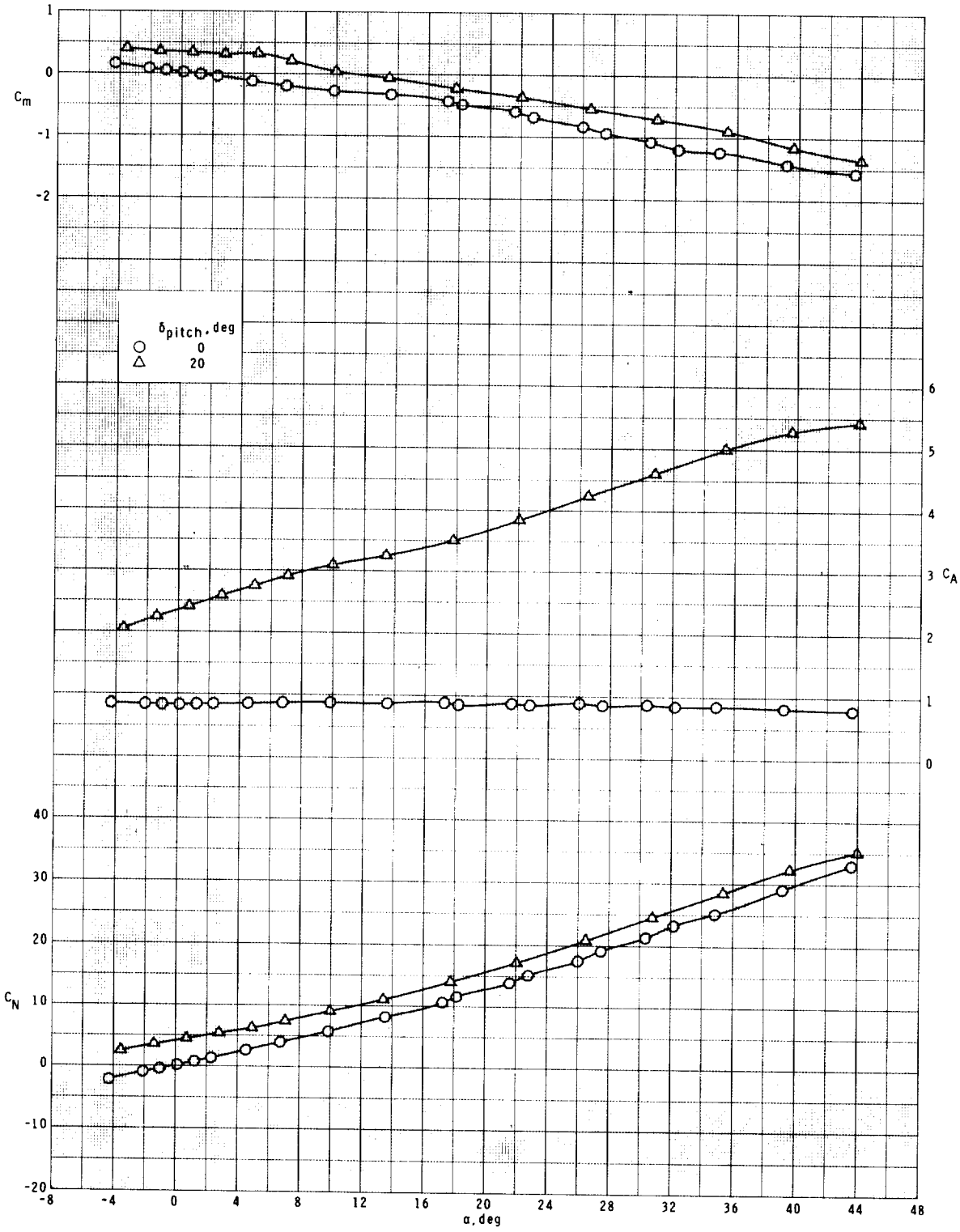

(c) M = 2.35.

Figure 4.- Continued.

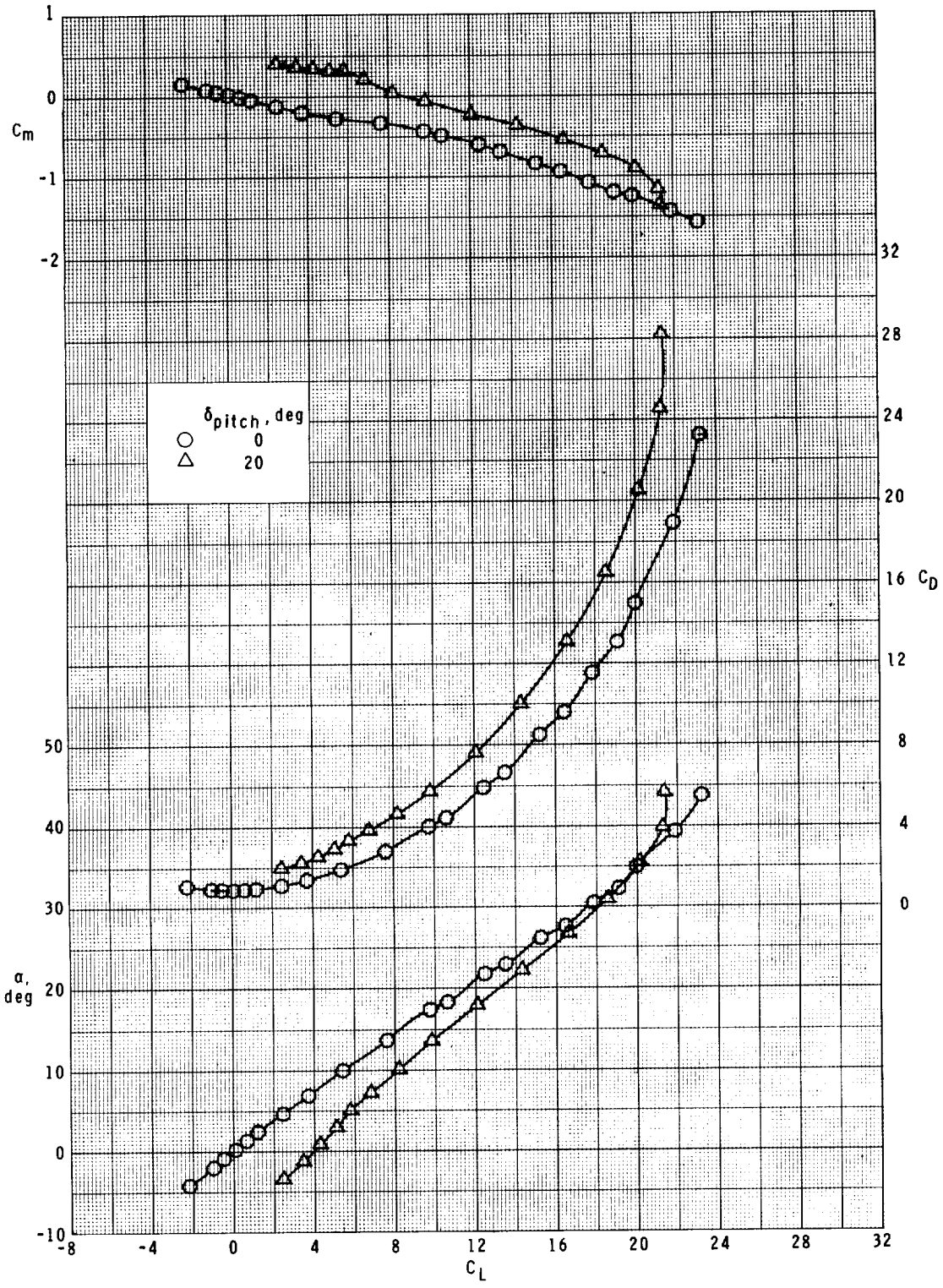

(c) Concluded.

Figure 4.- Continued.

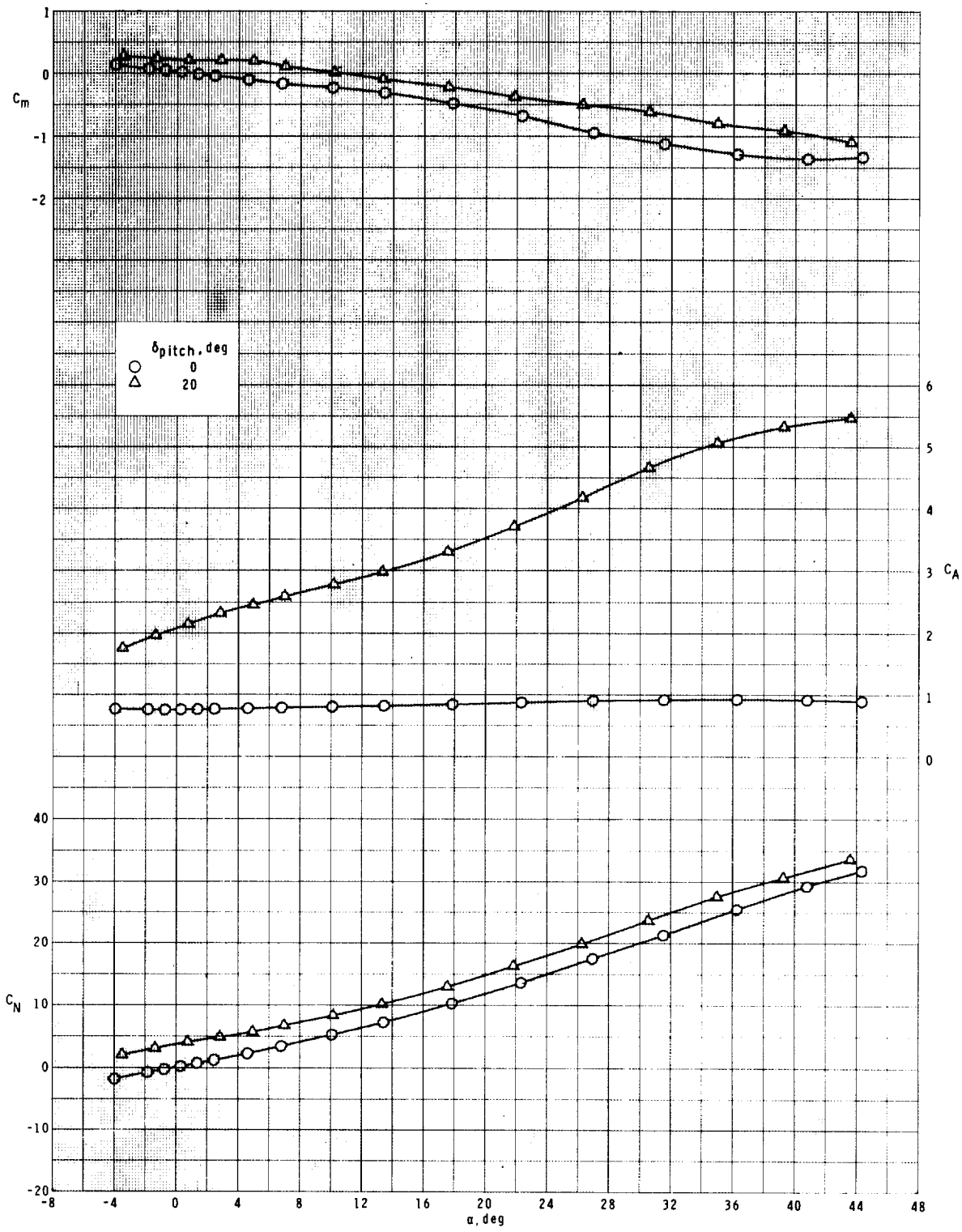

(d) M = 2.87.

Figure 4.- Continued.

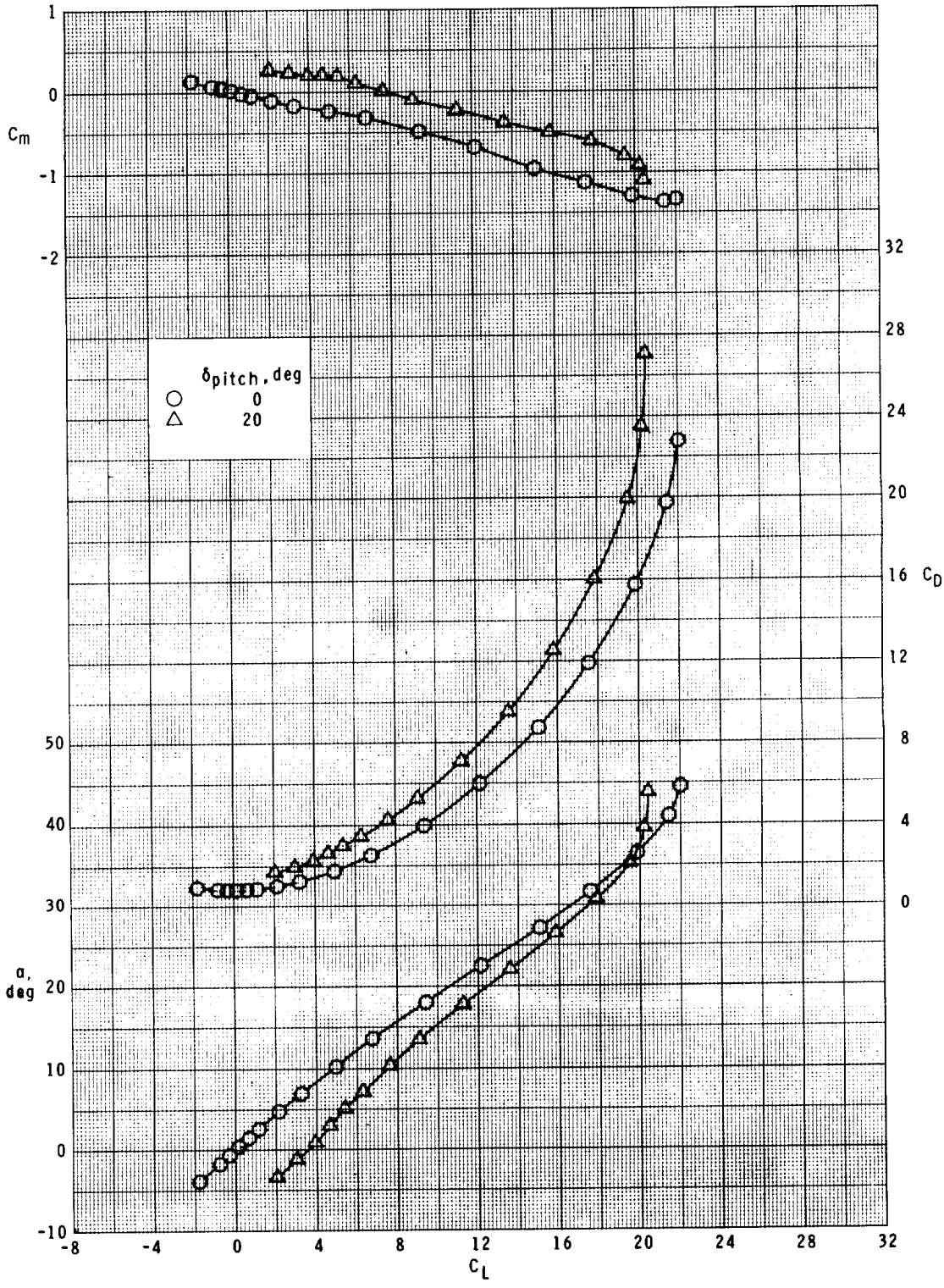

(d) Concluded.

Figure 4.- Continued.

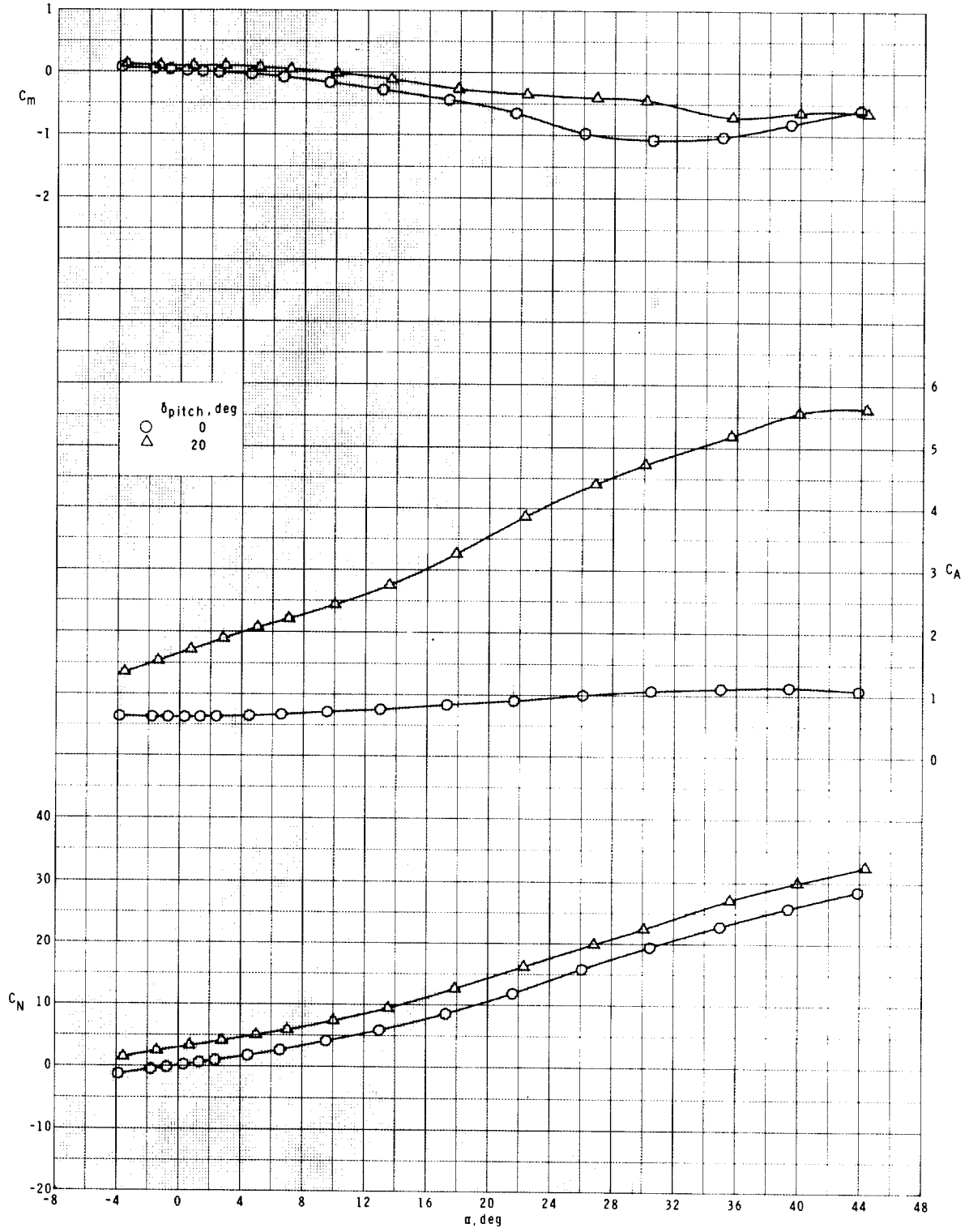

(e) M = 3.95.

Figure 4.- Continued.

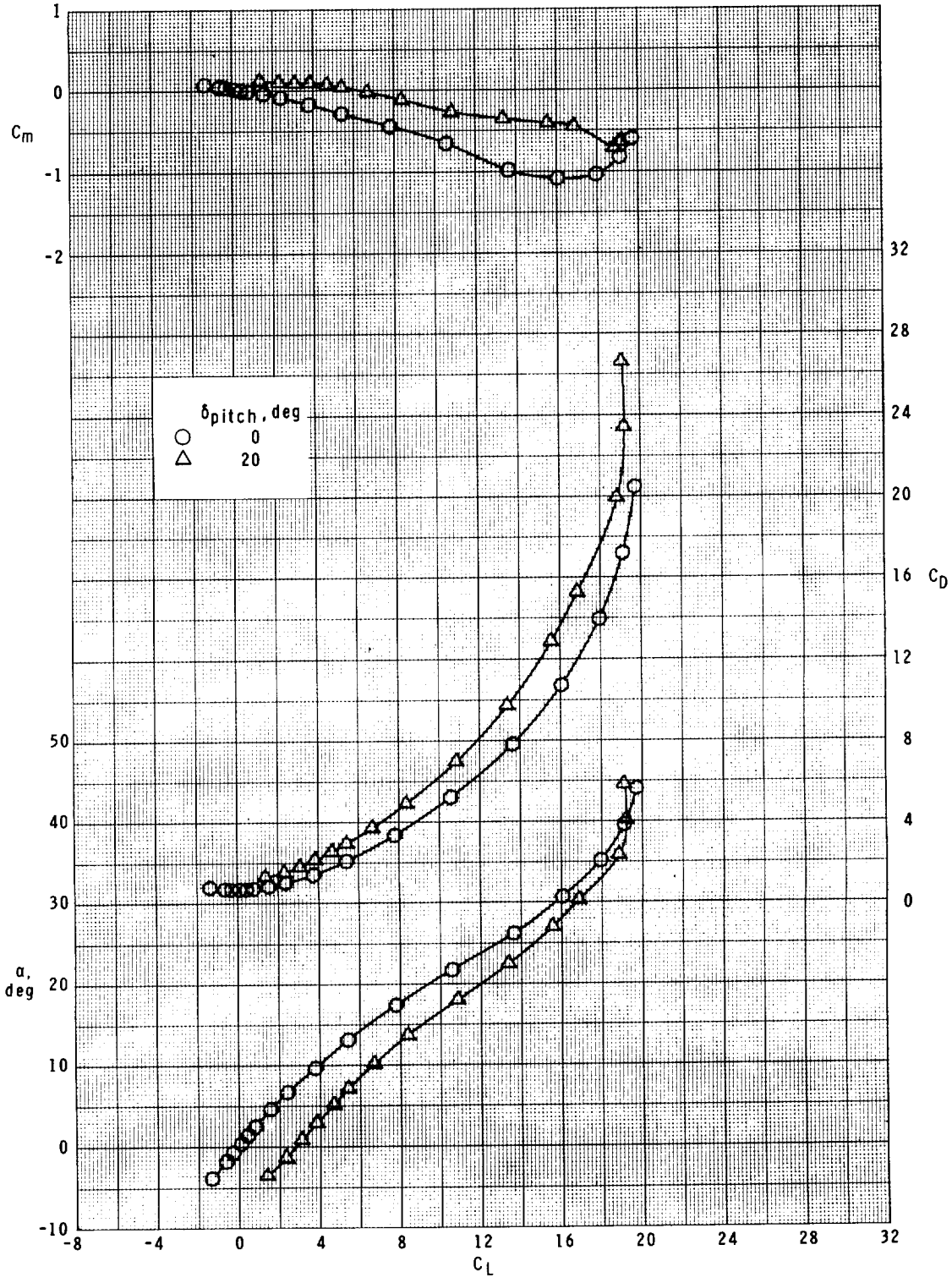

(e) Concluded.

Figure 4.- Continued.

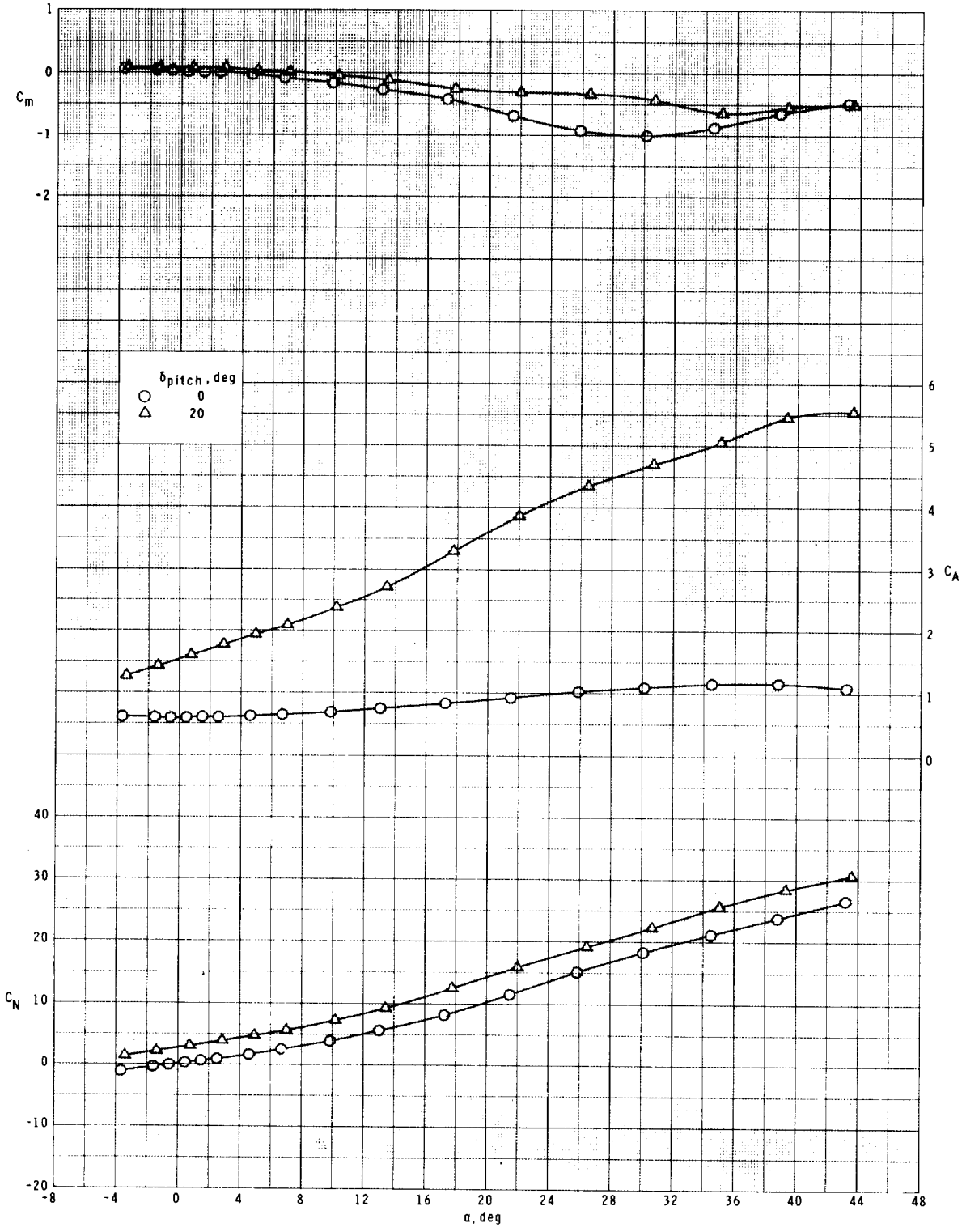

(f) M = 4.60.

Figure 4.- Continued.

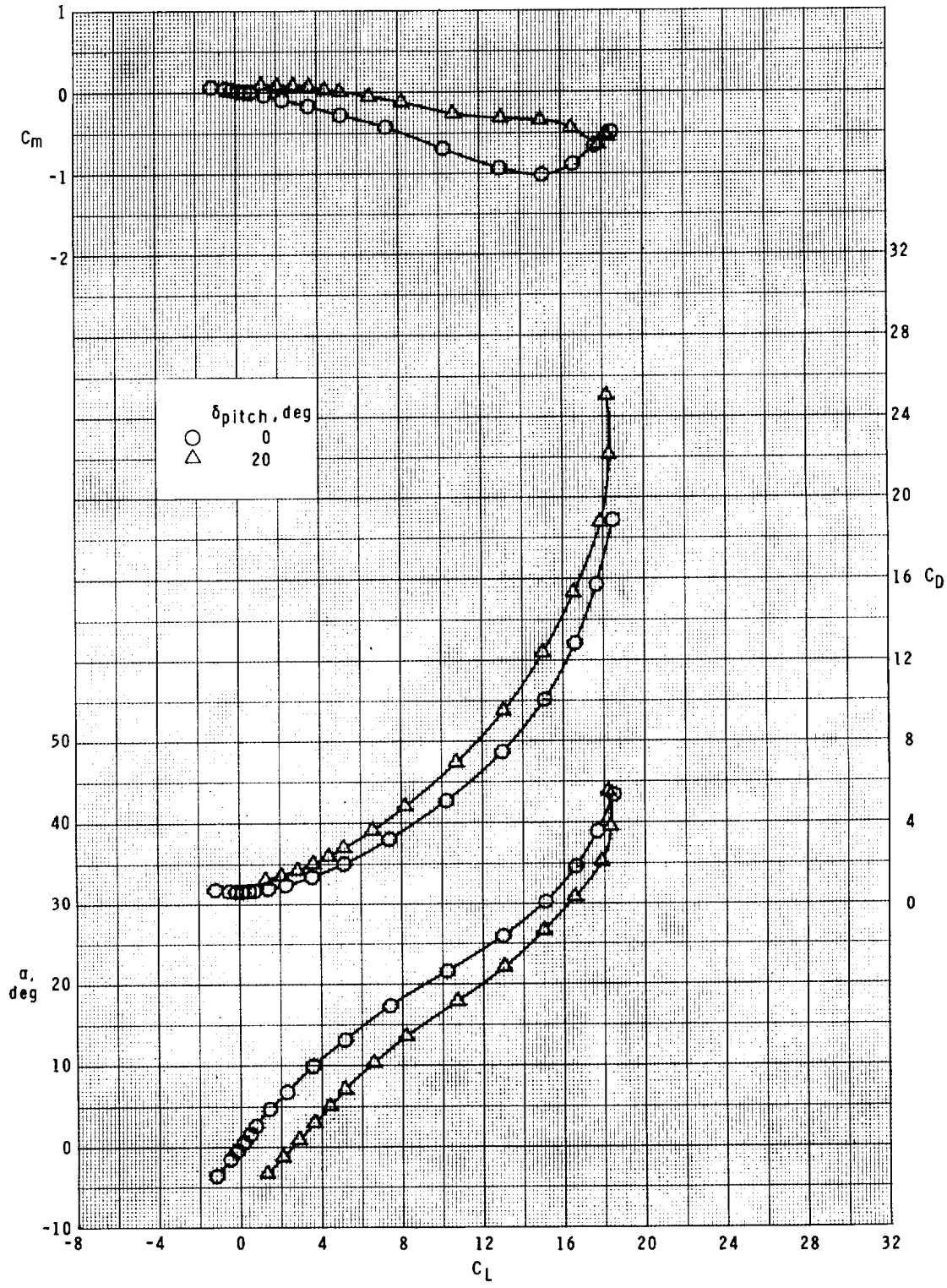

(f) Concluded.

Figure 4.- Concluded.

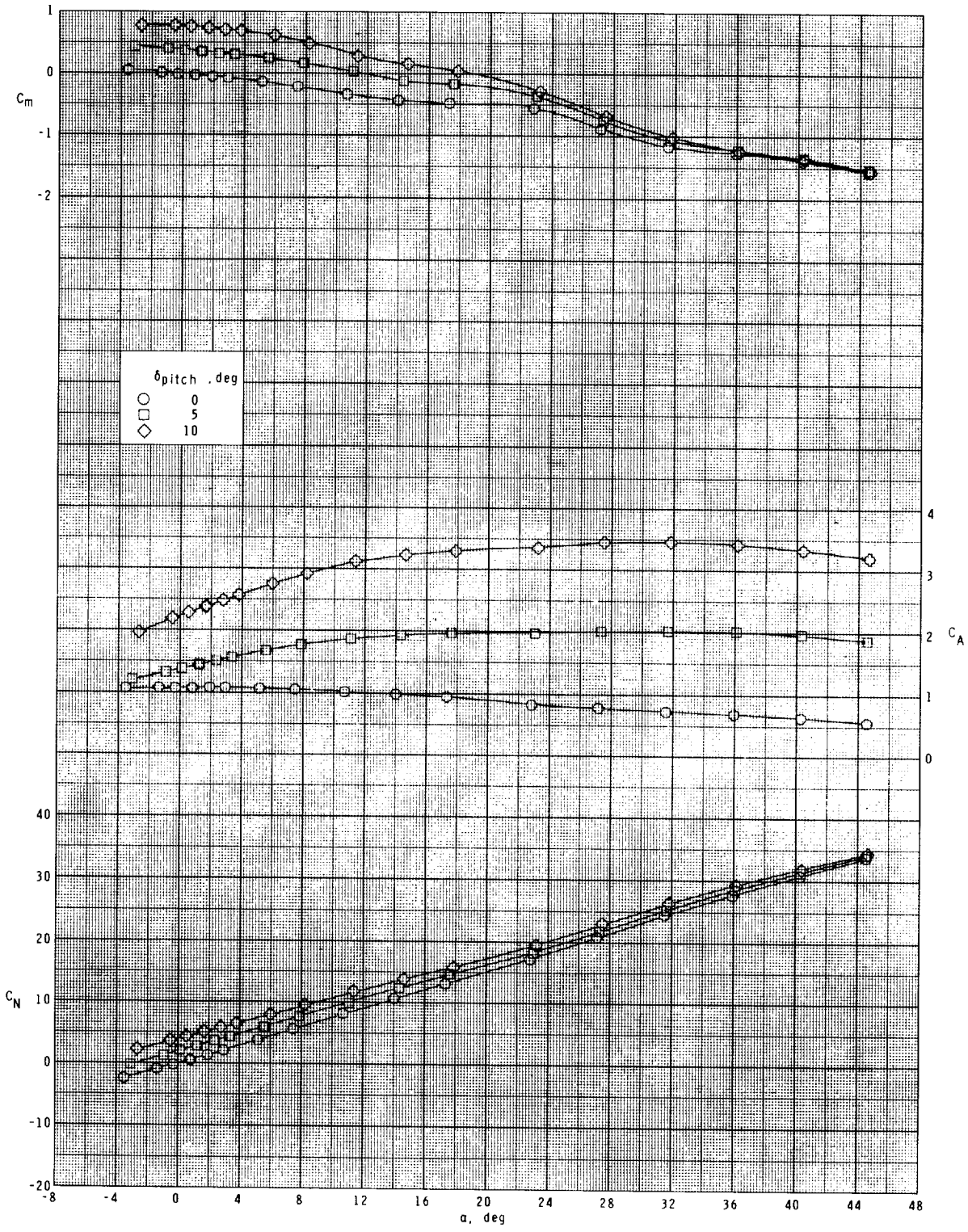

(a) M = 1.50.

Figure 5.- Pitch-control characteristics of wing-control configuration at $\phi = 45^{\circ}$.

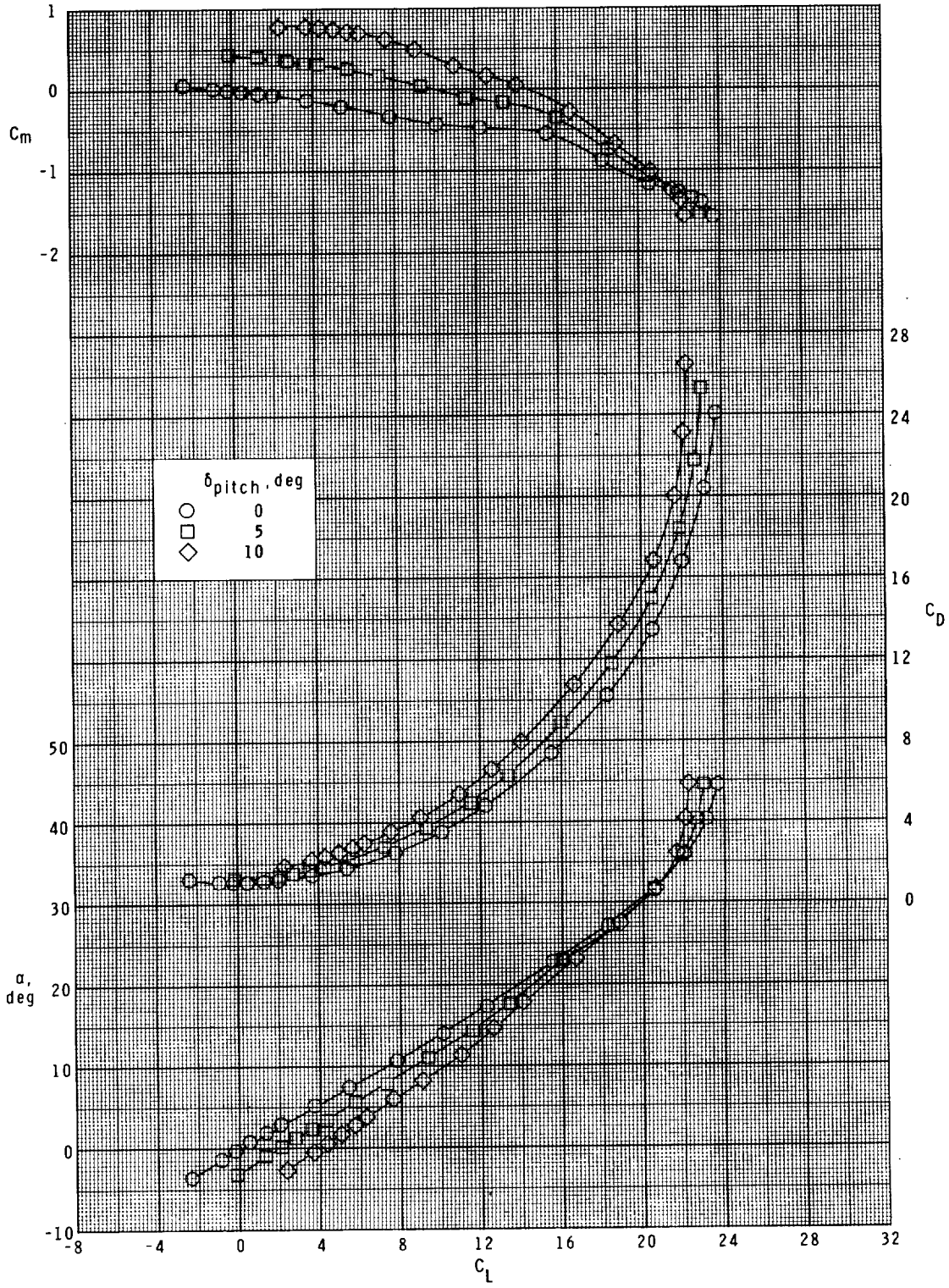

(a) Concluded.

Figure 5.- Continued.

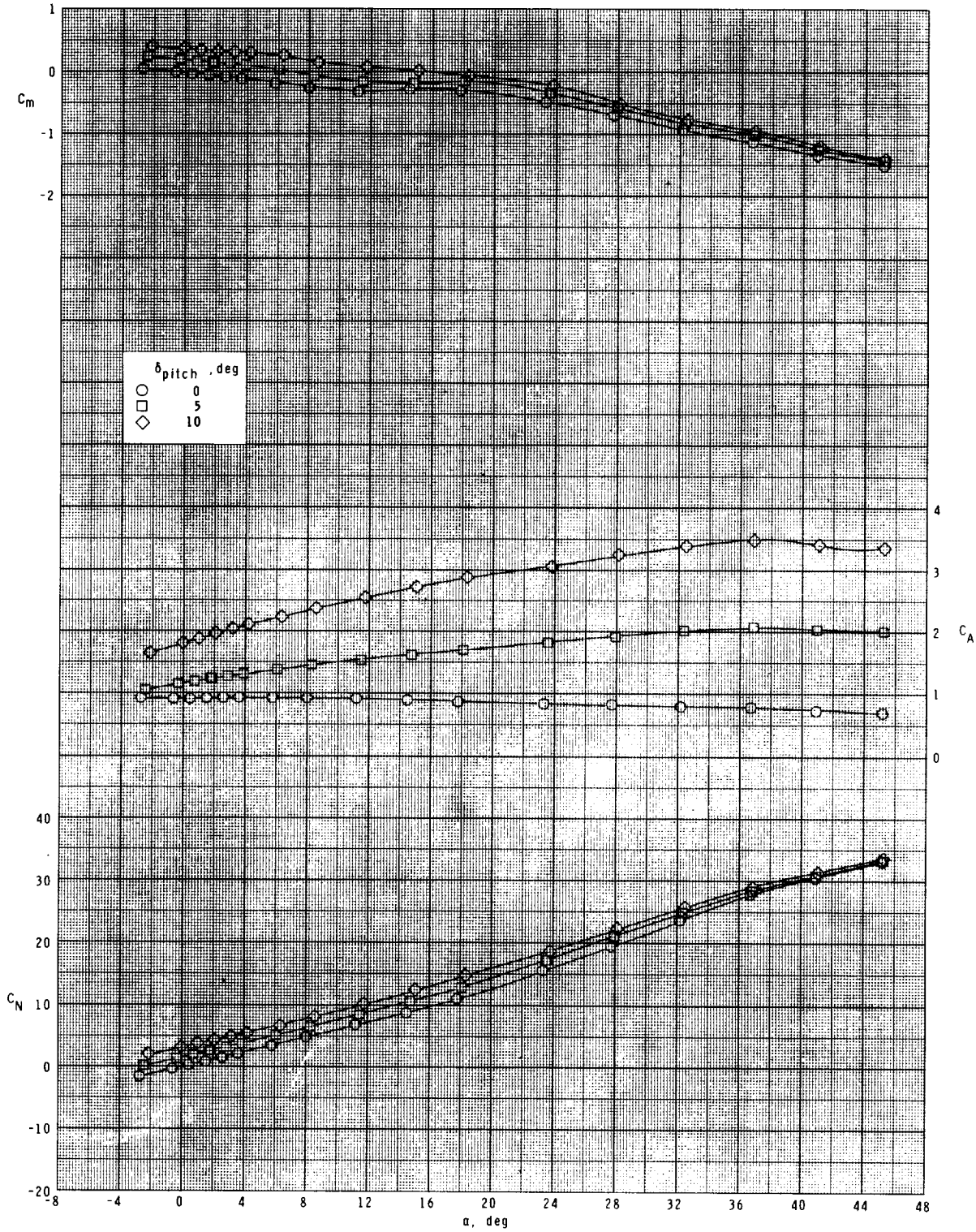

(b) M = 2.00.

Figure 5.- Continued.

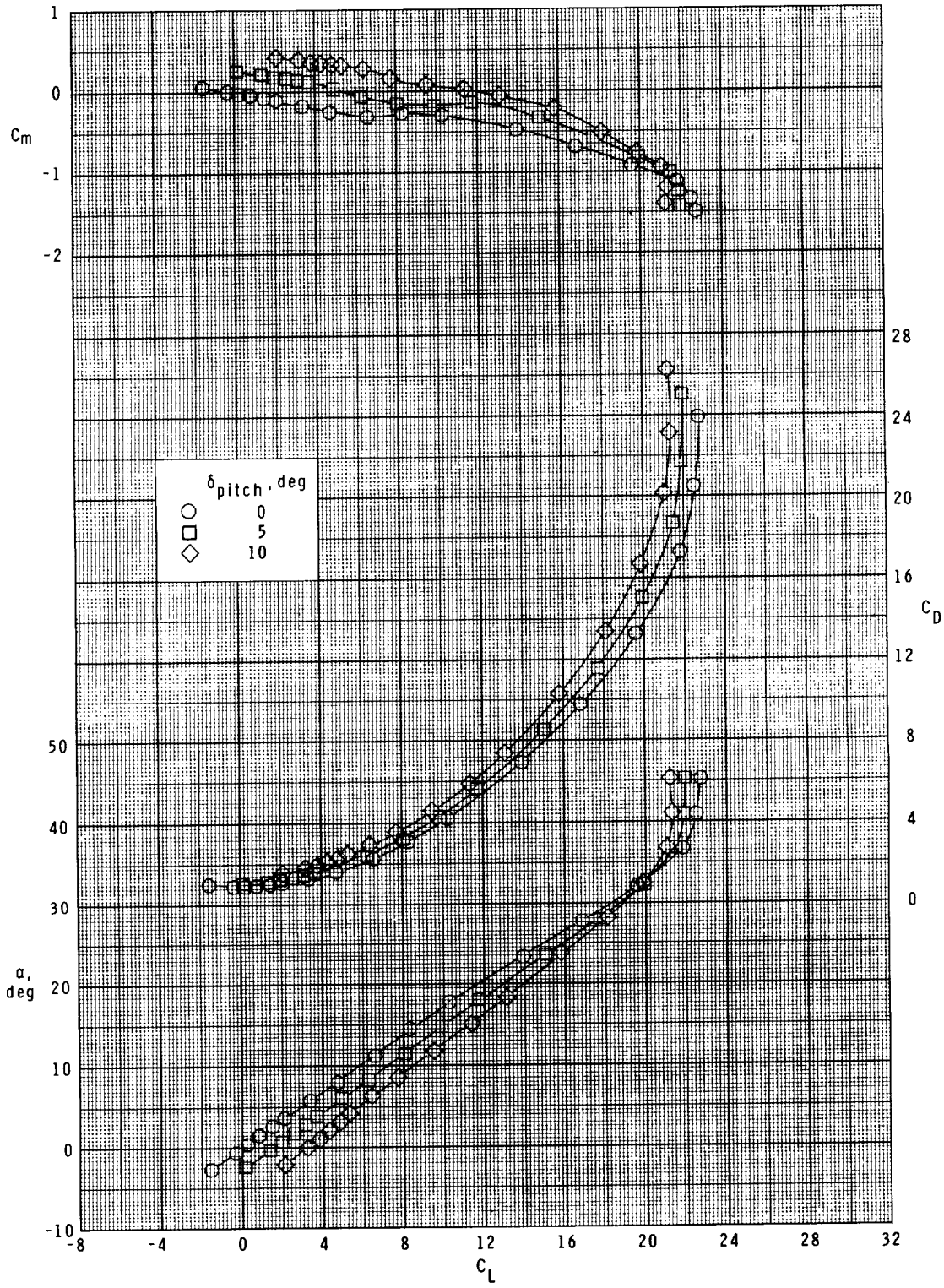

(b) Concluded.

Figure 5.- Continued.

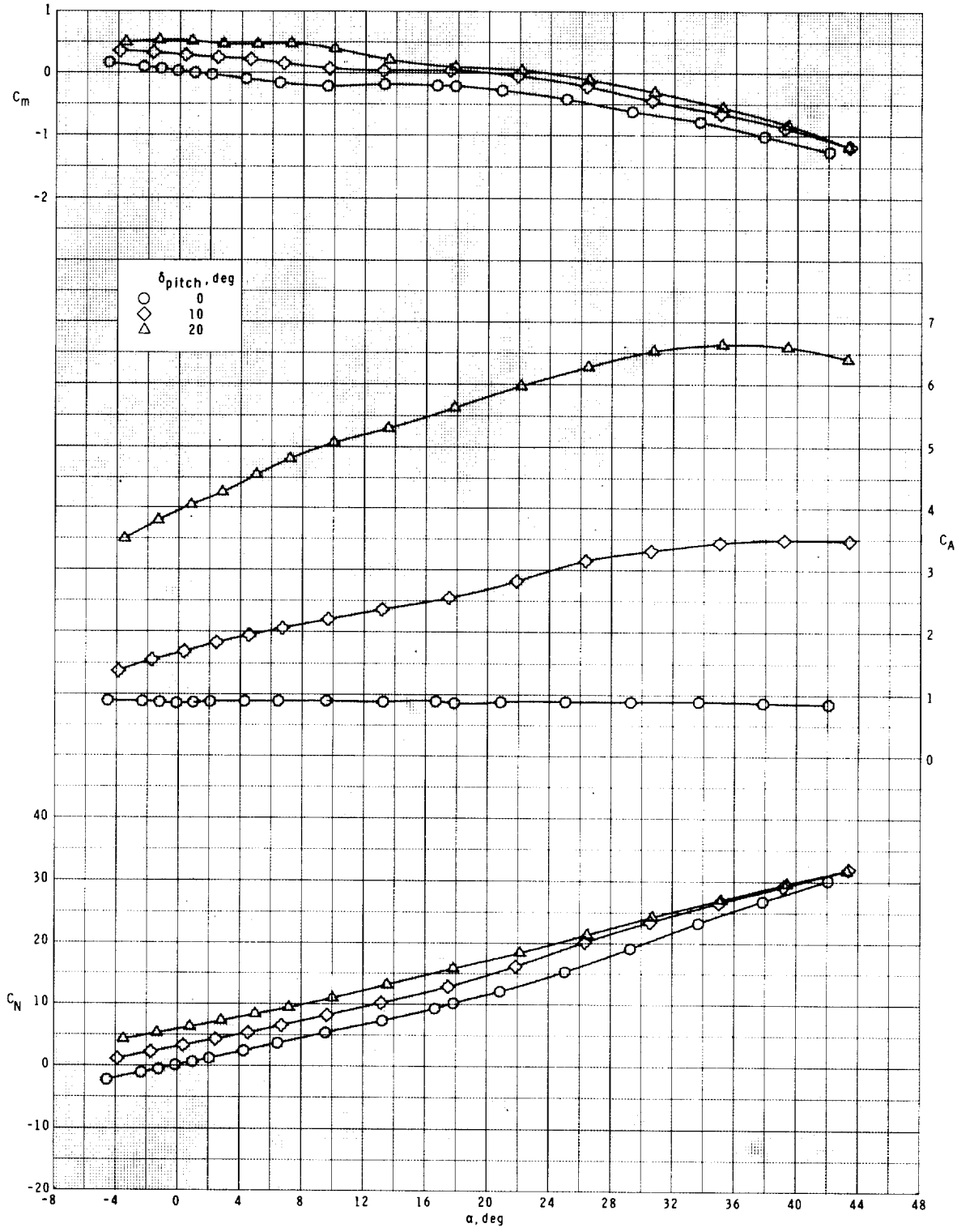

(c) M = 2.35.

Figure 5.- Continued.

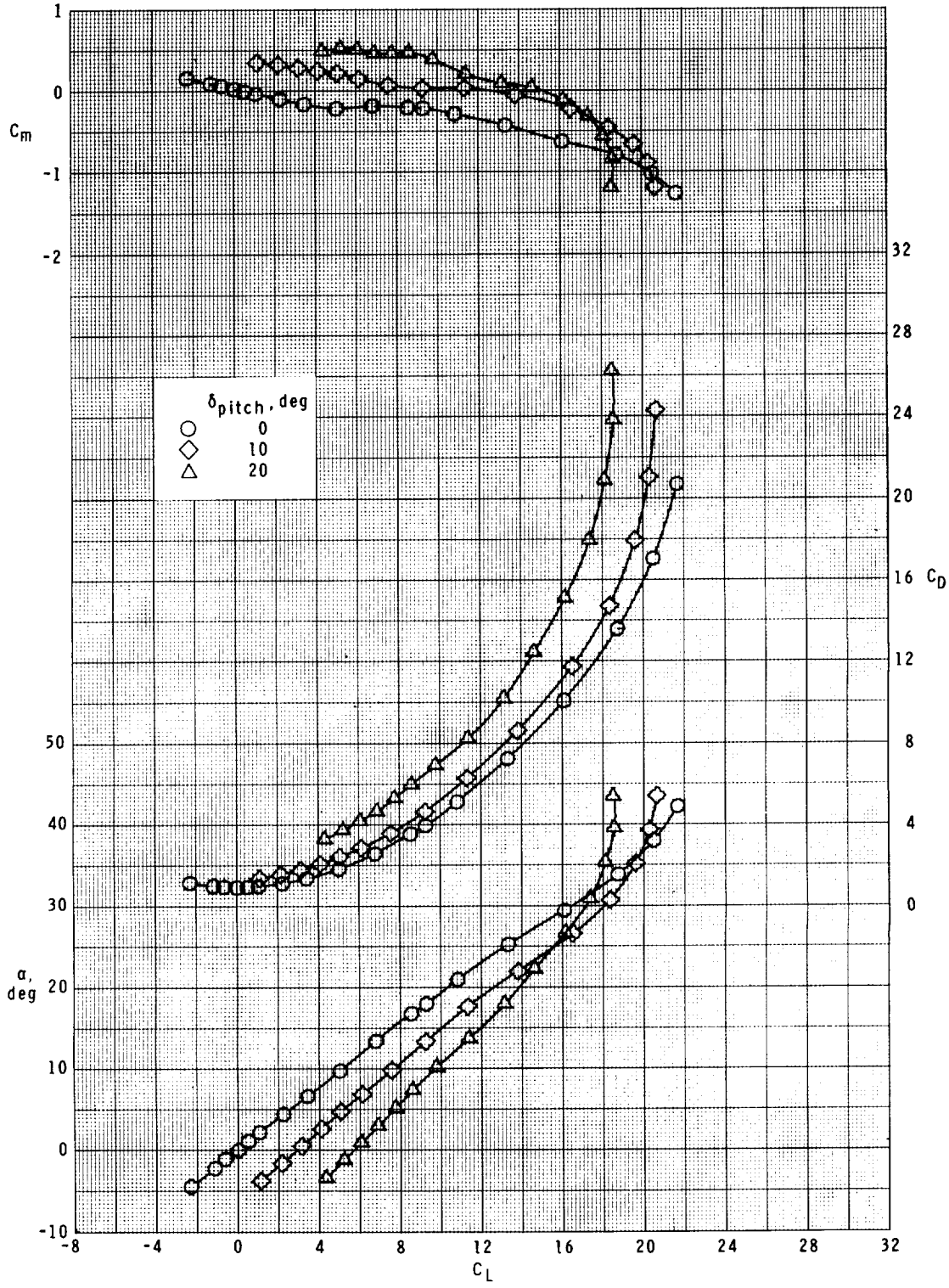

(c) Concluded.

Figure 5.- Continued.

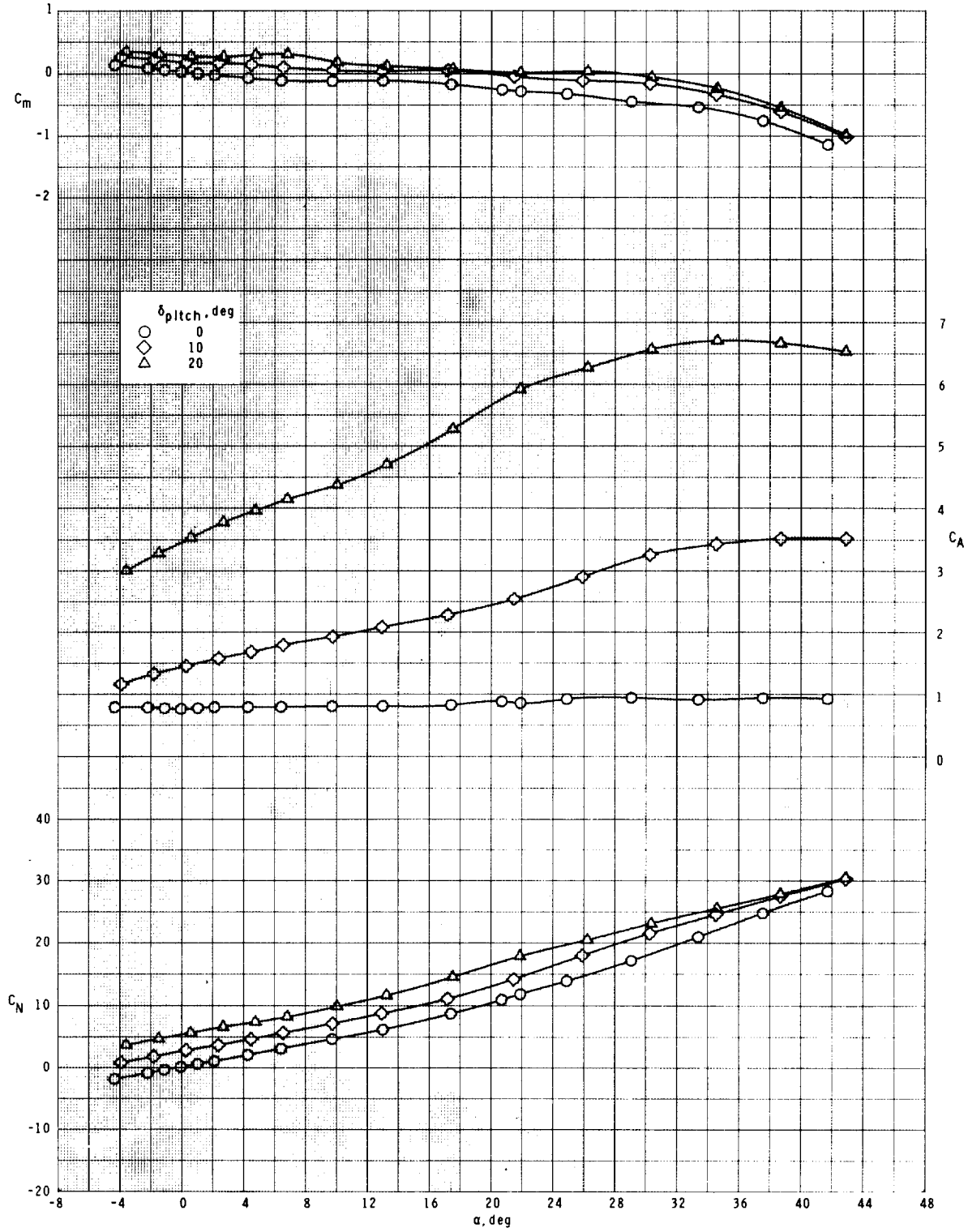

(d) M = 2.87.

Figure 5.- Continued.

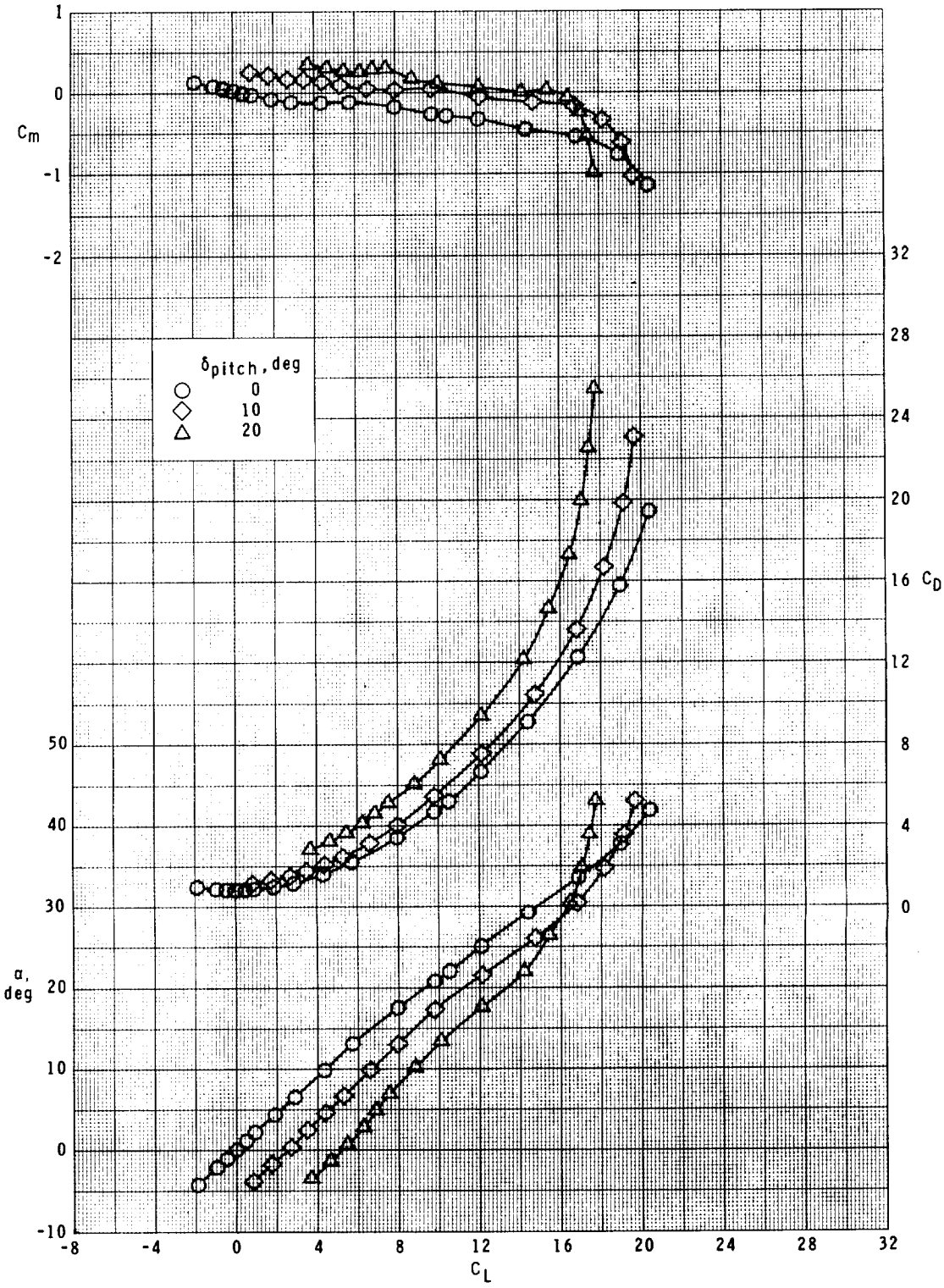

(d) Concluded.

Figure 5.- Continued.

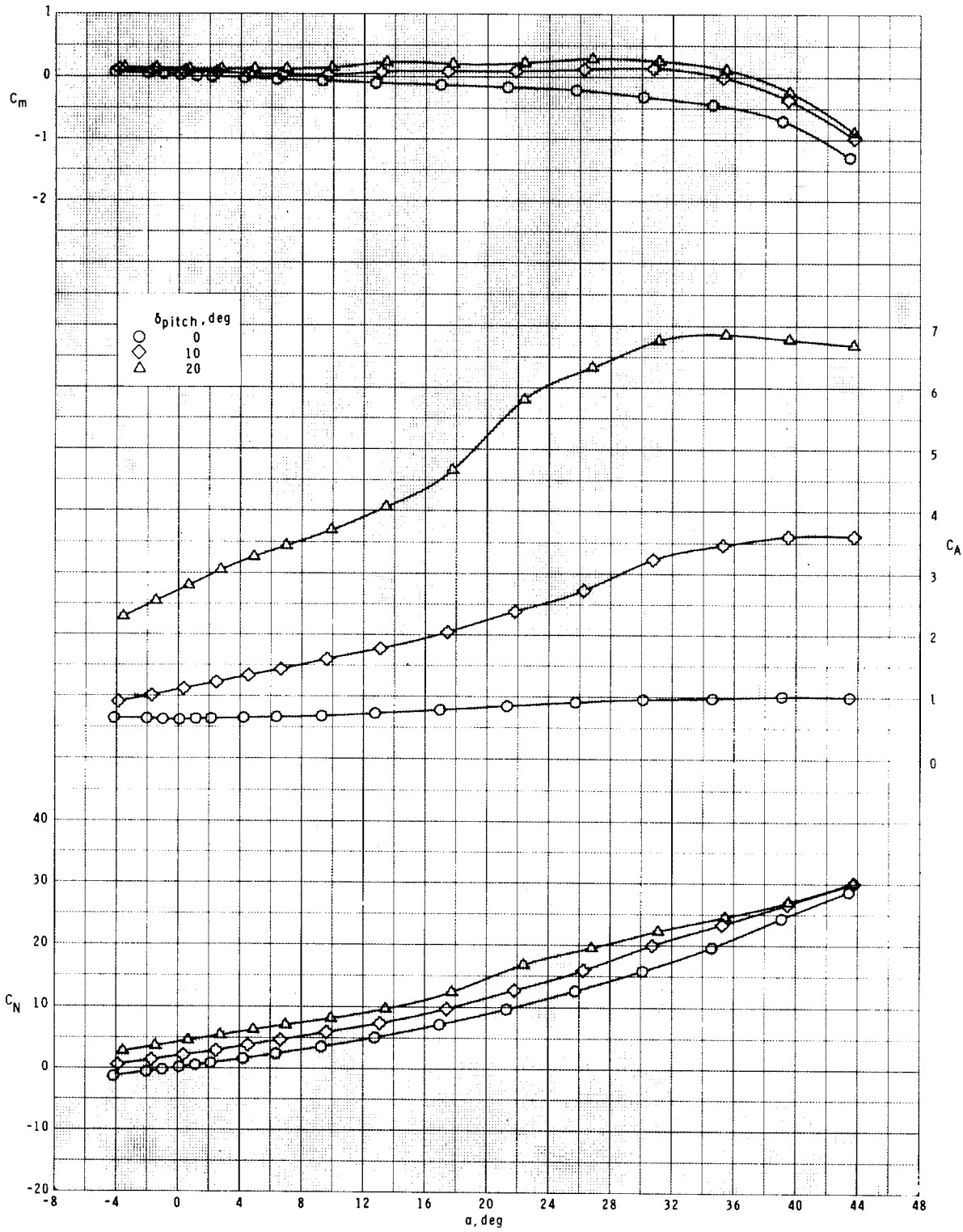

(e) M = 3.95.

Figure 5.- Continued.

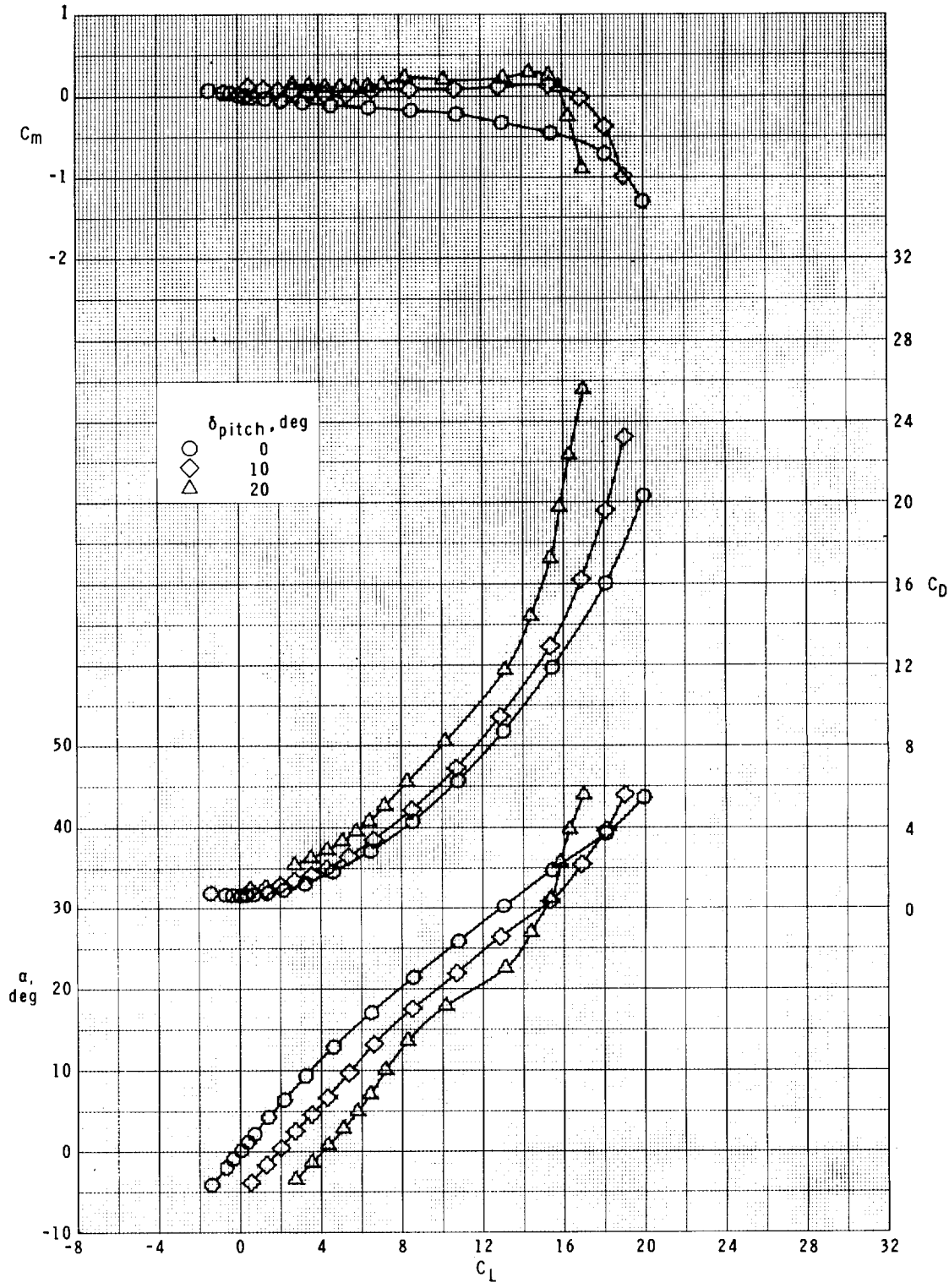

(e) Concluded.

Figure 5.- Continued.

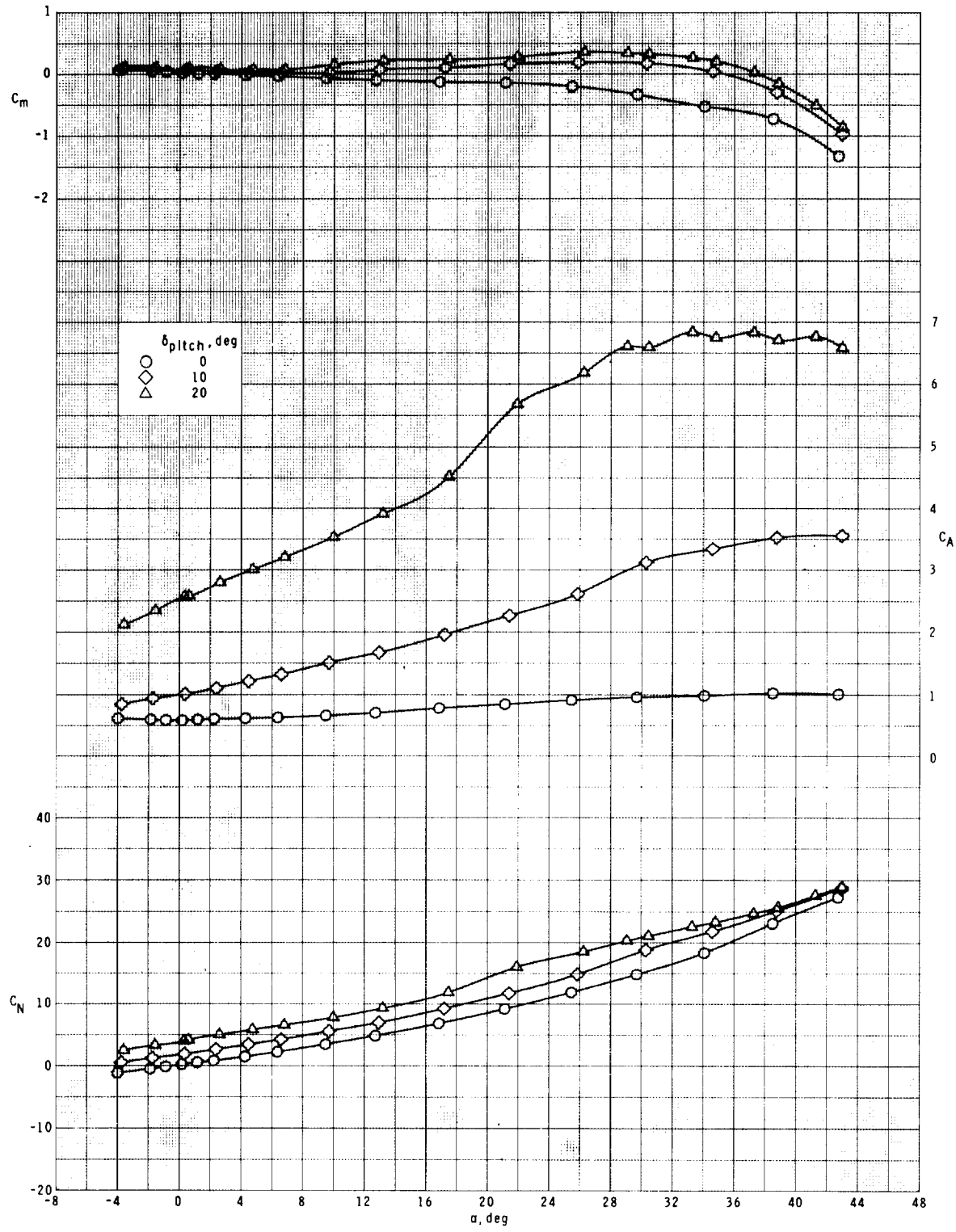

(f) M = 4.60.

Figure 5.- Continued.

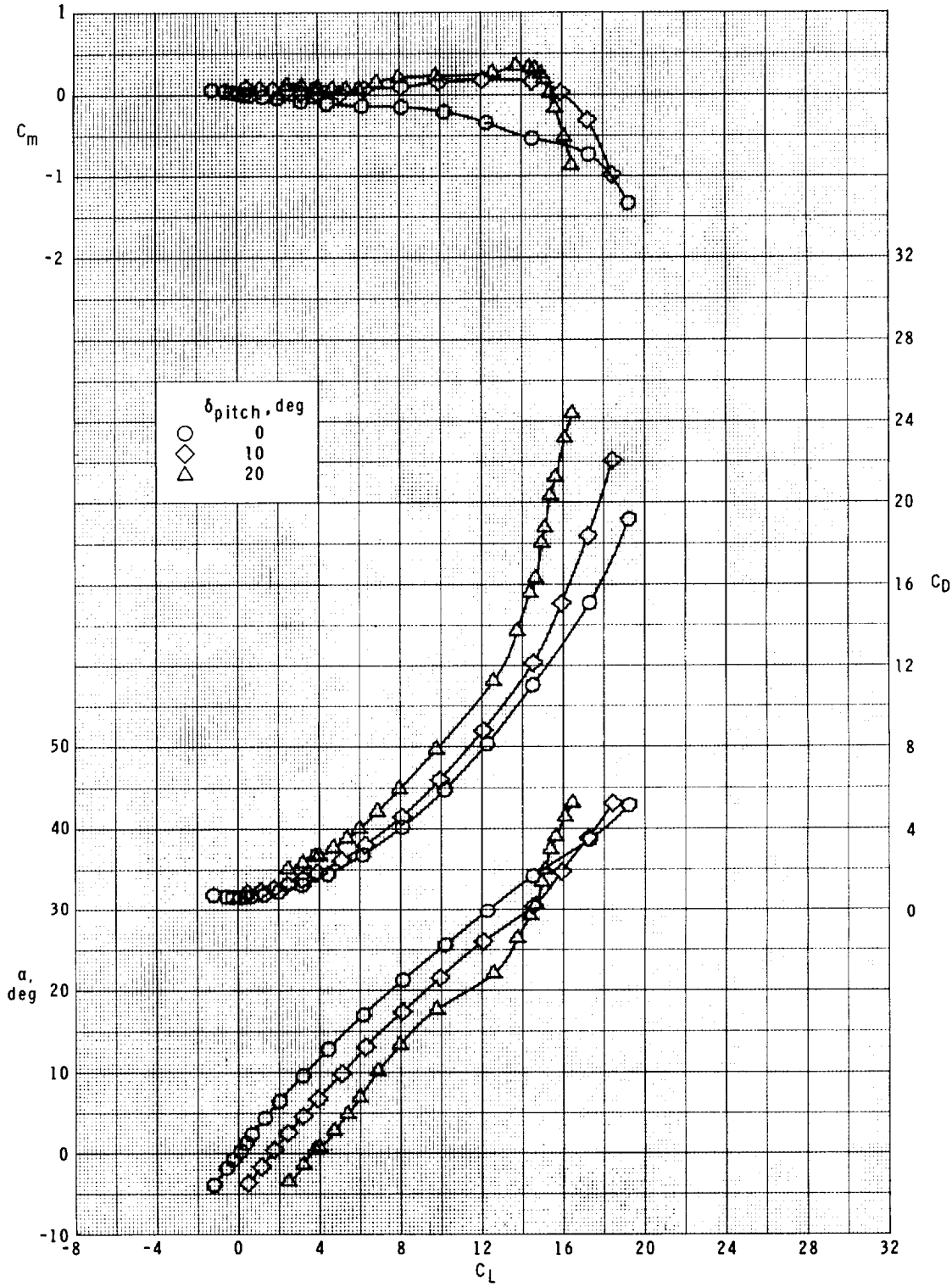

(f) Concluded.

Figure 5.- Concluded.

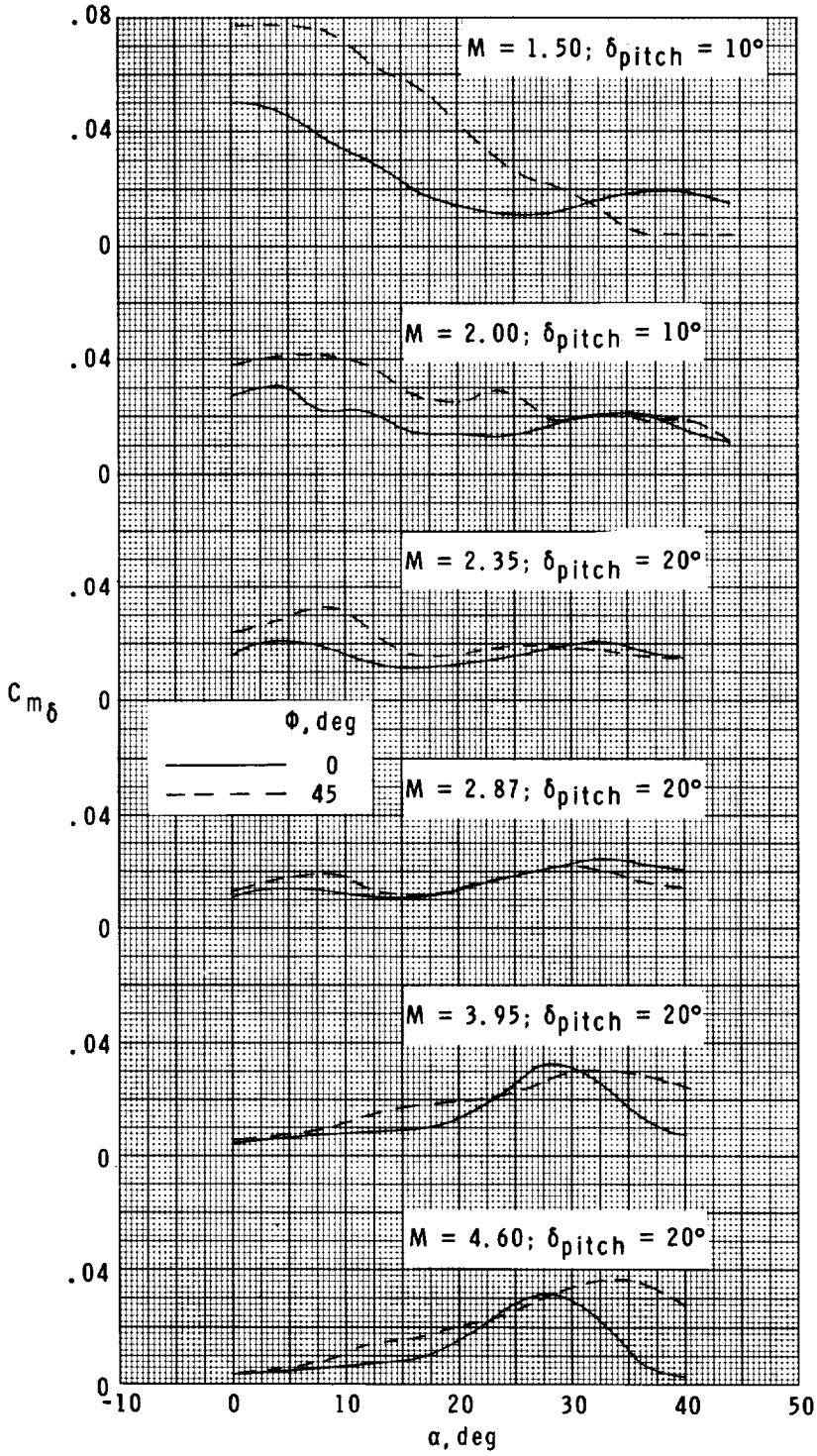

Figure 6.- Comparison of wing pitch-control effectiveness at $\phi = 0^{\circ}$ and 45°. $\delta_{pitch} = 10^{\circ}$ or 20°.

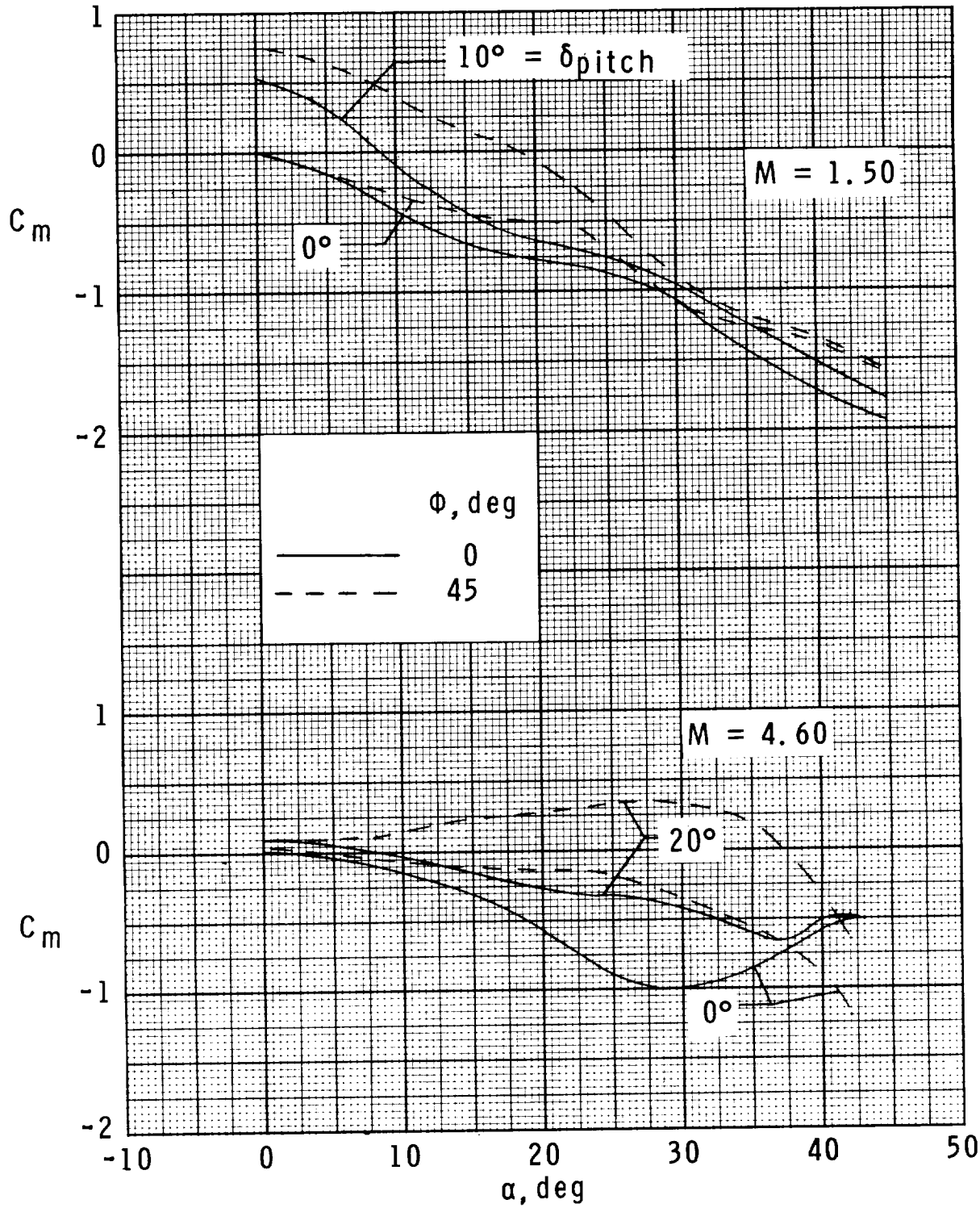

Figure 7.- Comparison of wing pitch-control characteristics at $\phi = 0^{\circ}$ and 45°. M = 1.50 and 4.60.

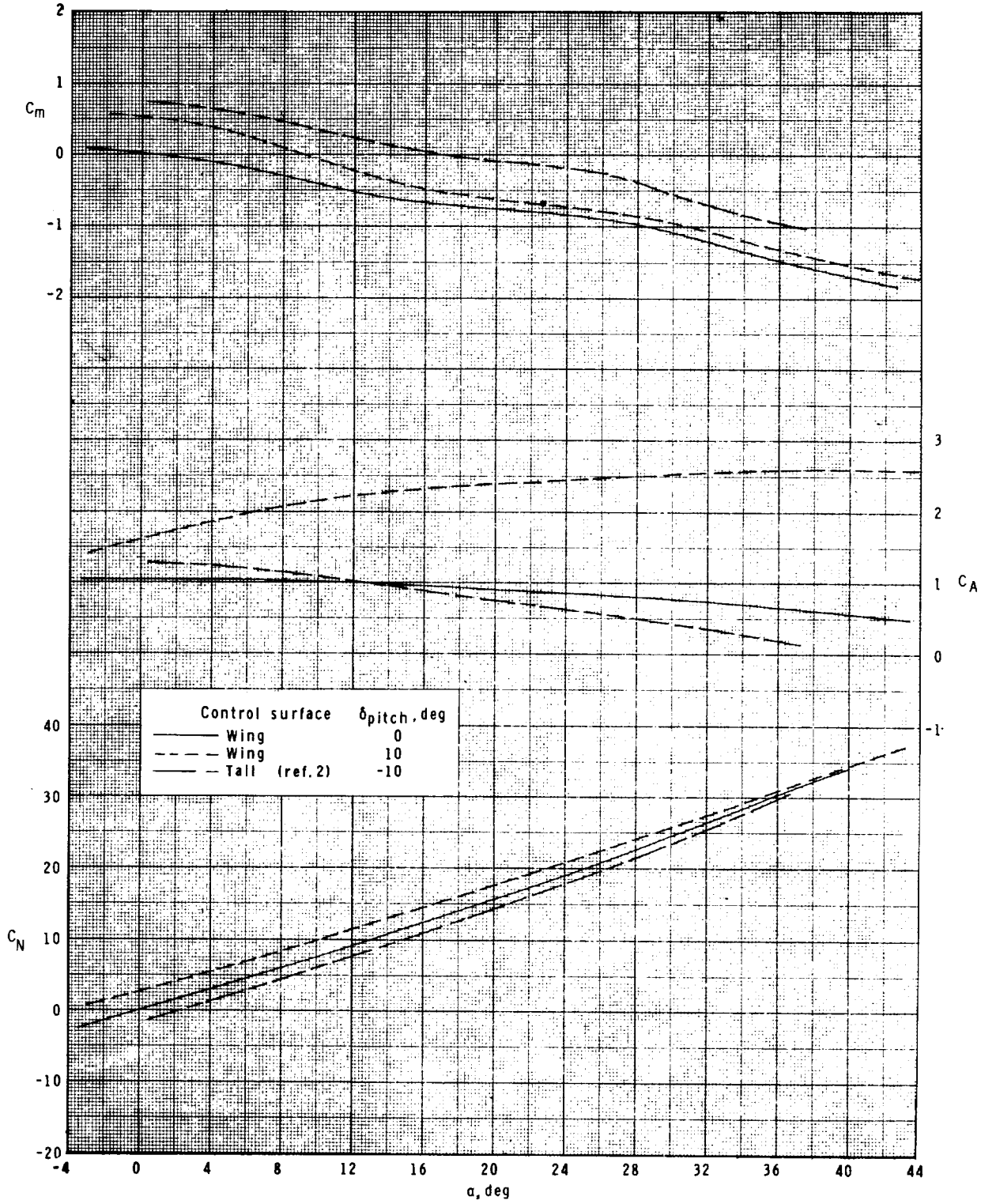

Figure 8.- Comparison of pitch-control characteristics of wing- and tail-control configurations. $\phi = 0^\circ$ and 45°.

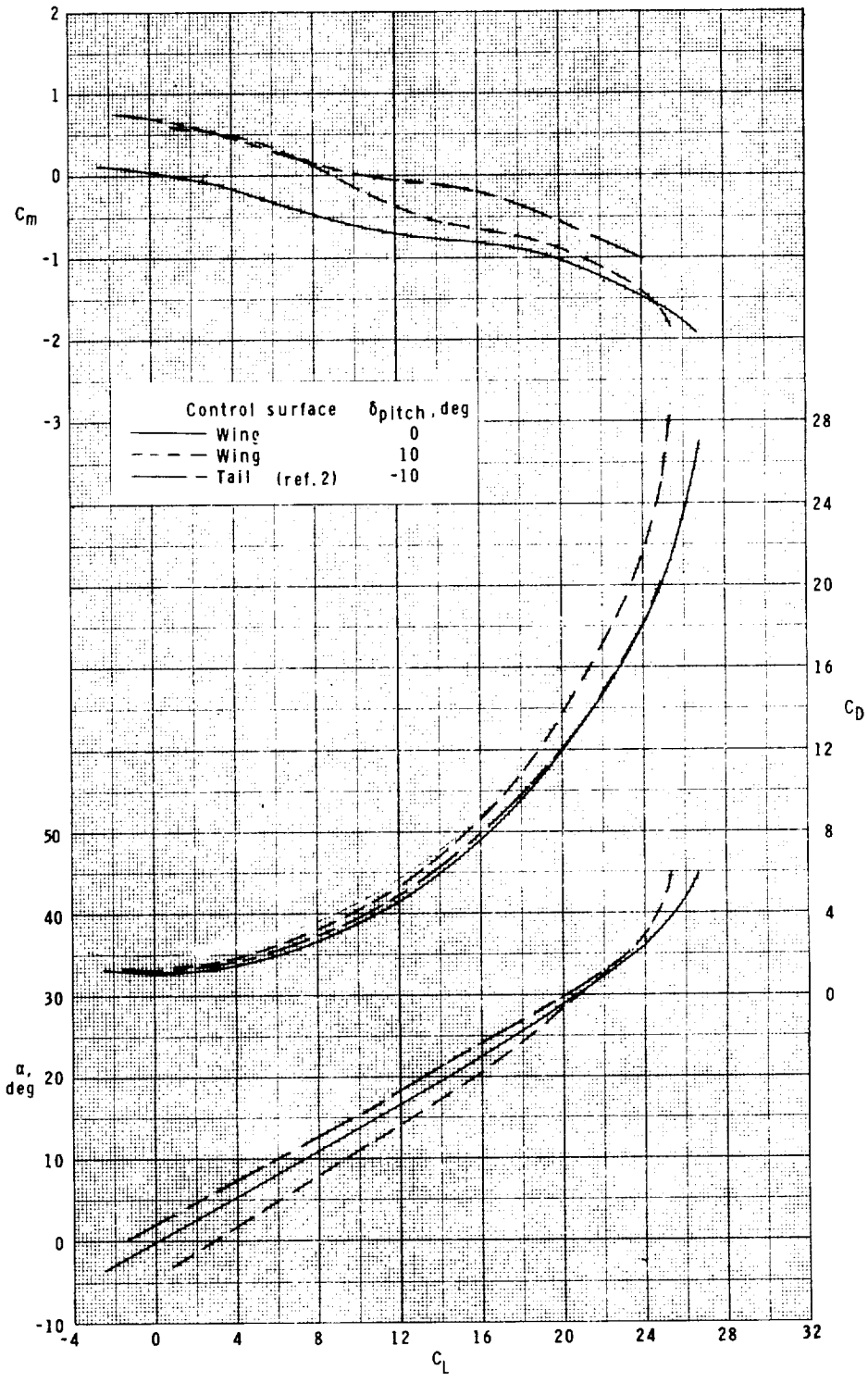

(a) Concluded.

Figure 8.- Continued.

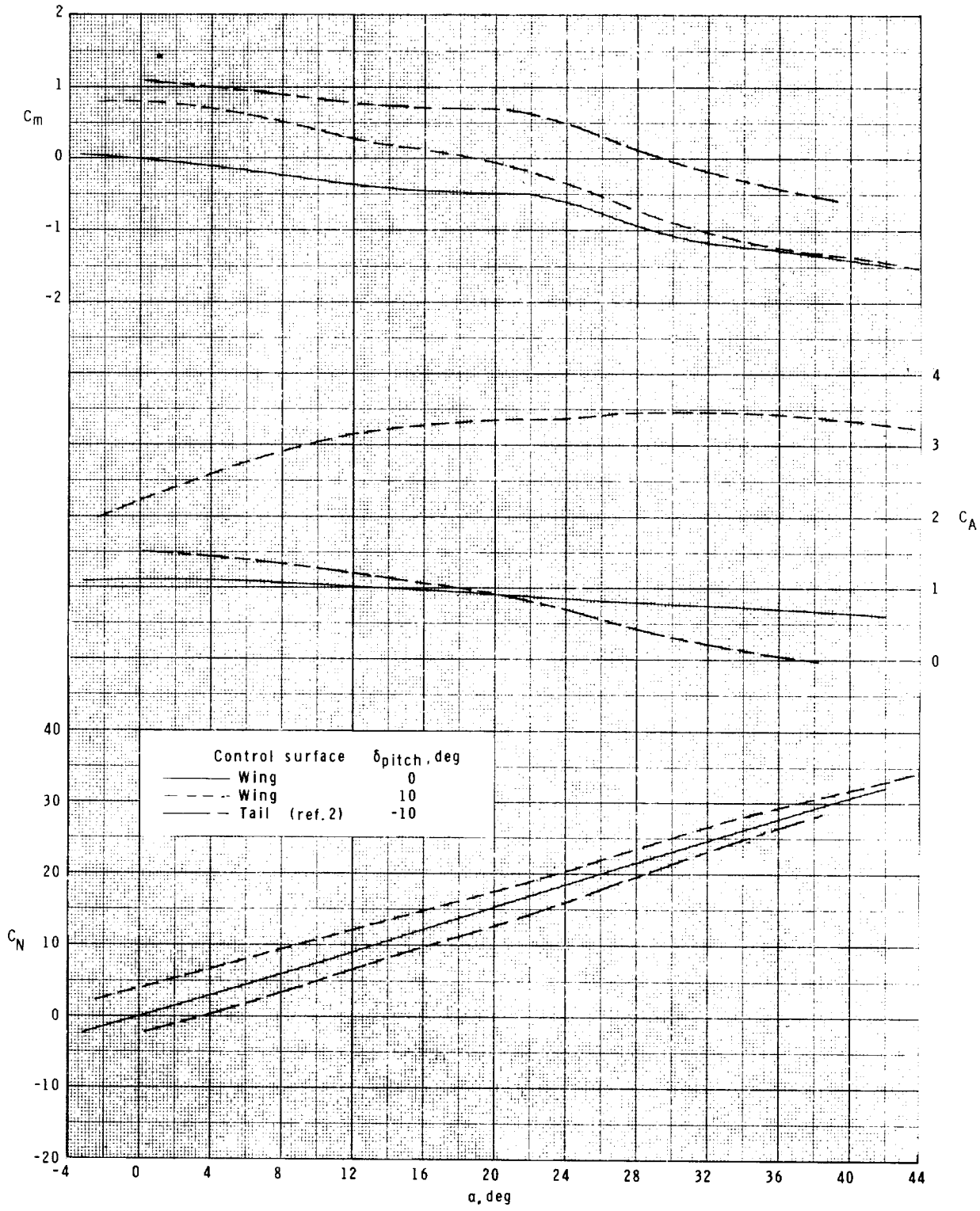

(b) M = 1.50; $\phi = 45^{\circ}$.

Figure 8.- Continued.

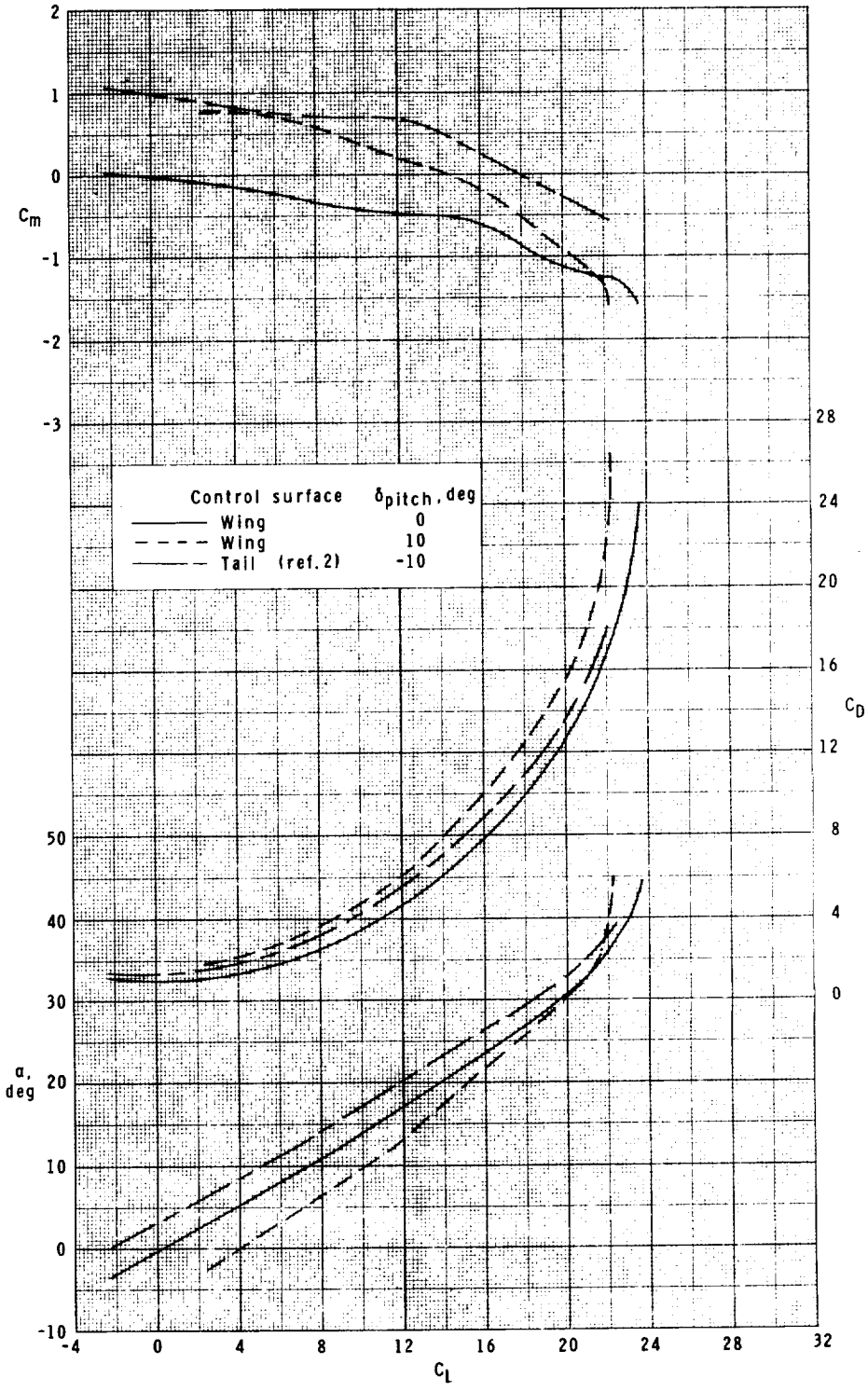

(b) Concluded.

Figure 8.- Continued.

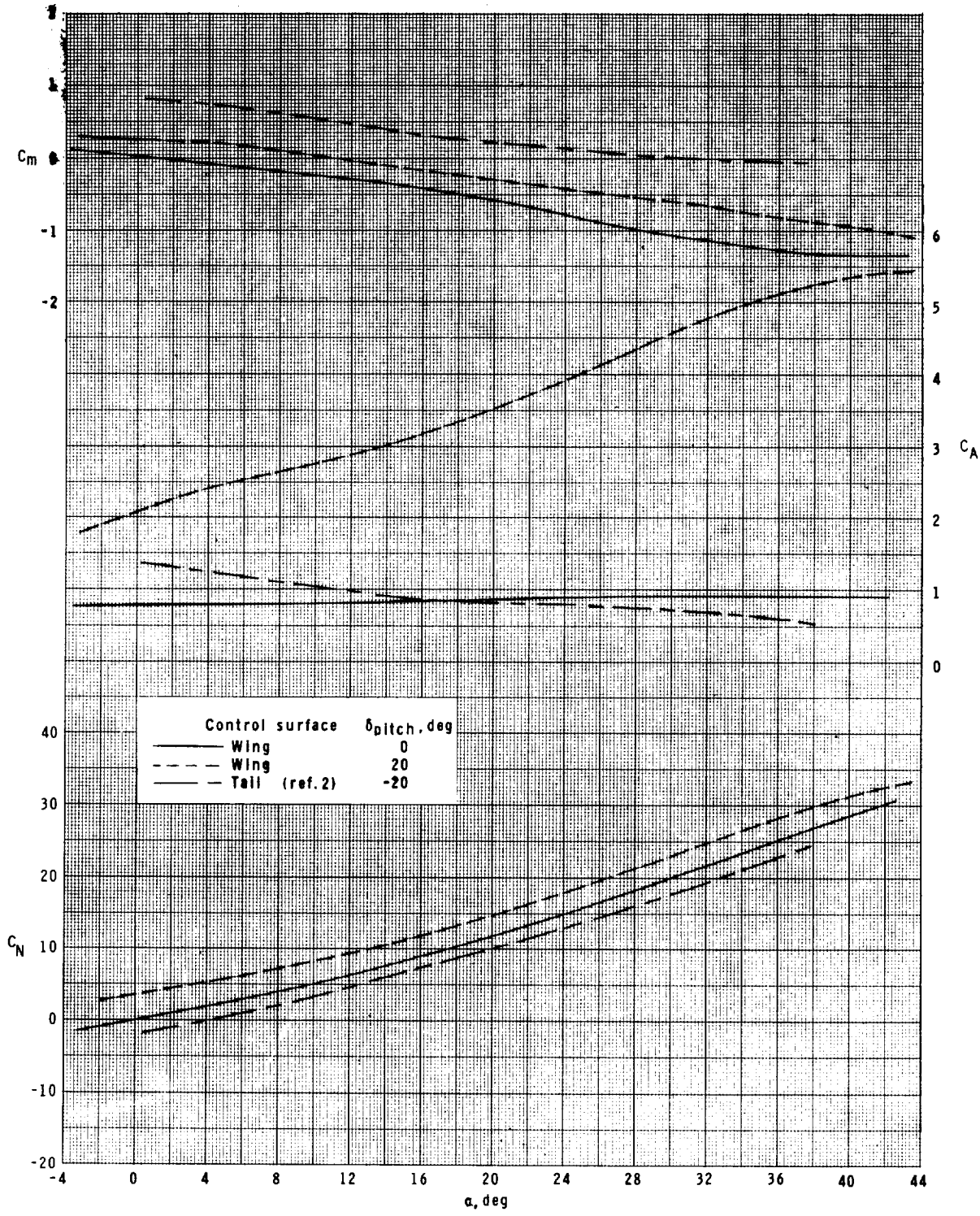

(c) M = 2.87; $\phi = 0^{\circ}$.

Figure 8.- Continued.

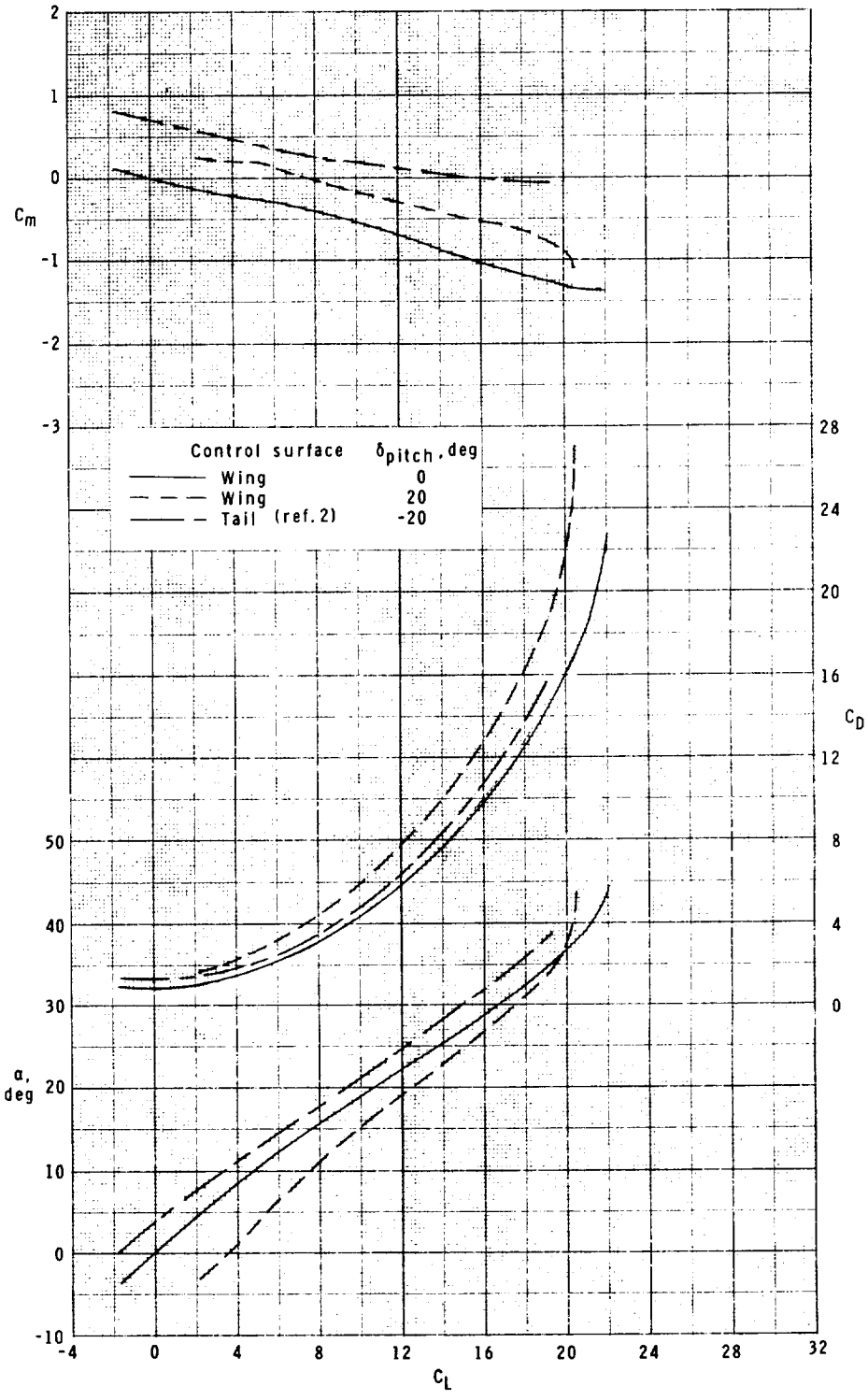

(c) Concluded.

Figure 8.- Continued.

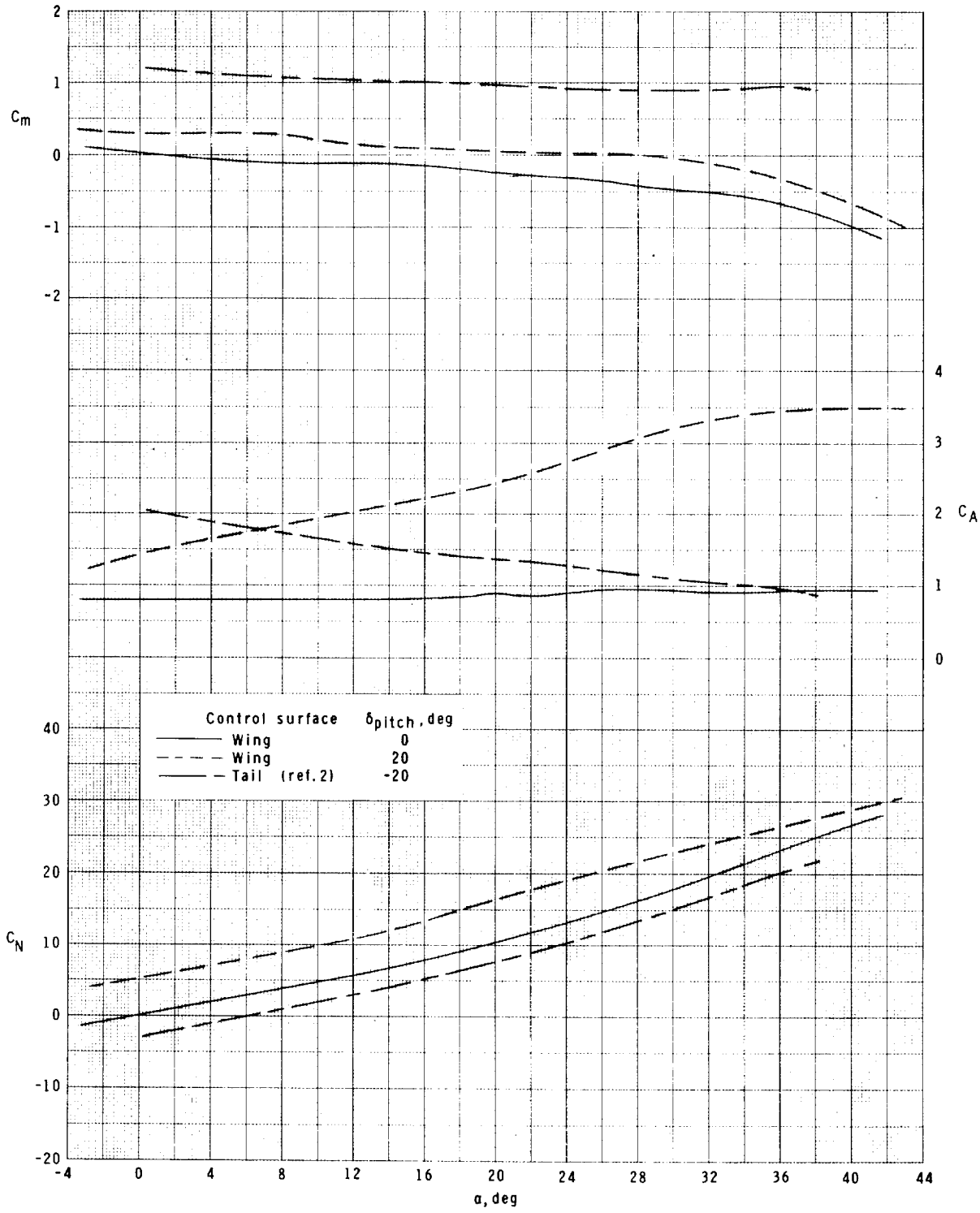

(d) M = 2.87; ϕ = 45°.

Figure 8.- Continued.

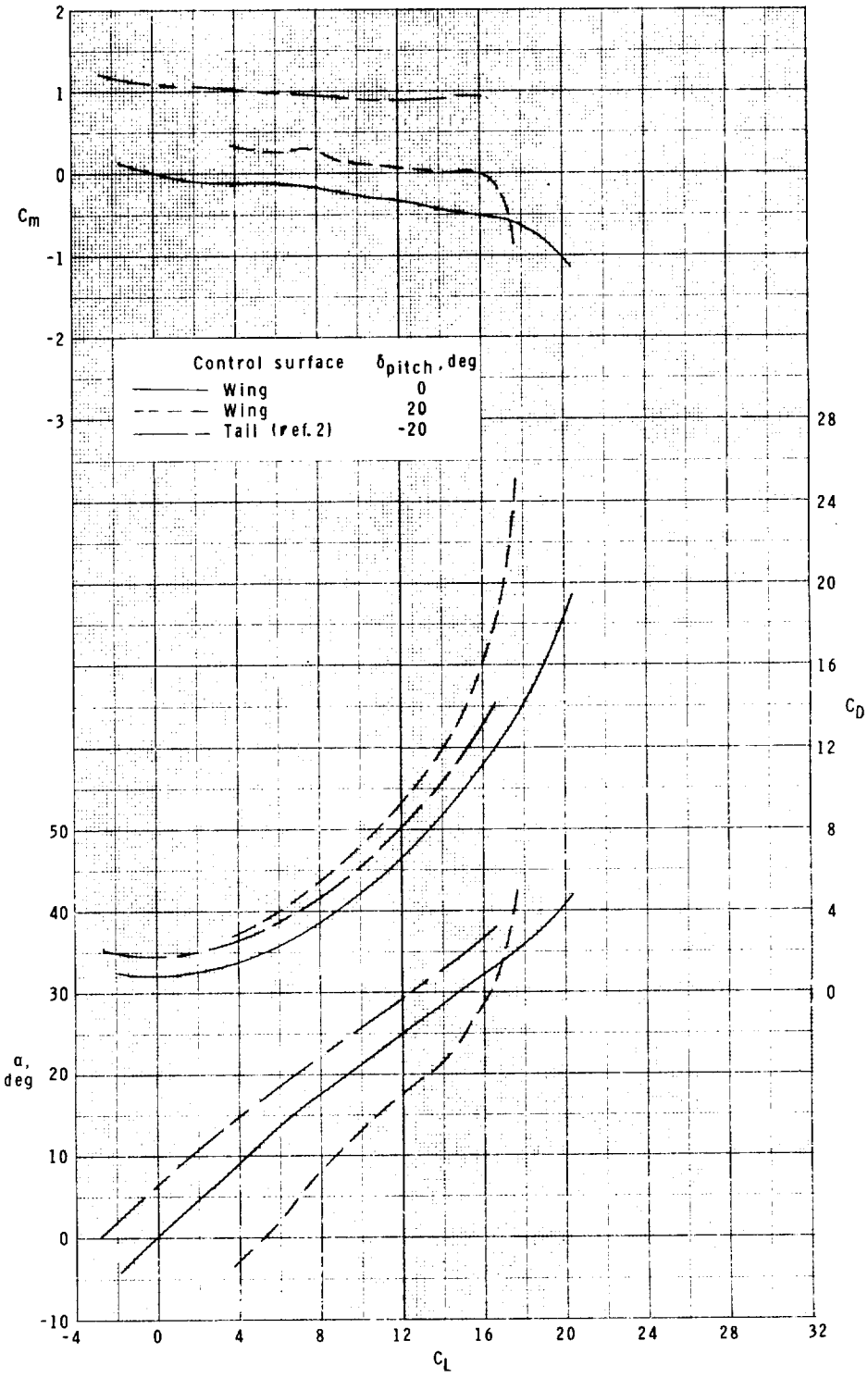

(d) Concluded.

Figure 8.- Continued.

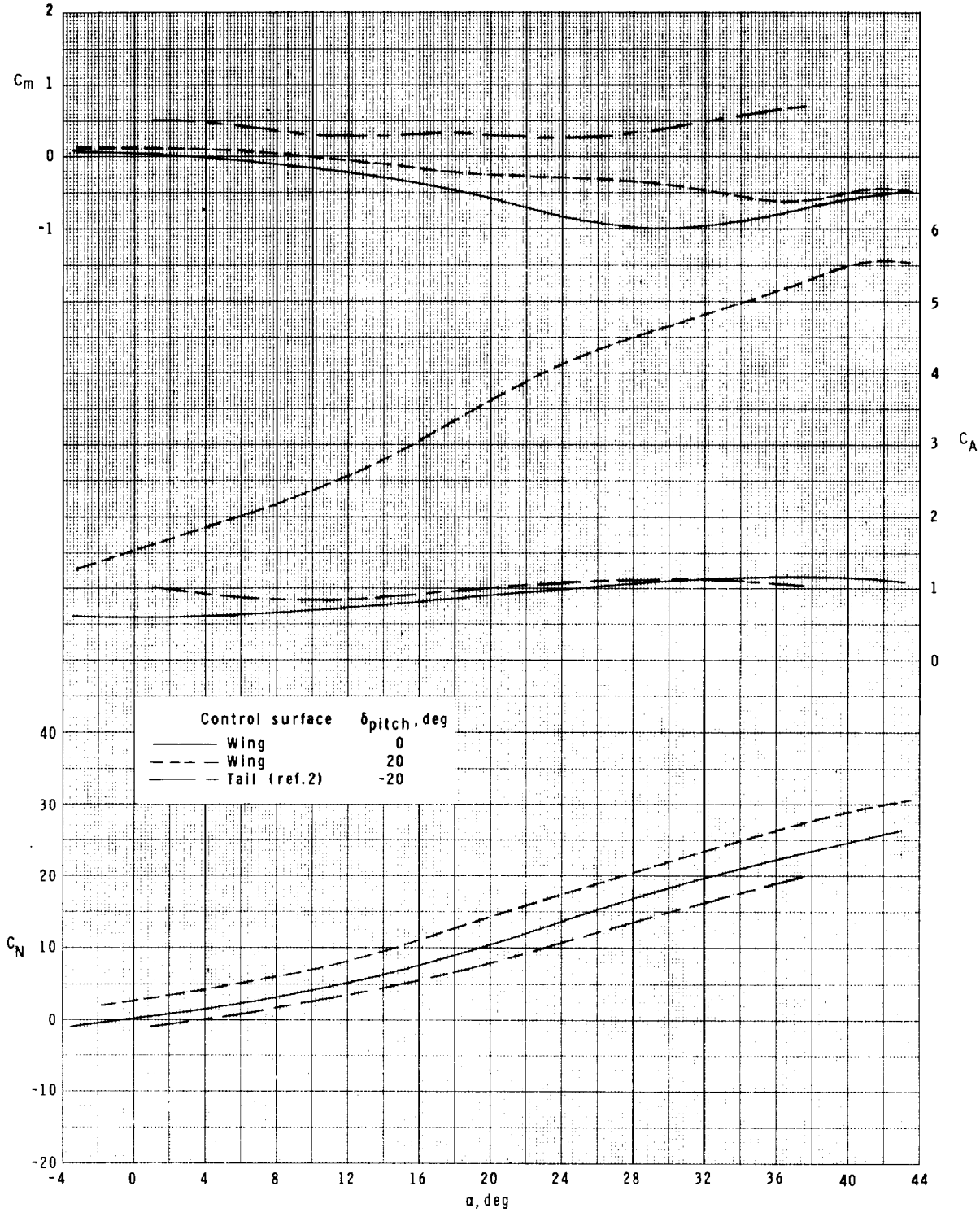

(e) M = 4.60; $\phi = 0^{o}$.

Figure 8.- Continued.

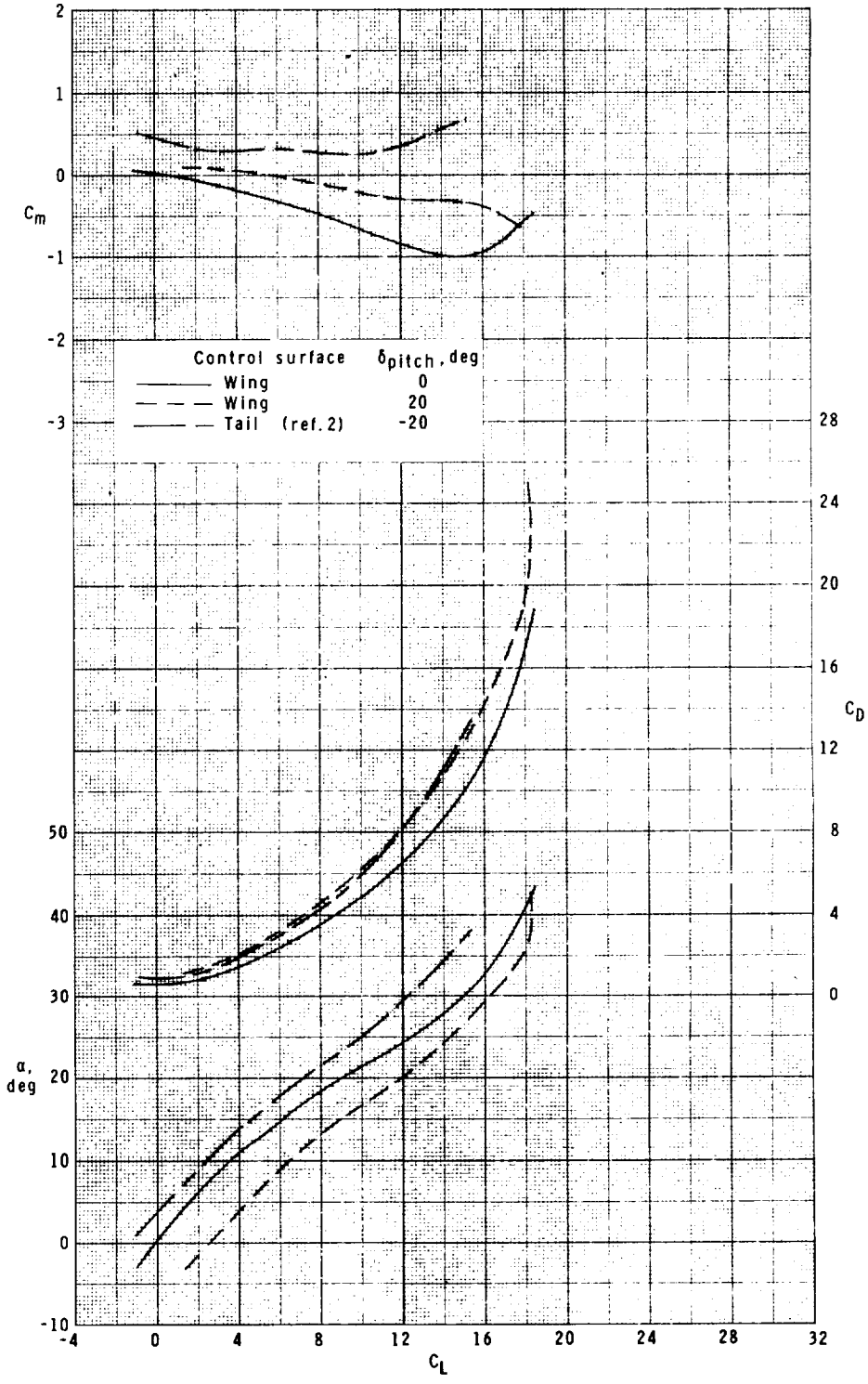

(e) Concluded.

Figure 8.- Continued.

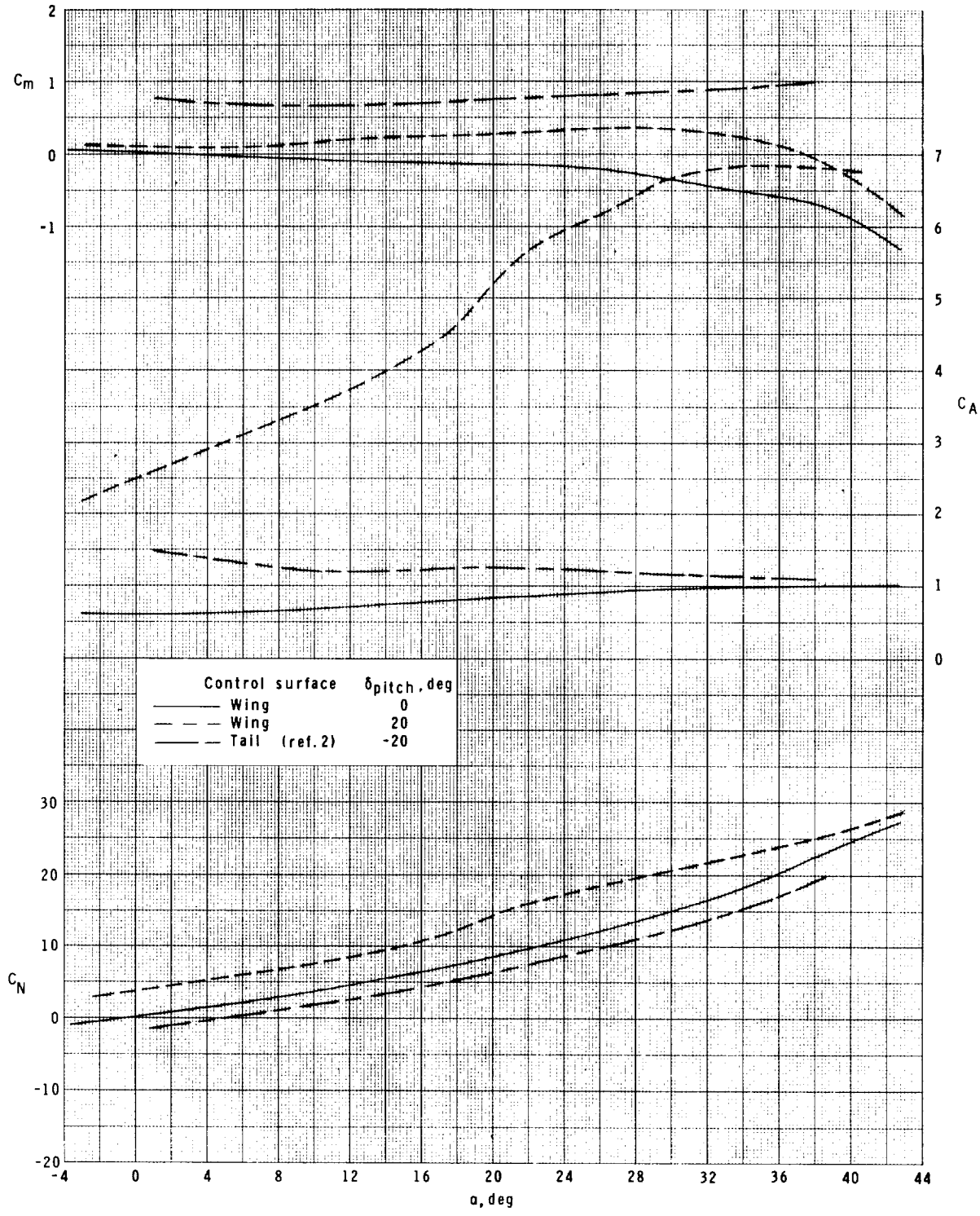

(f) M = 4.60; ϕ = 45°.

Figure 8.- Continued.

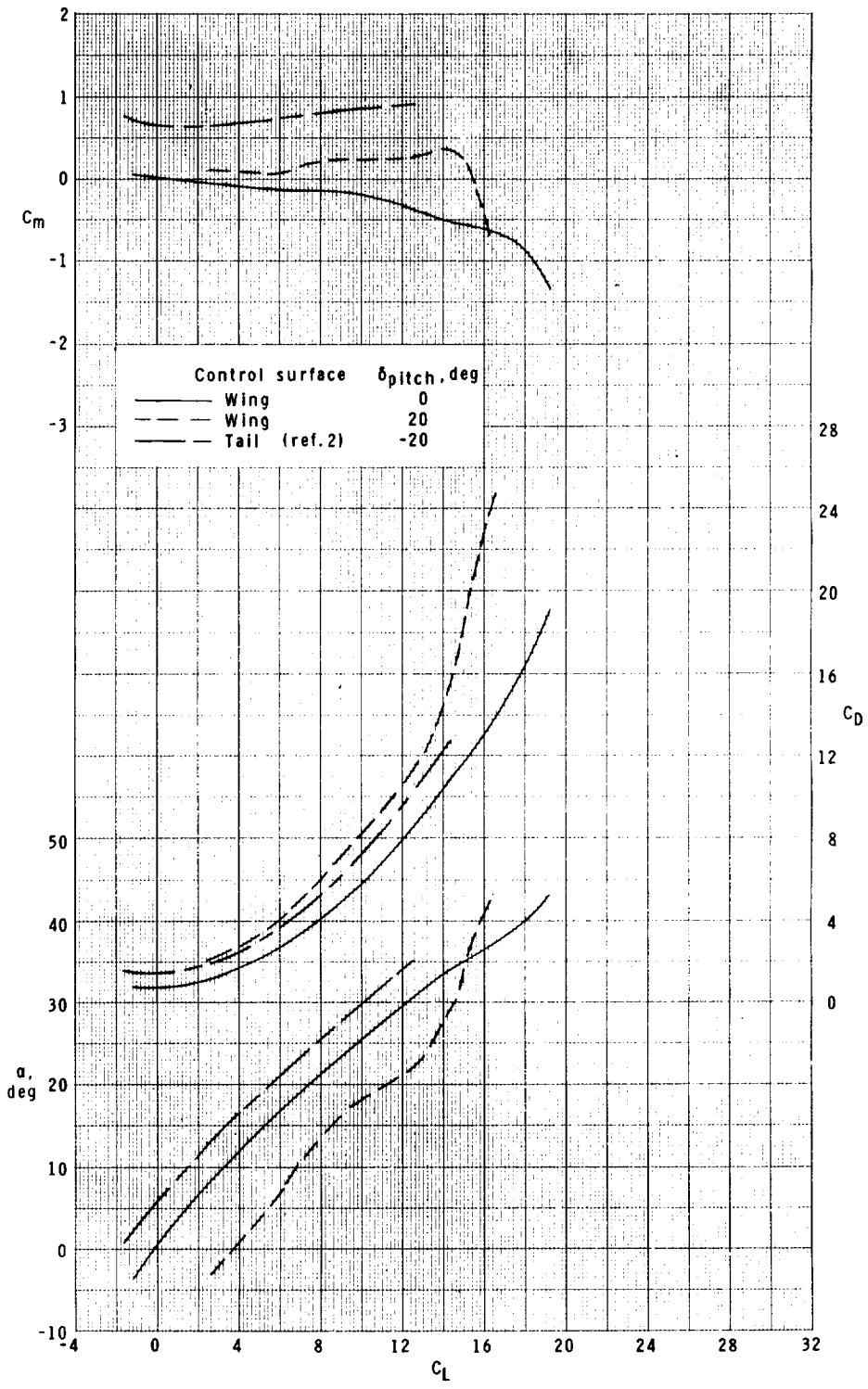

(f) Concluded.

Figure 8.- Concluded.

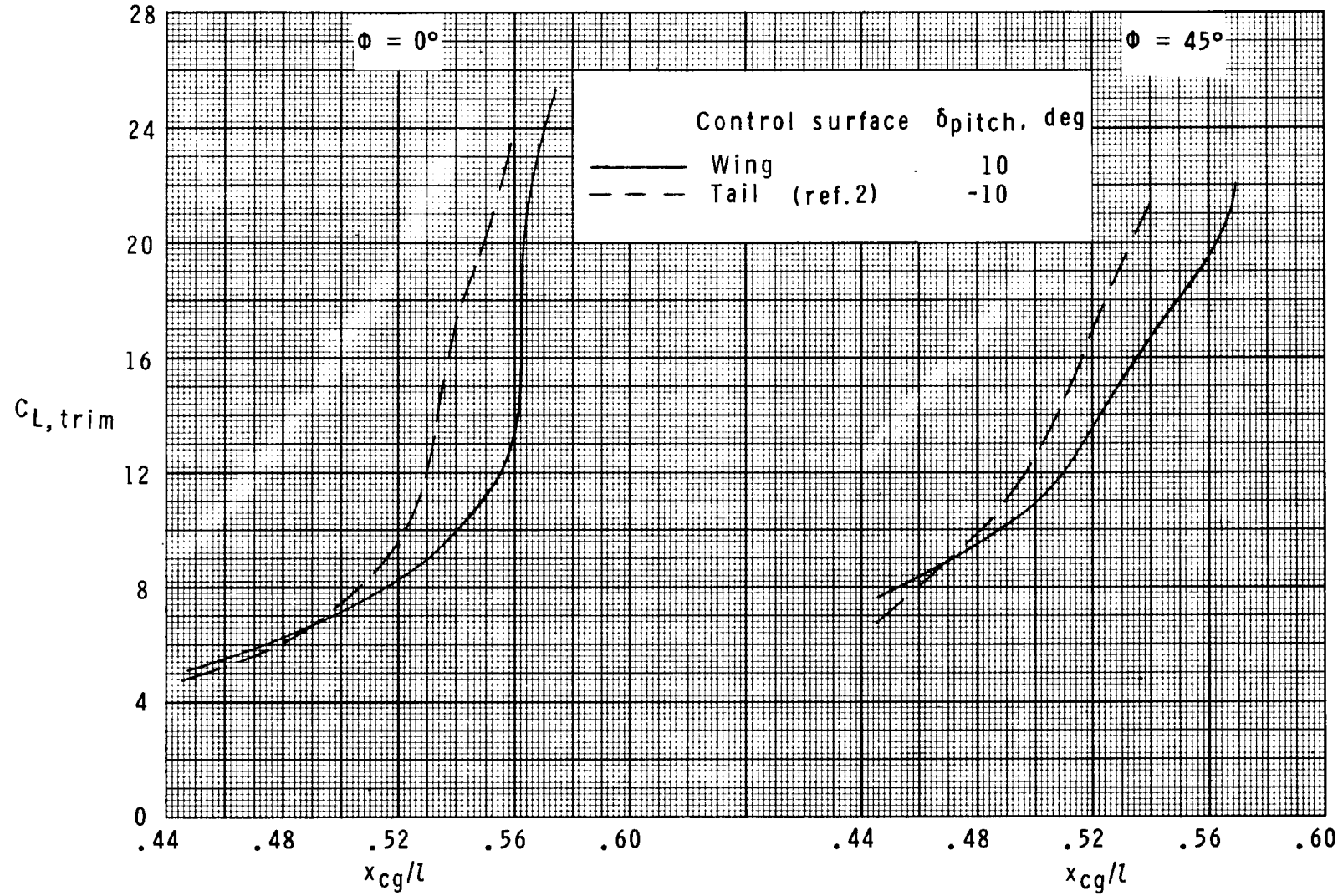

(a) M = 1.50.

Figure 9.- Comparison of trimmed-lift characteristics for wing- and tail-control configurations. $\phi = 0^{o}$ and 45^{o}.

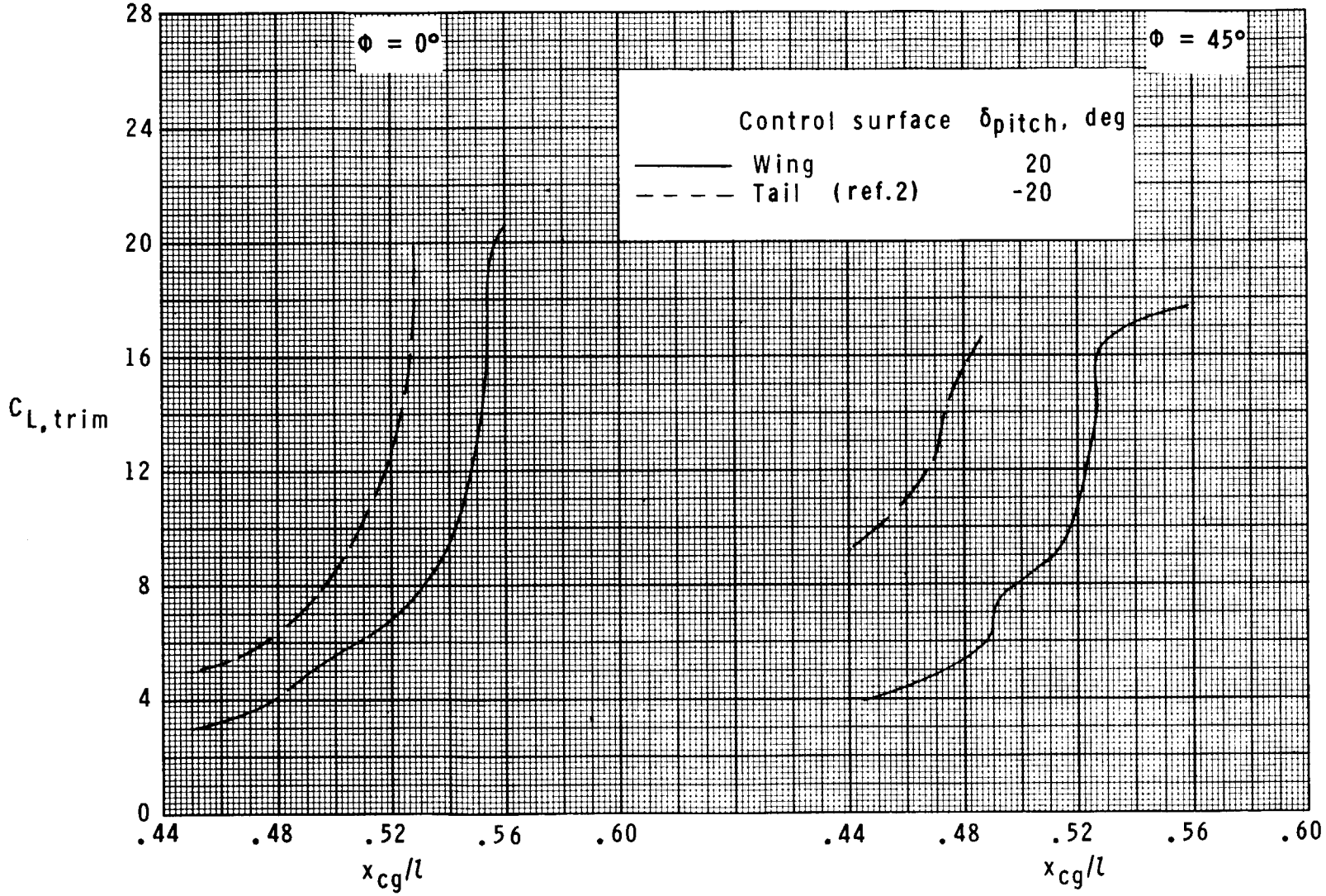

(b) M = 2.87.

Figure 9.- Continued.

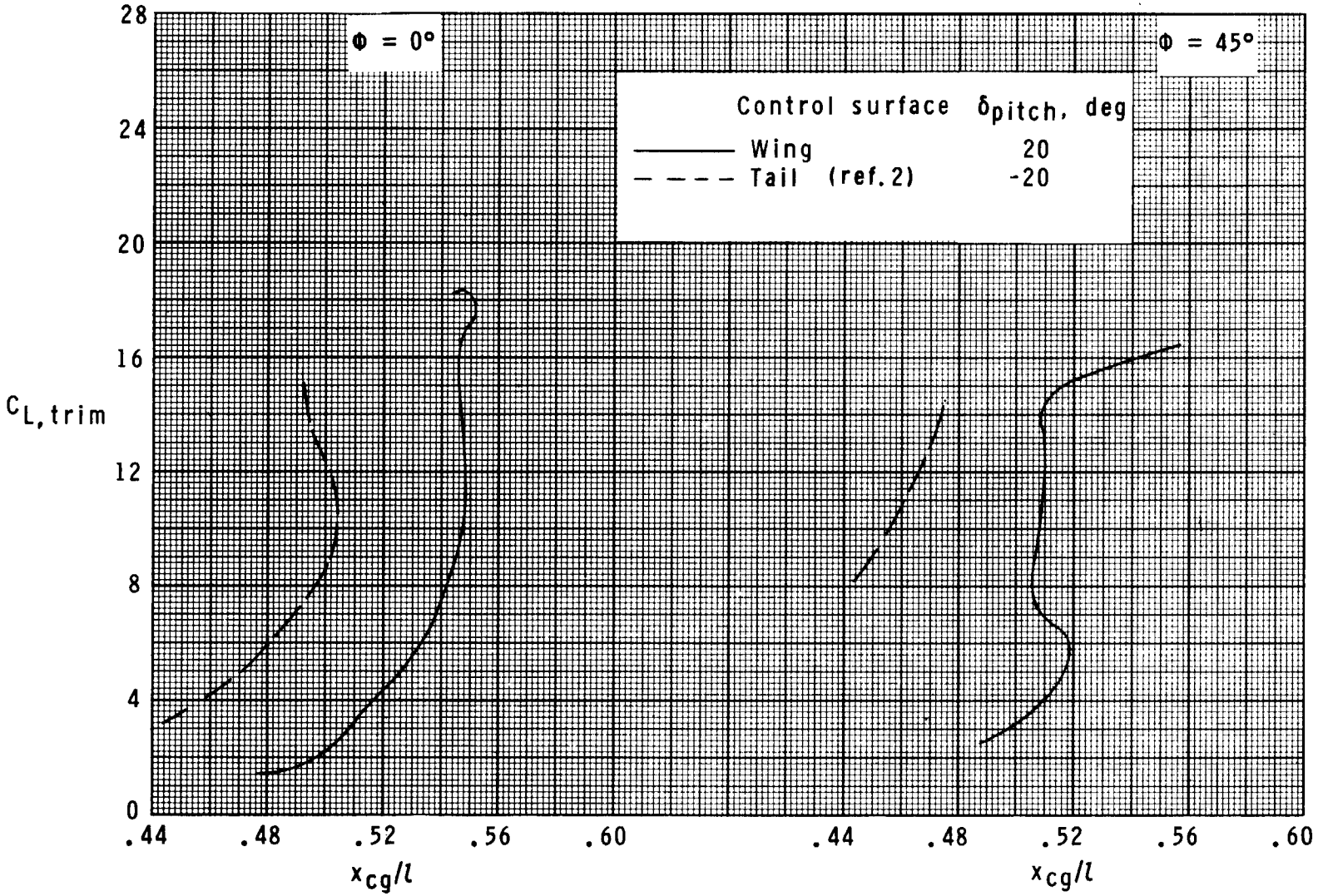

(c) M = 4.60.

Figure 9.- Concluded.

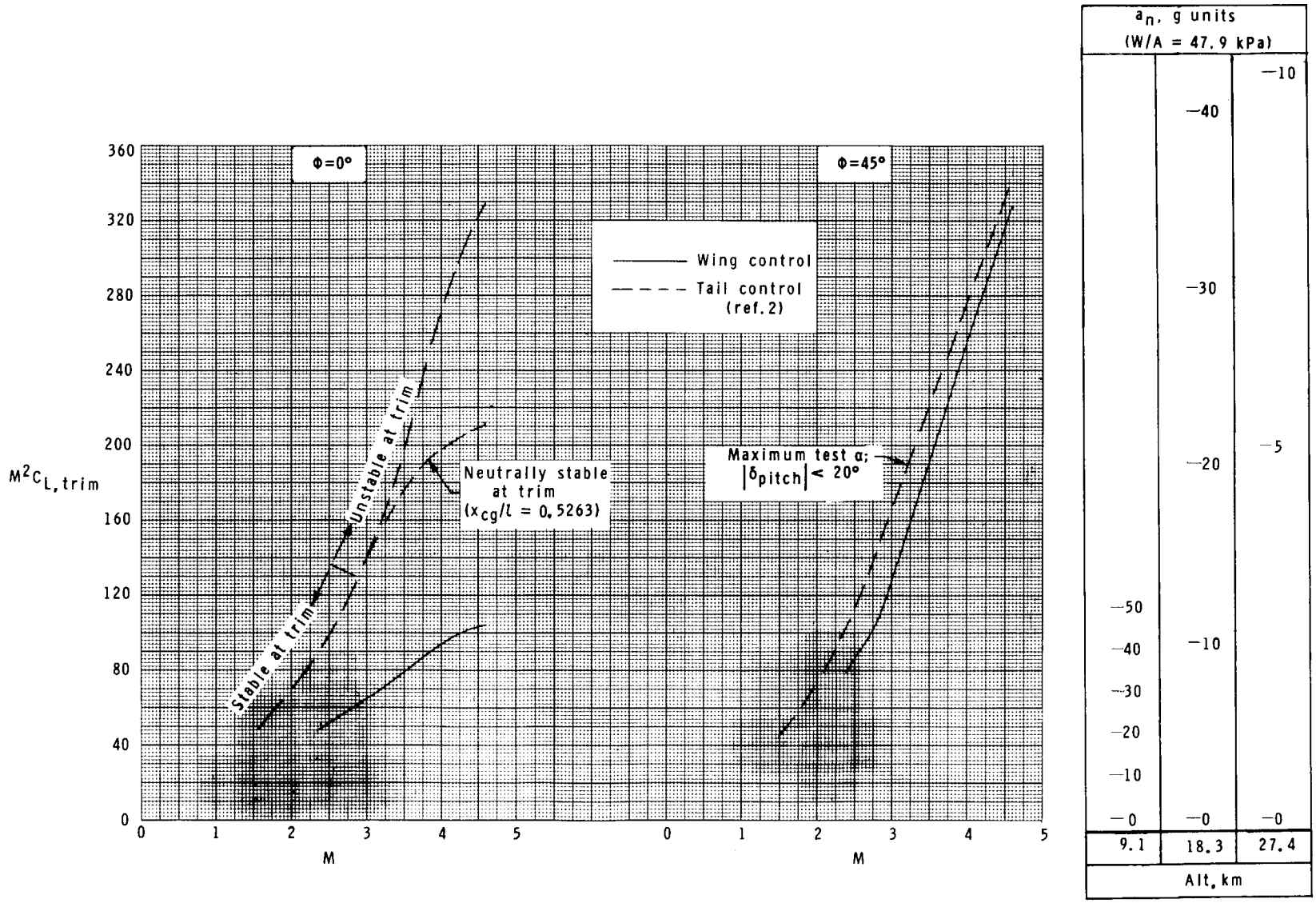

Figure 10.- Comparison of normal-acceleration capability of wing- and tail-control configurations for $|\delta_{pitch}| = 20°$. $\phi = 0°$ and 45°.

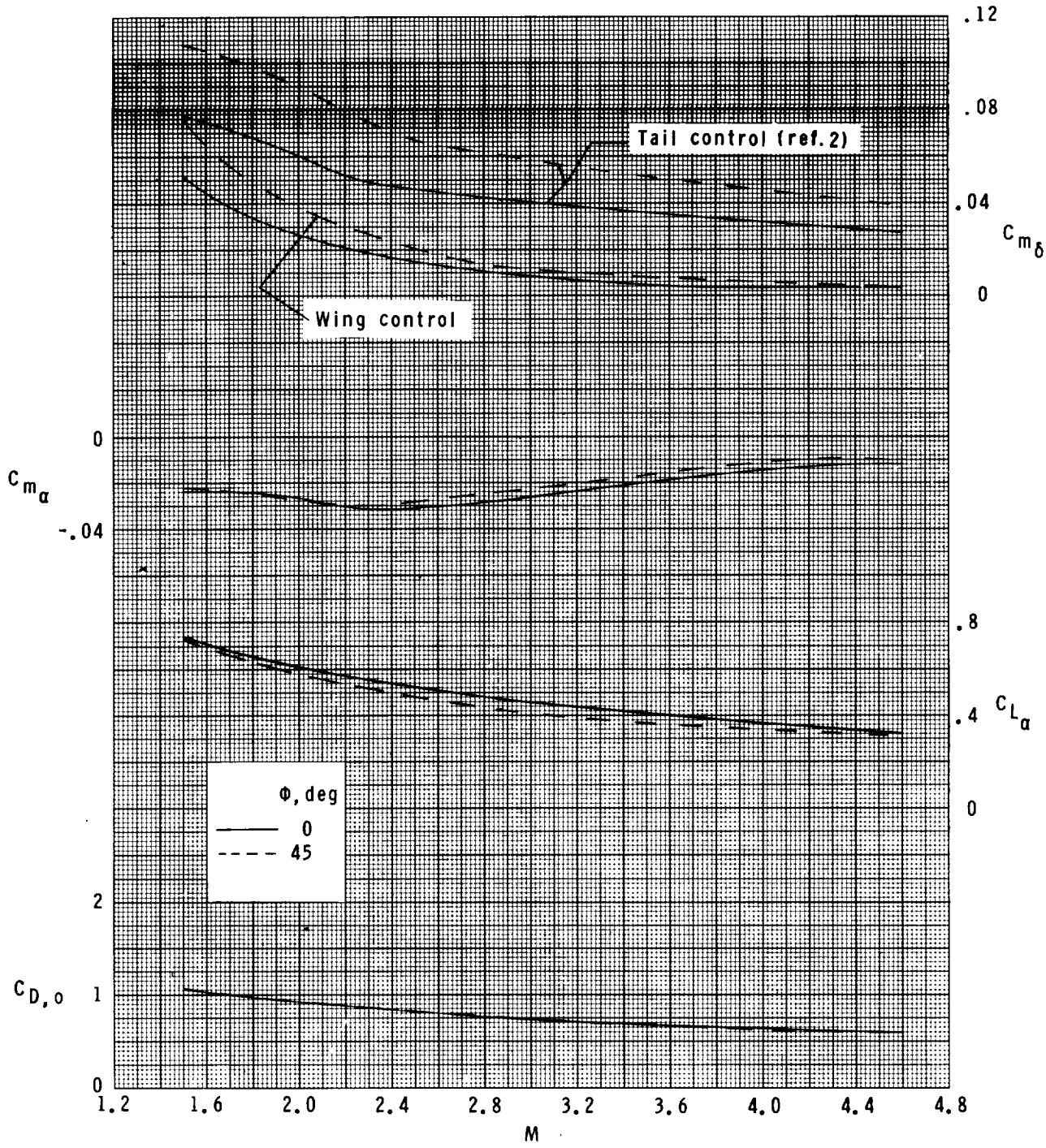

(a) C_{m_δ}, C_{m_α}, C_{L_α}, and $C_{D,o}$.

Figure 11.- Summary of longitudinal characteristics. $\phi = 0^o$ and 45^o.

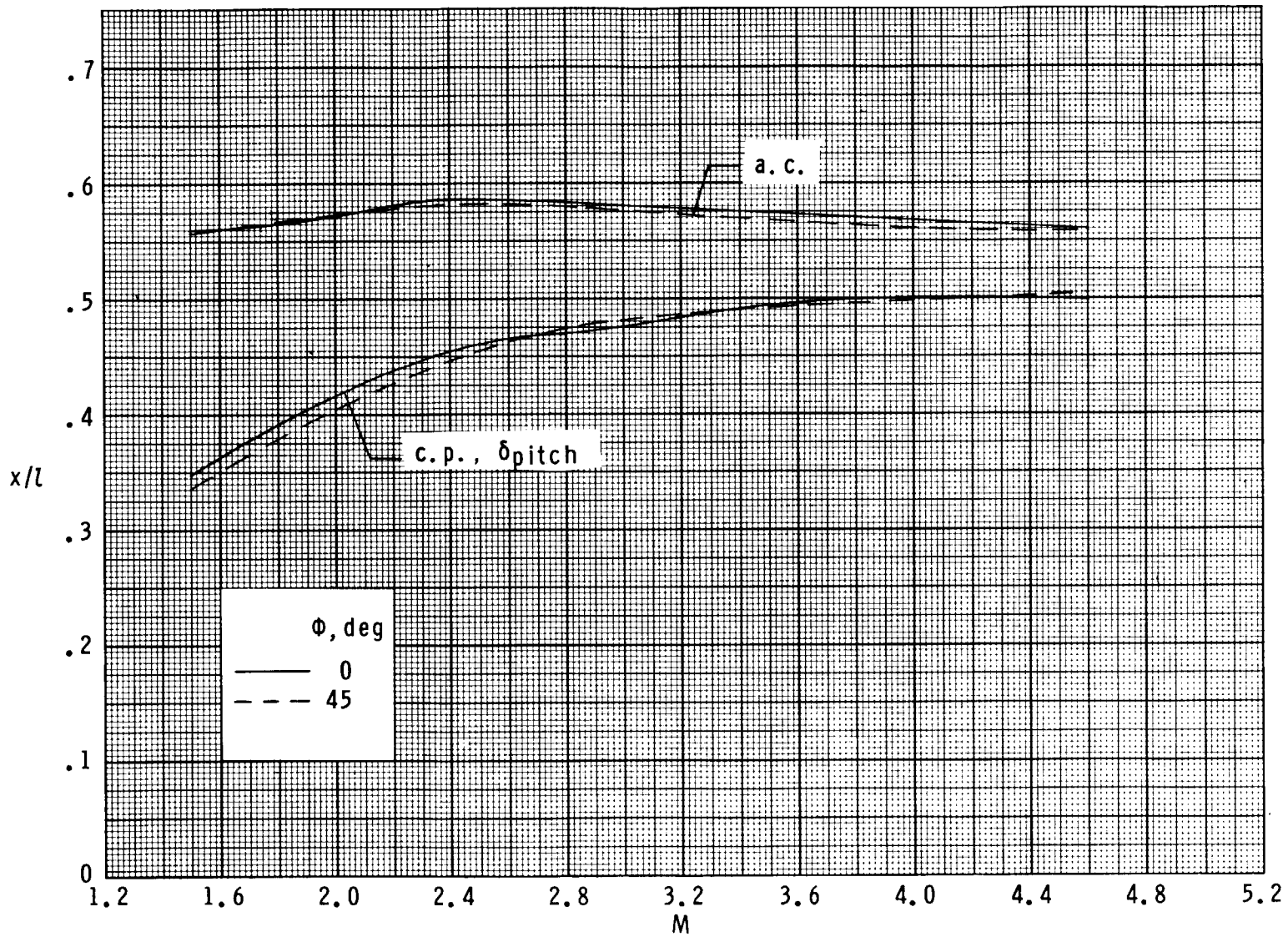

(b) x_{ac}/l and $(x_{cp}/l)_{\delta_{pitch}}$.

Figure 11.- Concluded.

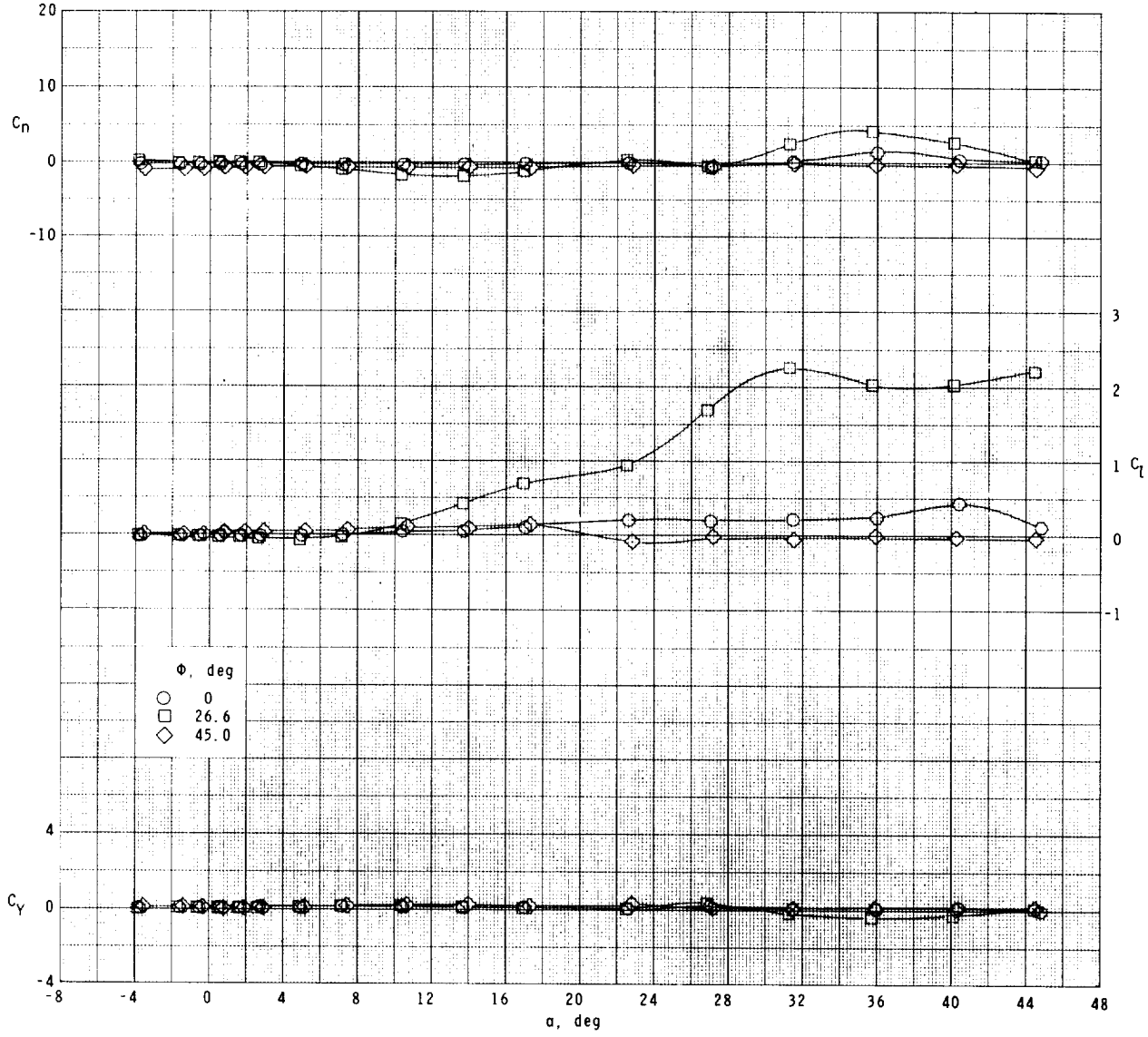

(a) M = 1.50.

Figure 12.- Effect of ϕ on lateral characteristics. $\delta = 0^{o}$.

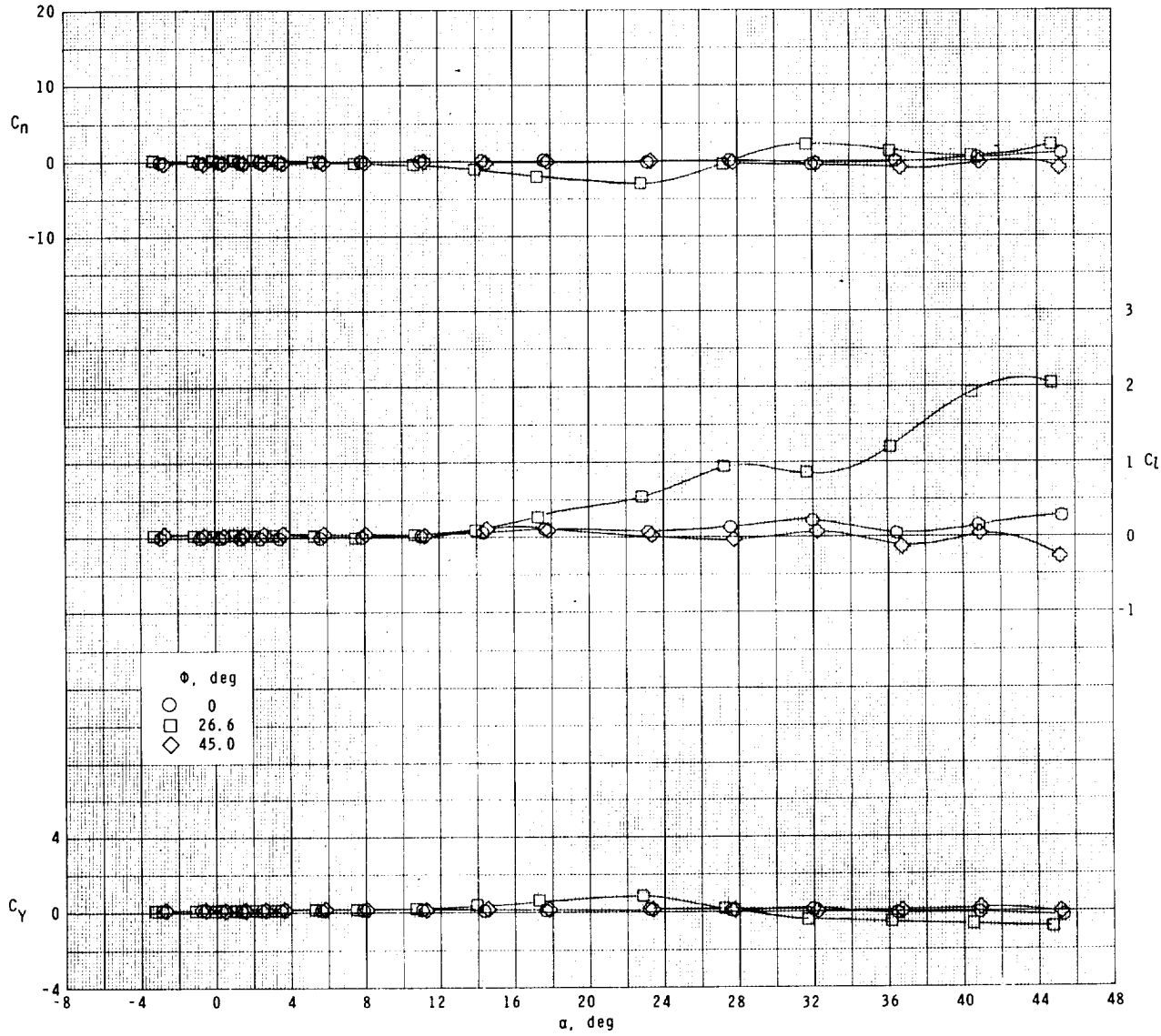

(b) M = 2.00.

Figure 12.- Continued.

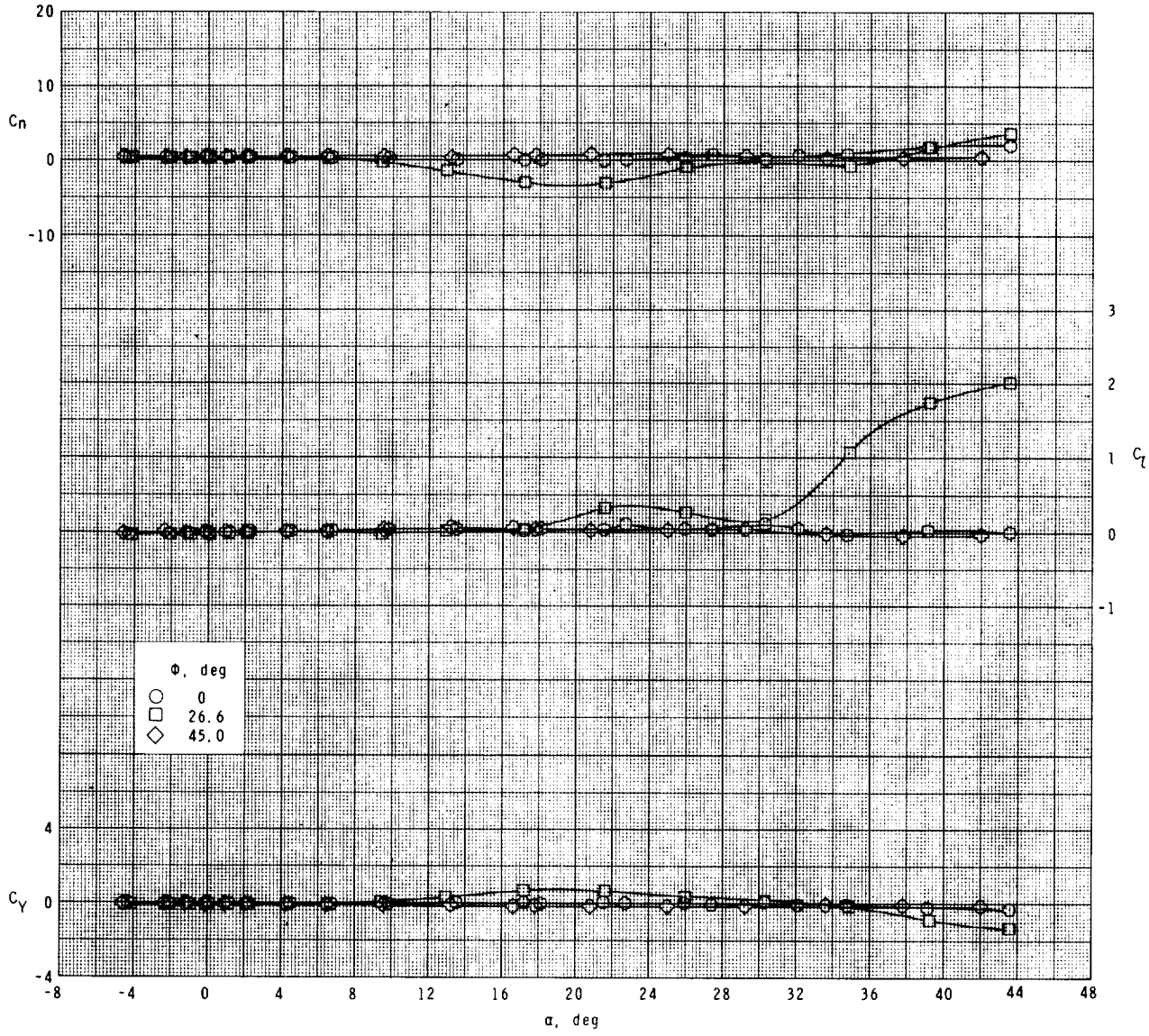

(c) M = 2.35.

Figure 12.- Continued.

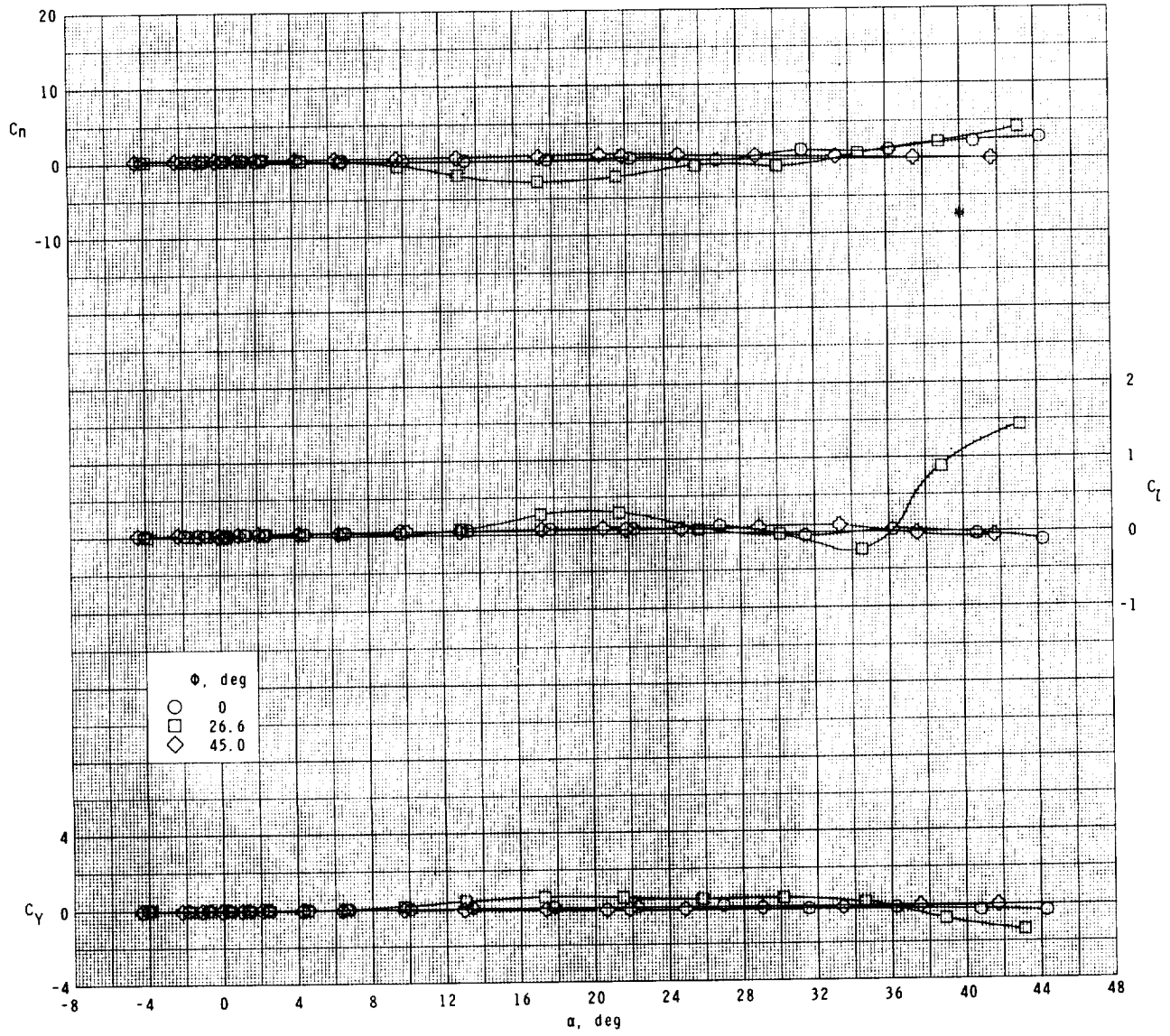

(d) M = 2.87.

Figure 12.- Continued.

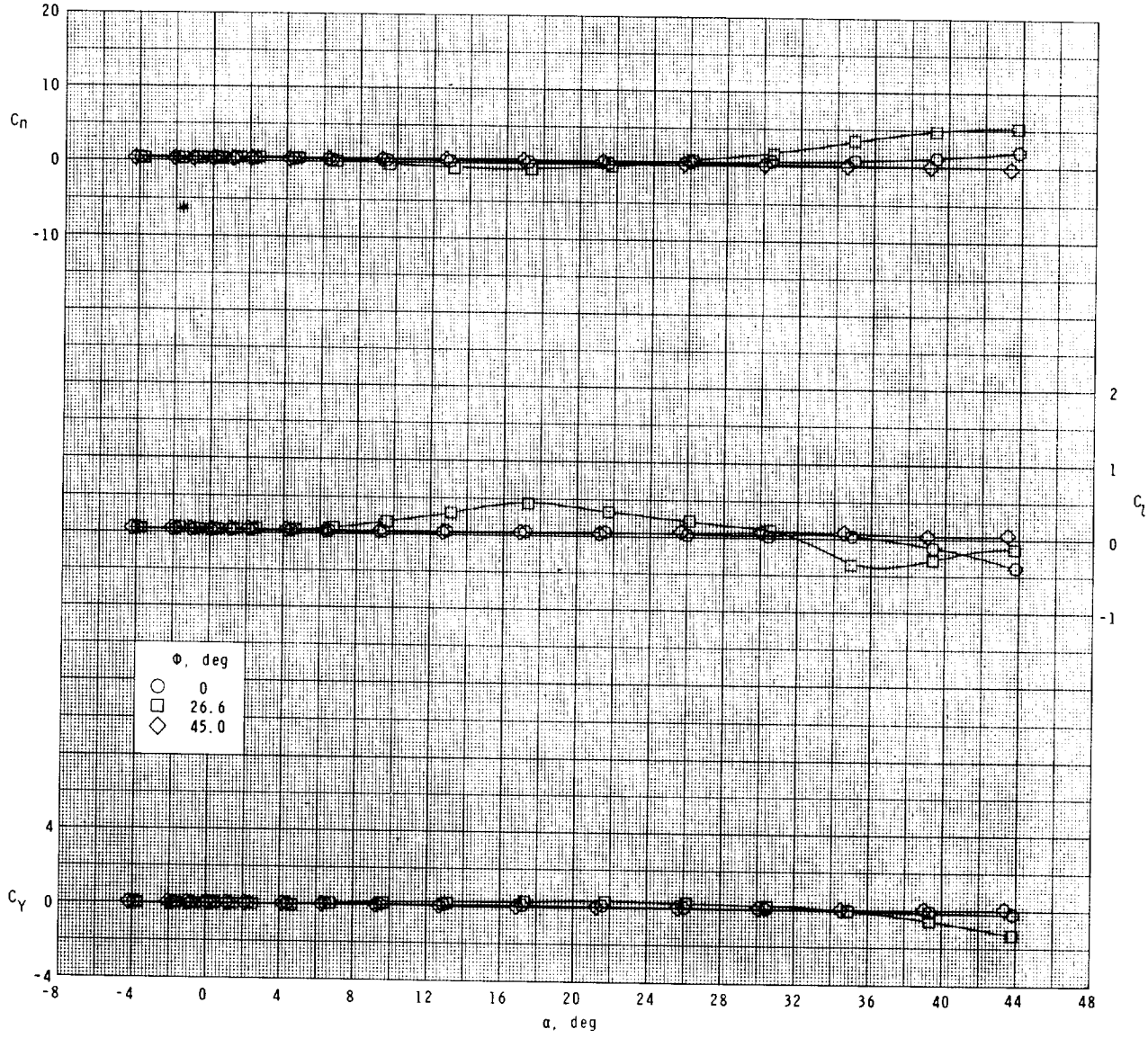

(e) M = 3.95.

Figure 12.- Continued.

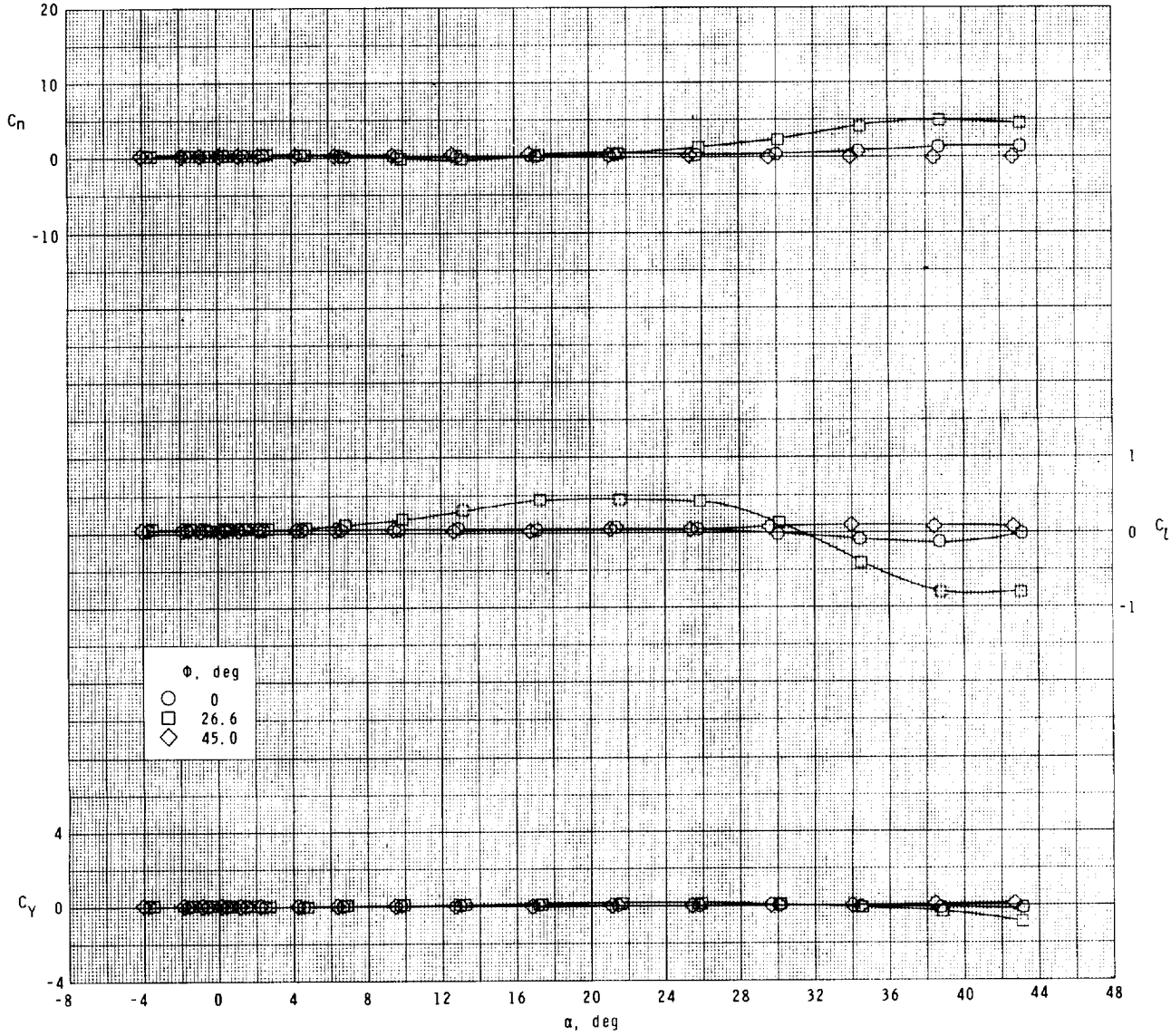

(f) M = 4.60.

Figure 12.- Concluded.

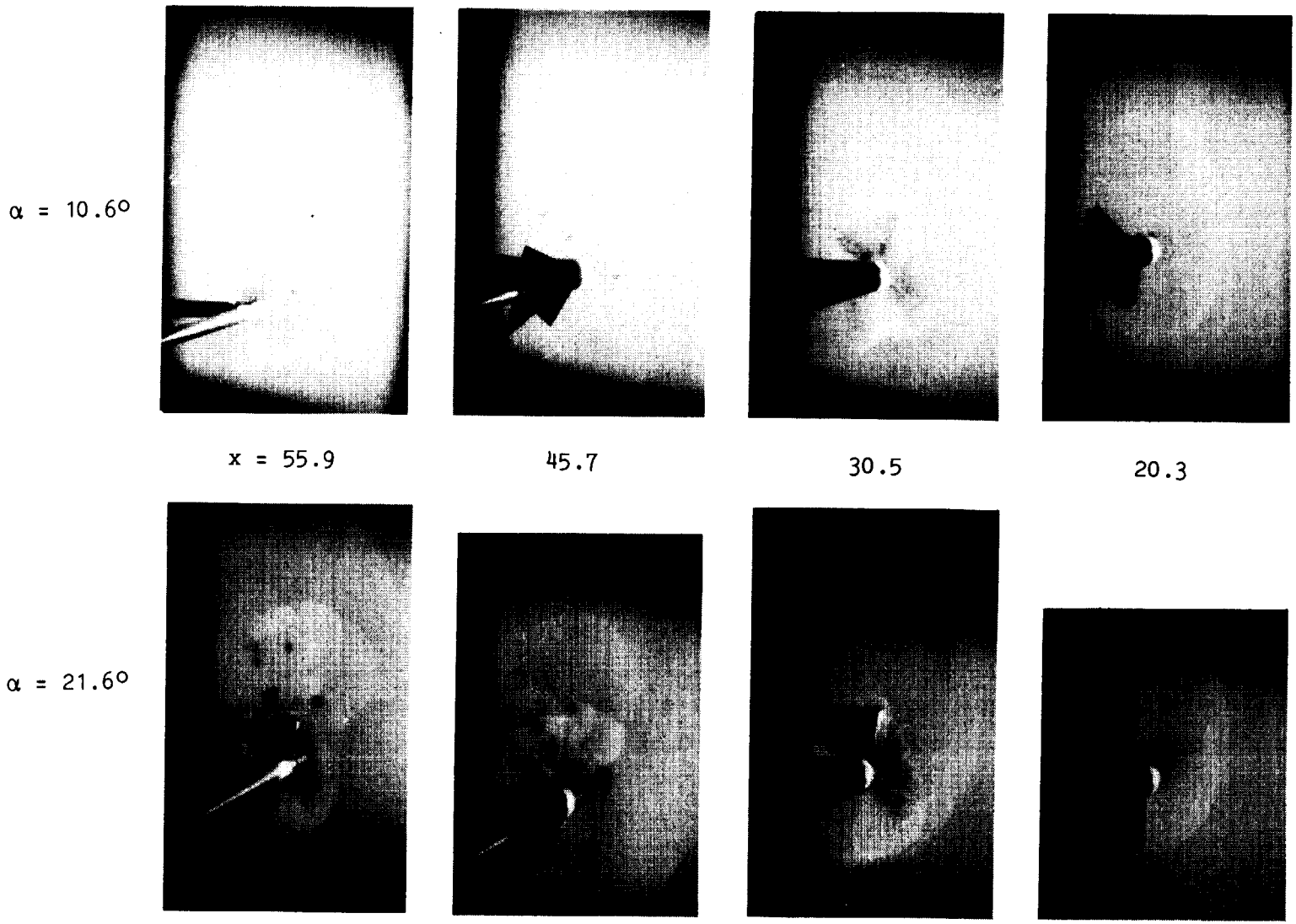

(a) $\alpha = 10.6^{\circ}$ and 21.6°.

Figure 13.- Vapor-screen photographs. $\phi = 26.6^{\circ}$; $M = 2.35$ (nominal).

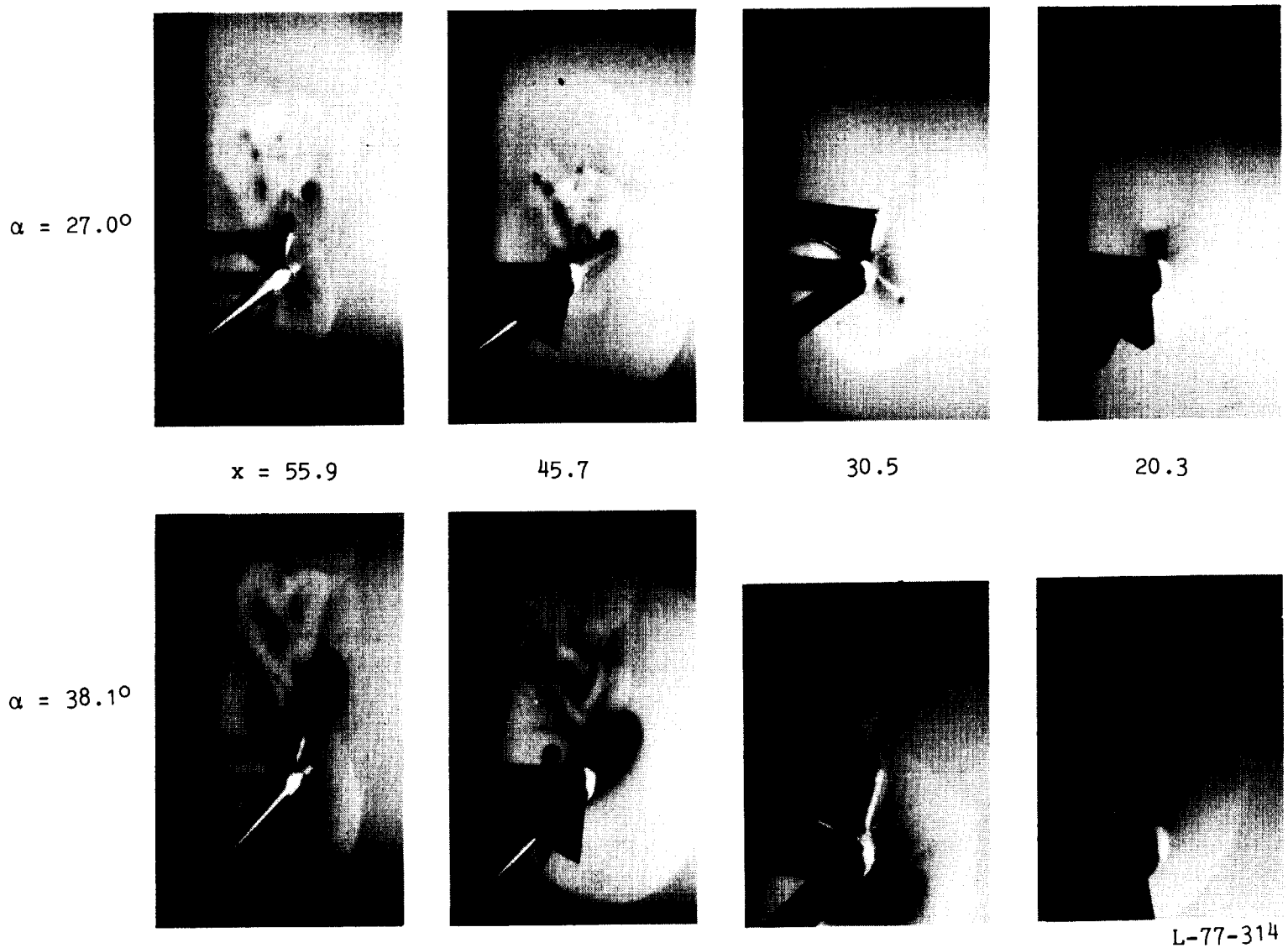

(b) $\alpha = 27.0^{\circ}$ and 38.1°.

Figure 13.- Concluded.

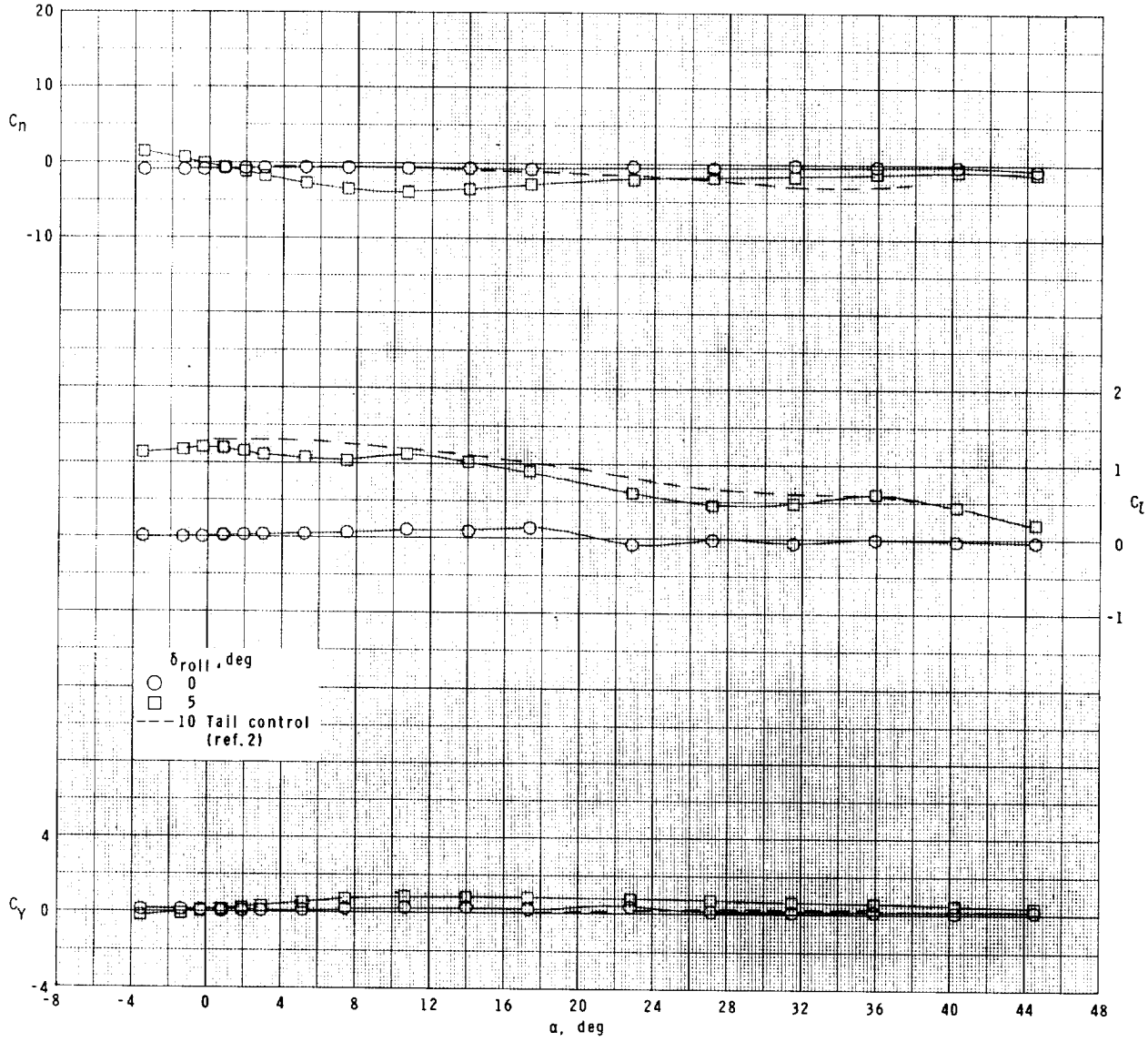

(a) M = 1.50.

Figure 14.- Comparison of two-panel roll-control characteristics for wing- and tail-control configurations at $\phi = 45^o$. Control surfaces 1 and 3 deflected.

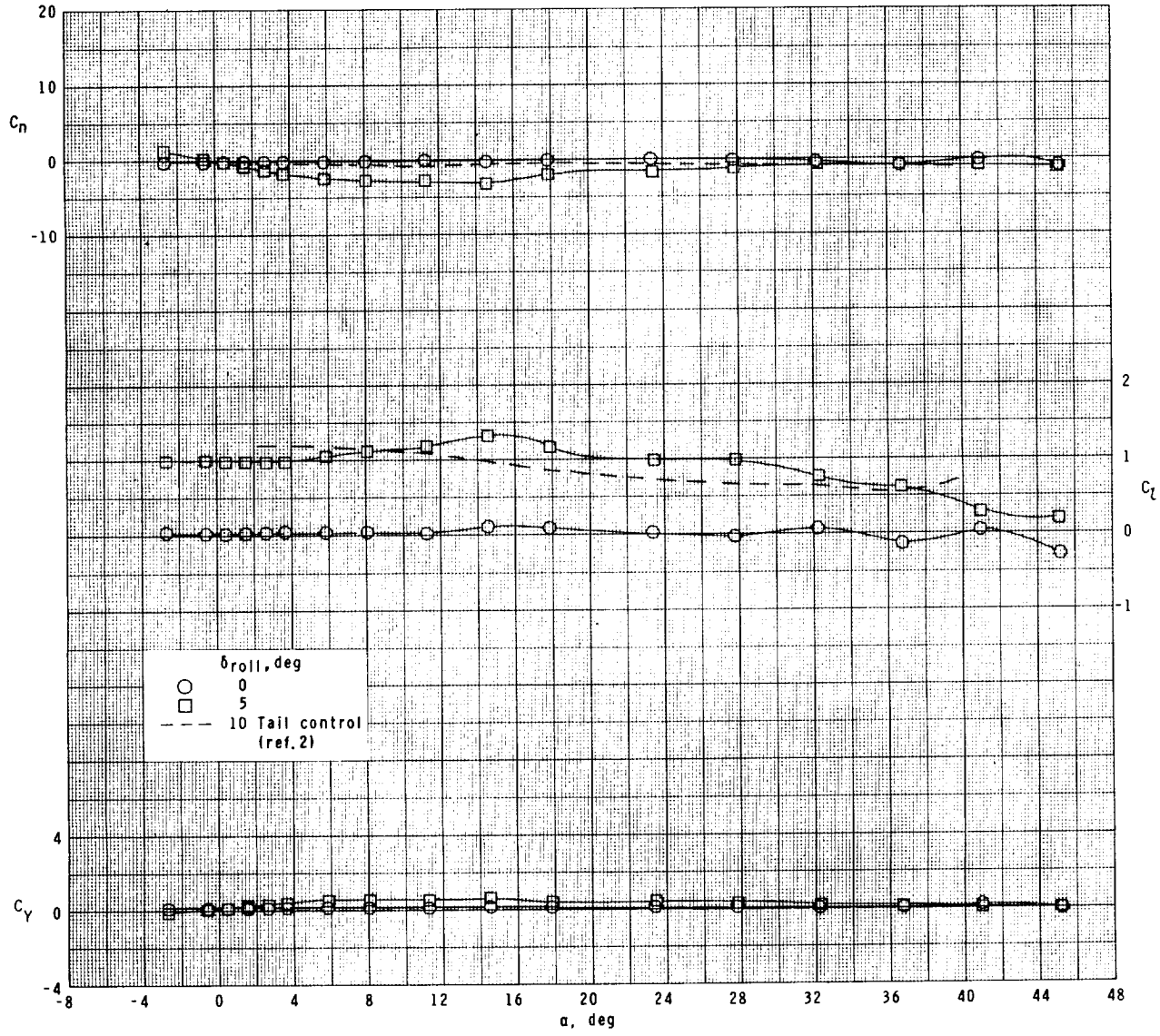

(b) M = 2.00.

Figure 14.- Continued.

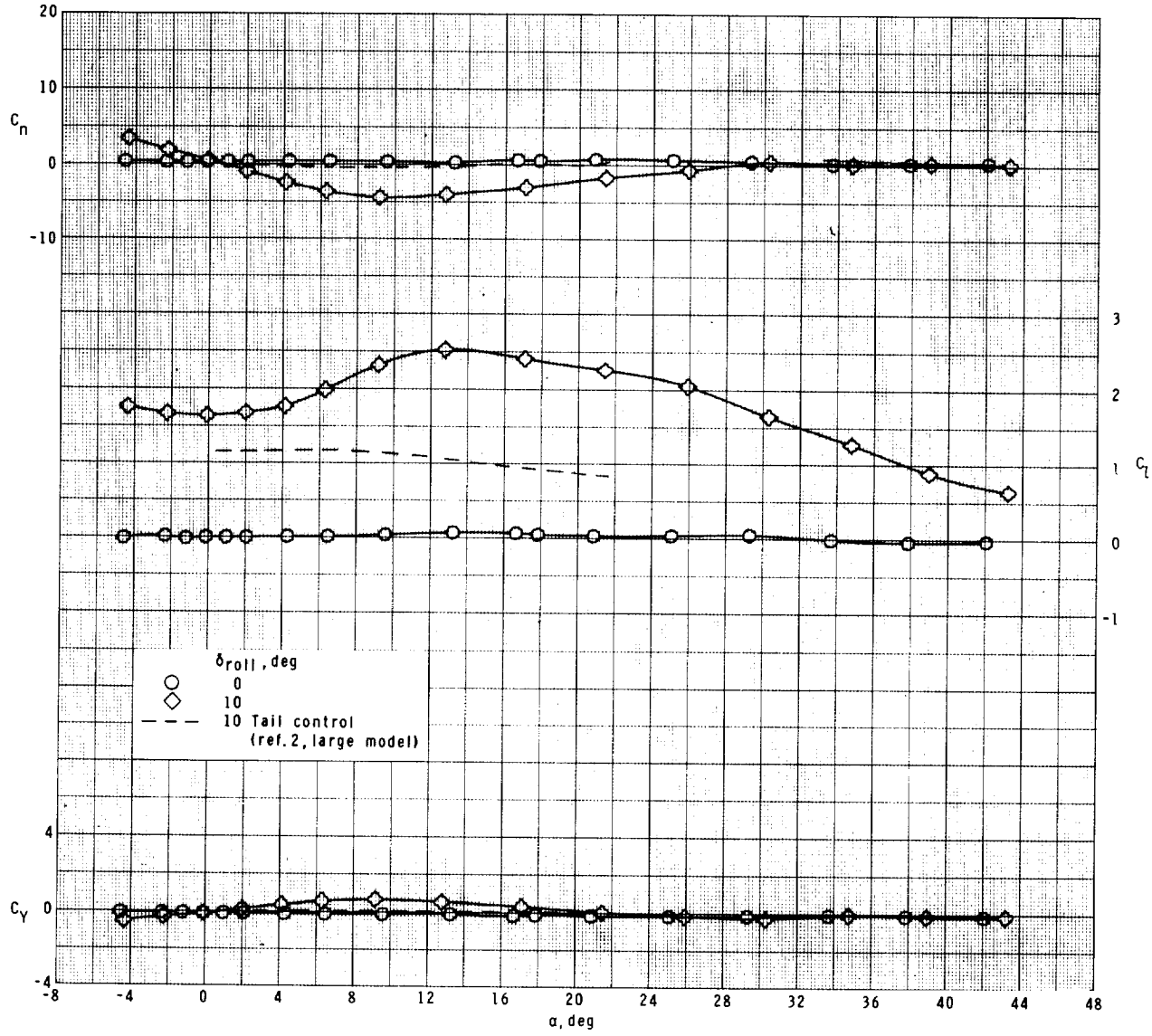

(c) M = 2.35.

Figure 14.- Continued.

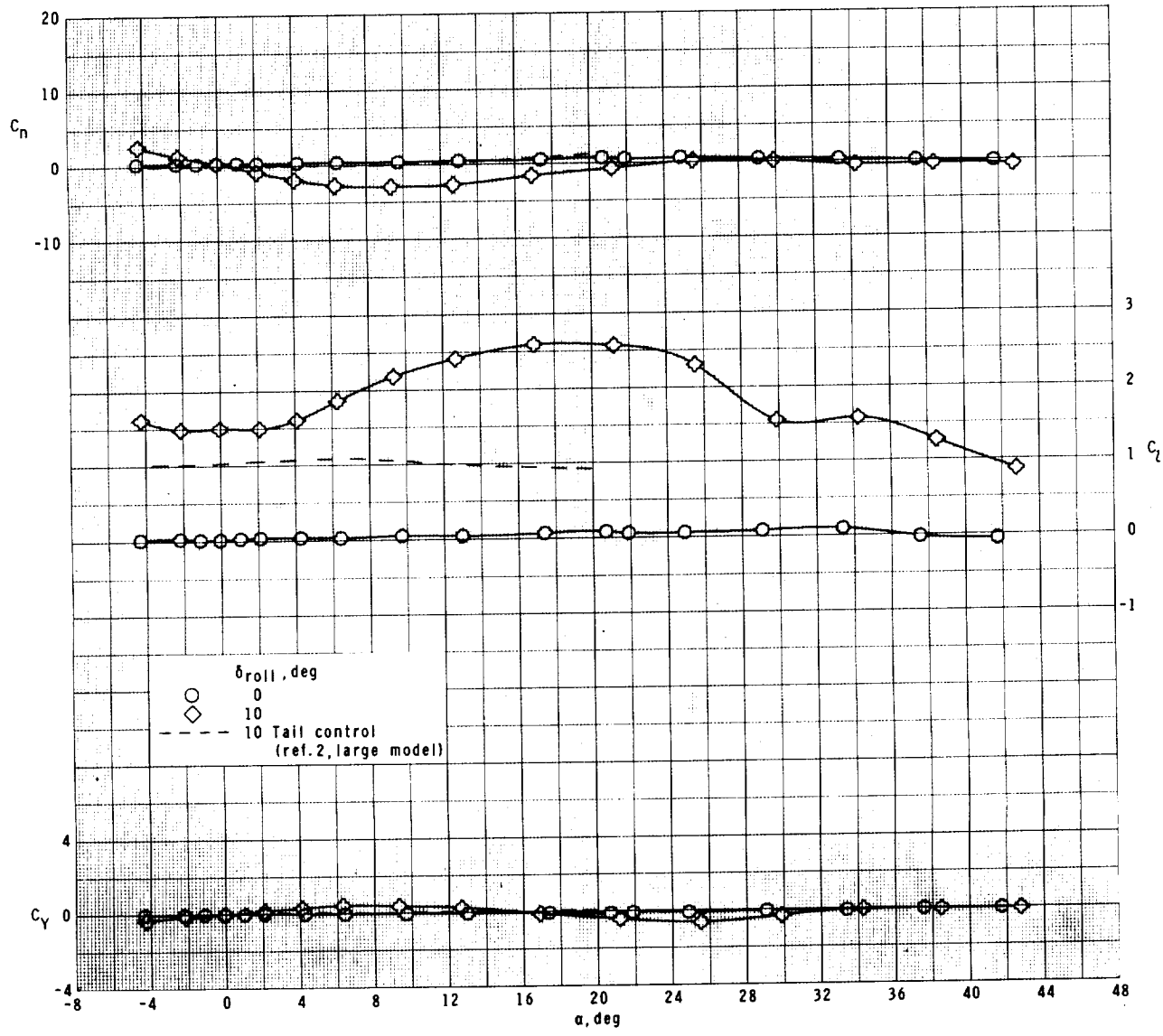

(d) M = 2.87.

Figure 14.- Continued.

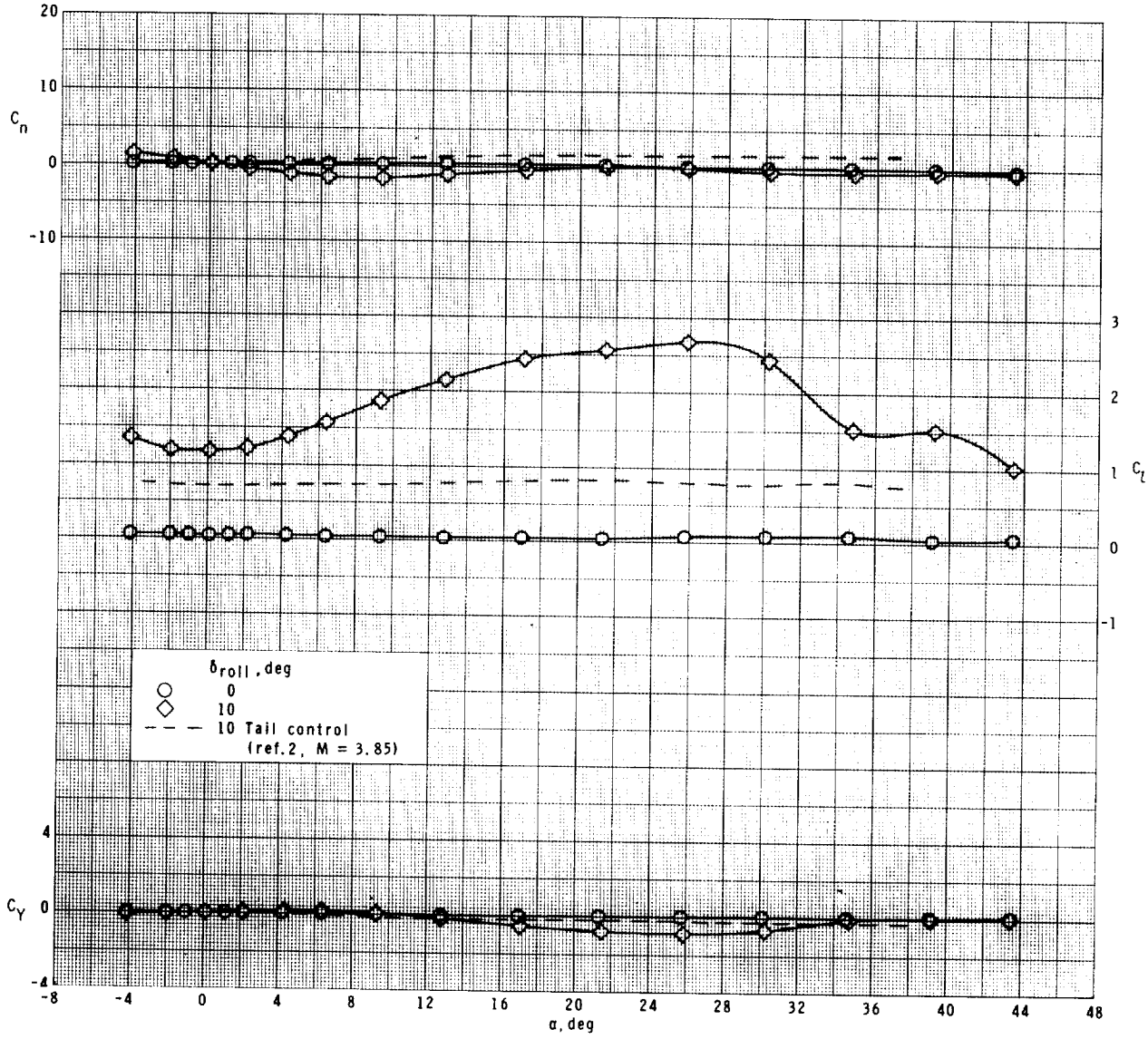

(e) M = 3.95.

Figure 14.- Continued.

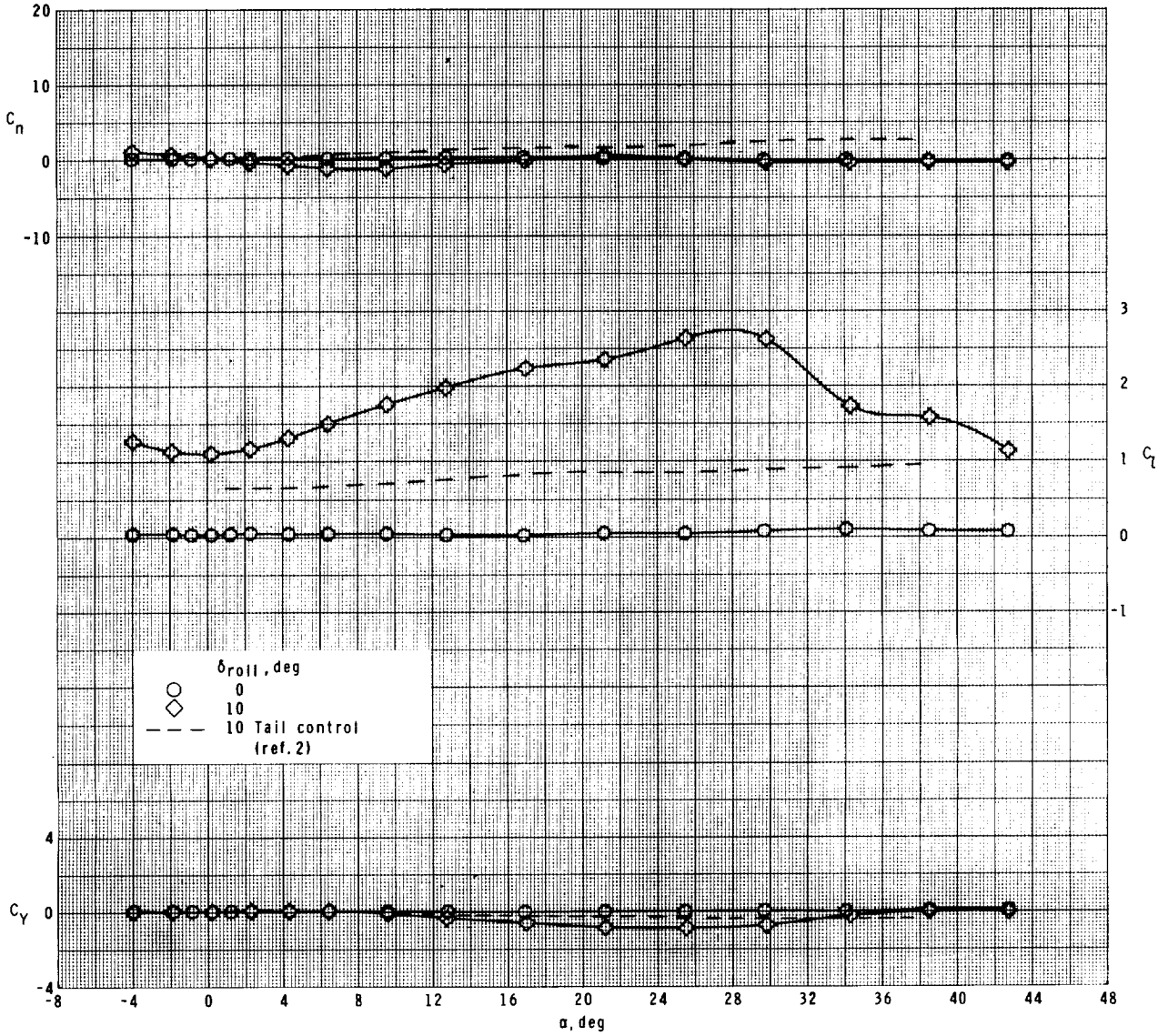

(f) M = 4.60.

Figure 14.- Concluded.

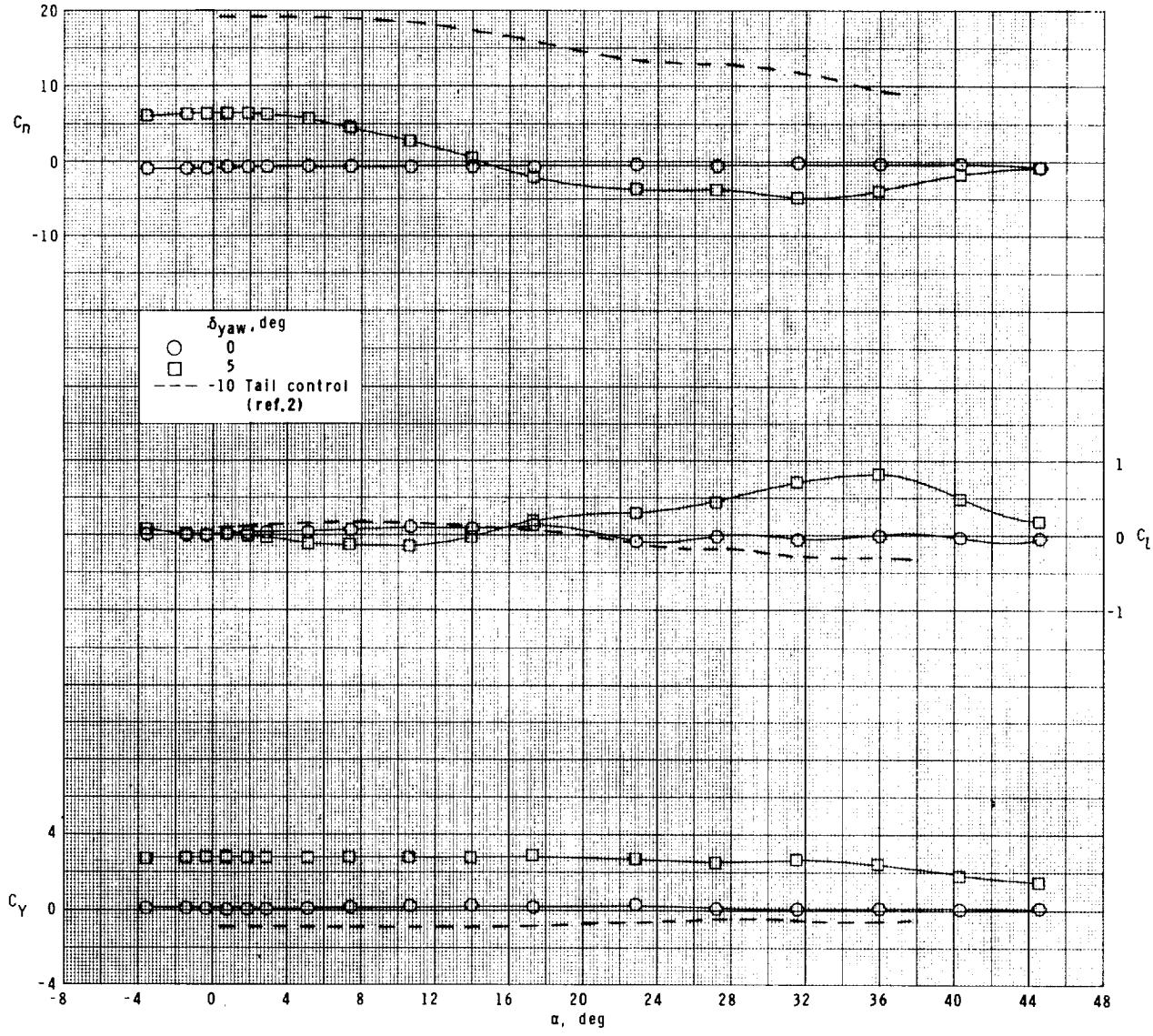

(a) M = 1.50.

Figure 15.- Comparison of yaw-control characteristics for wing- and tail-control configurations. $\phi = 45^{\circ}$.

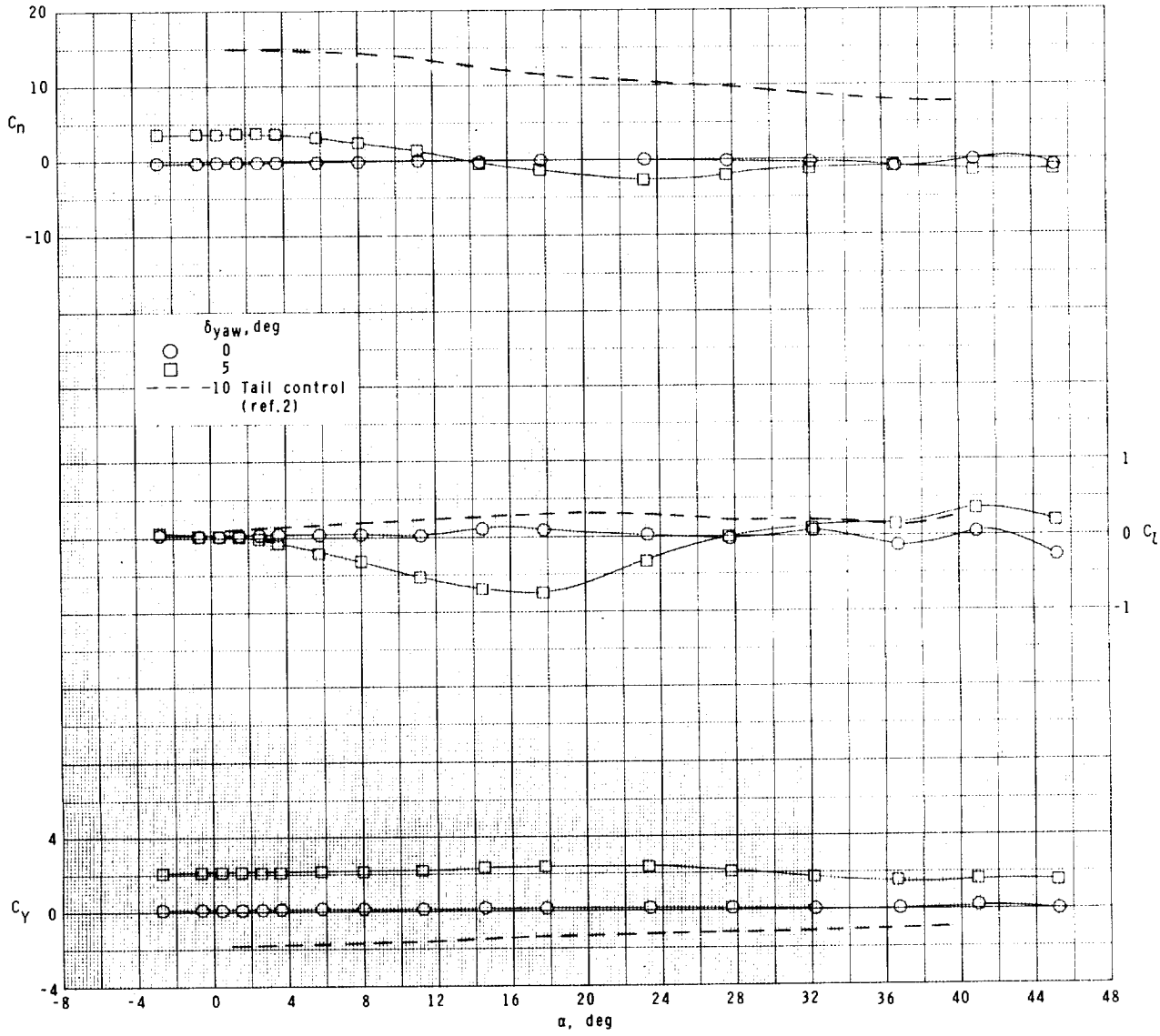

(b) M = 2.00.

Figure 15.- Continued.

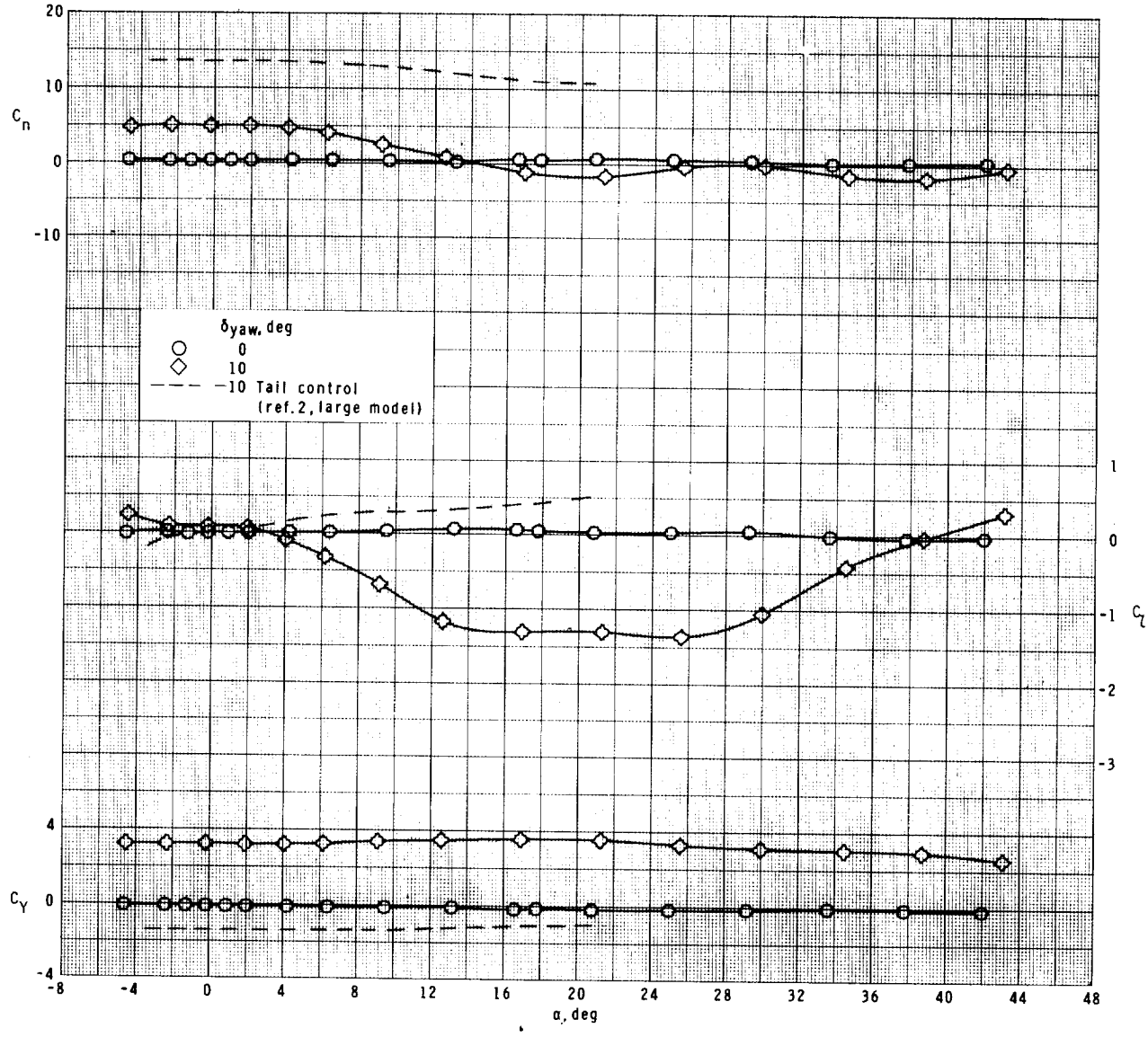

(c) M = 2.35.

Figure 15.- Continued.

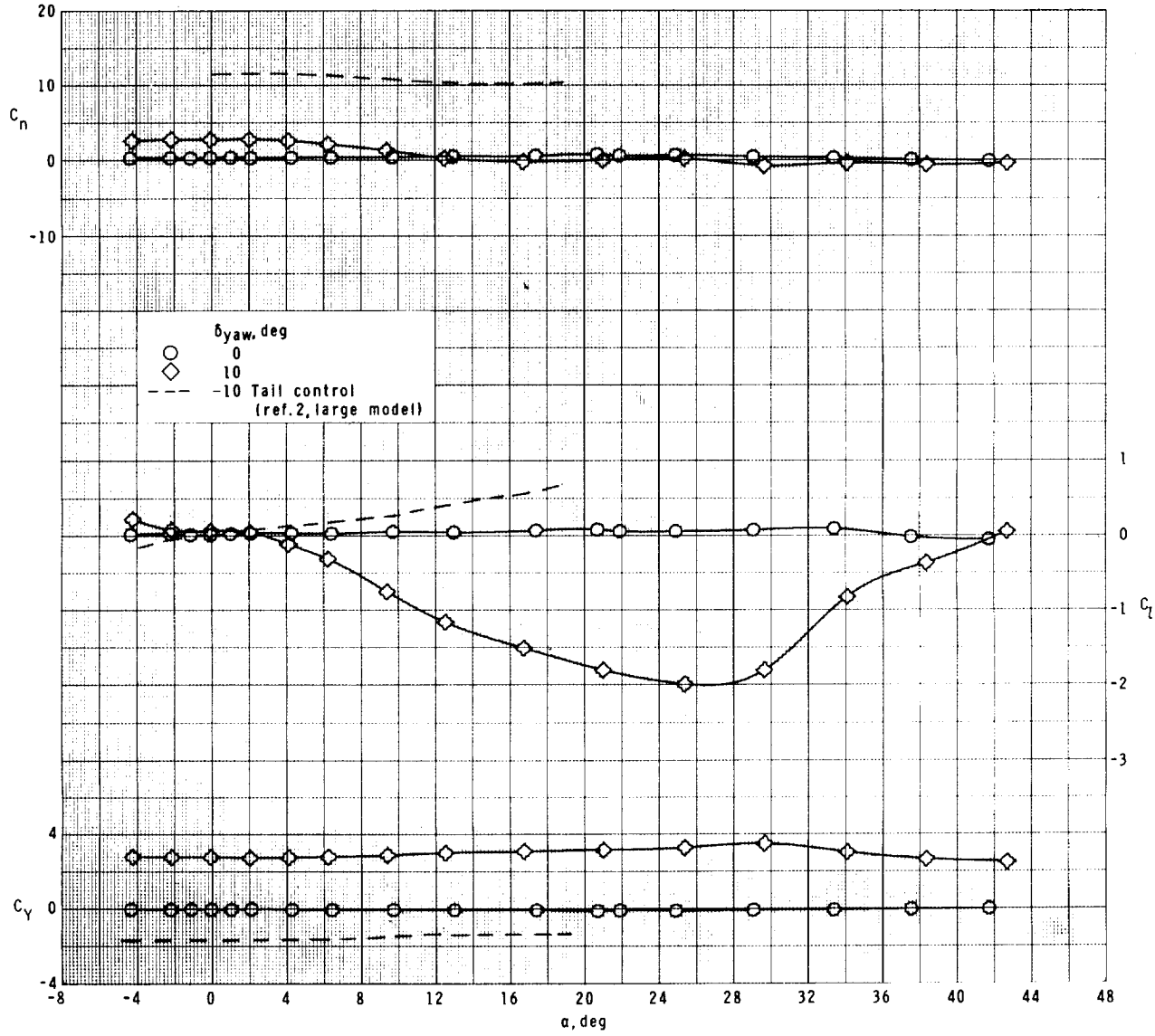

(d) M = 2.87.

Figure 15.- Continued.

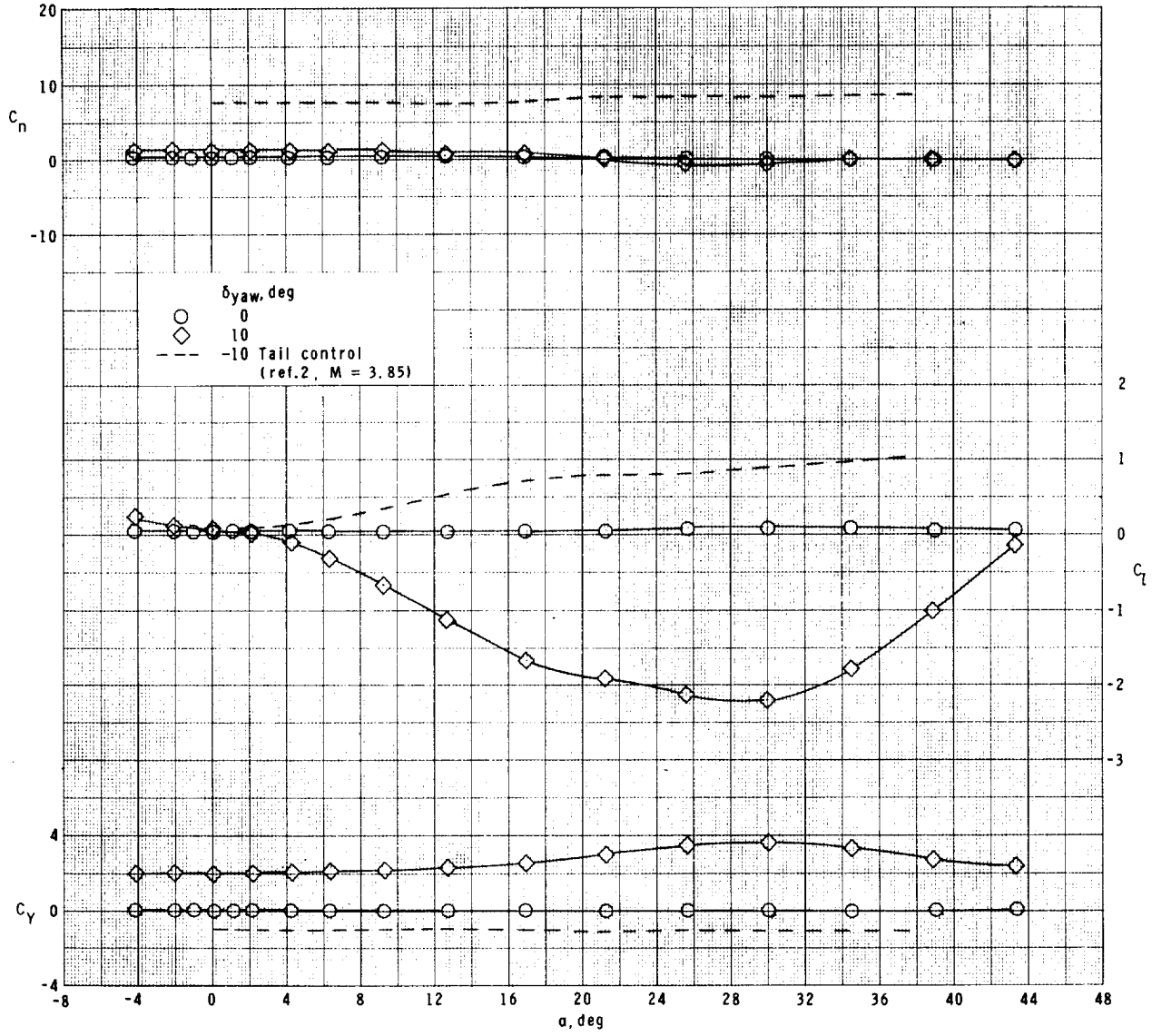

(e) M = 3.95.

Figure 15.- Continued.

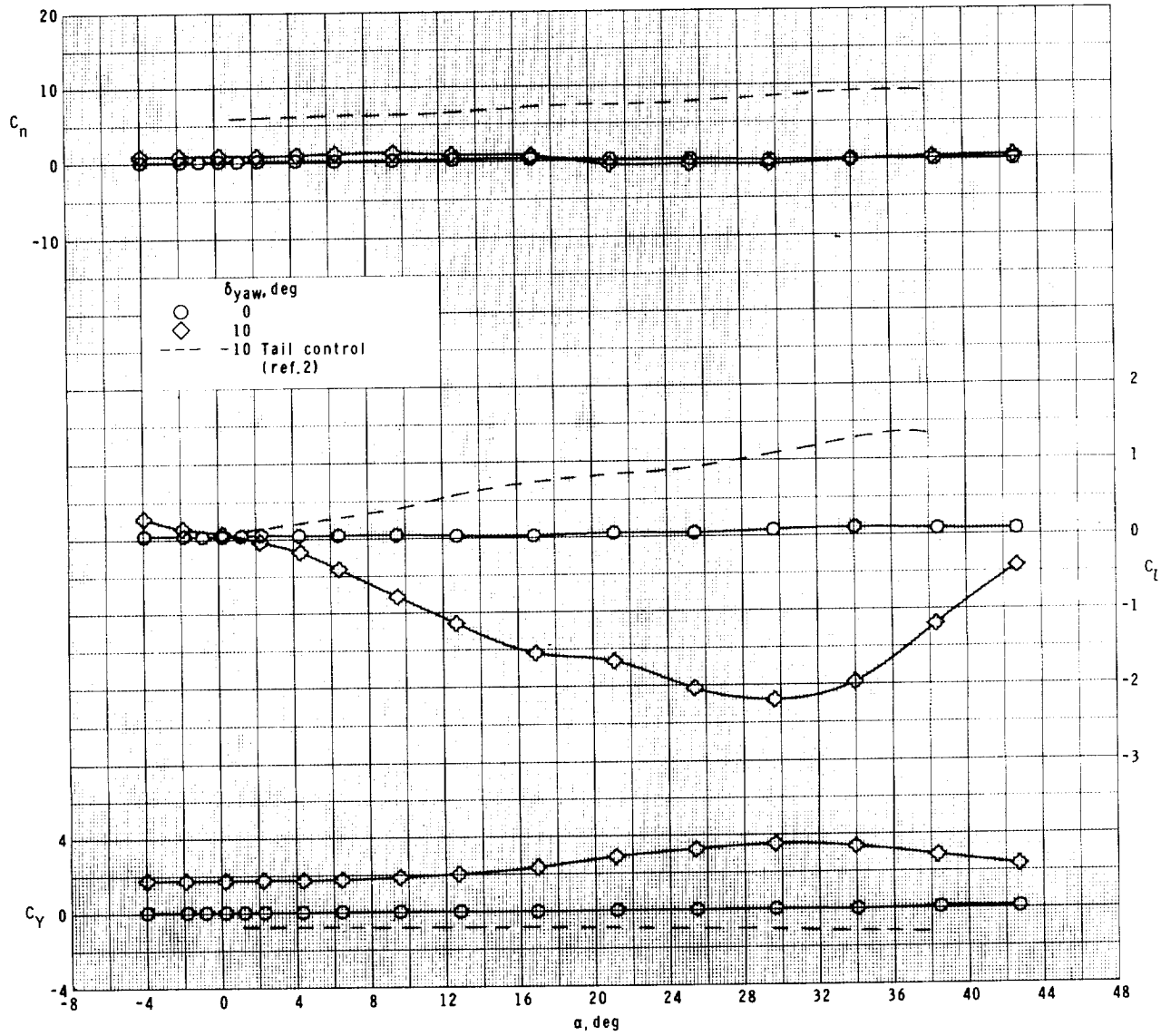

(f) M = 4.60.

Figure 15.- Concluded.

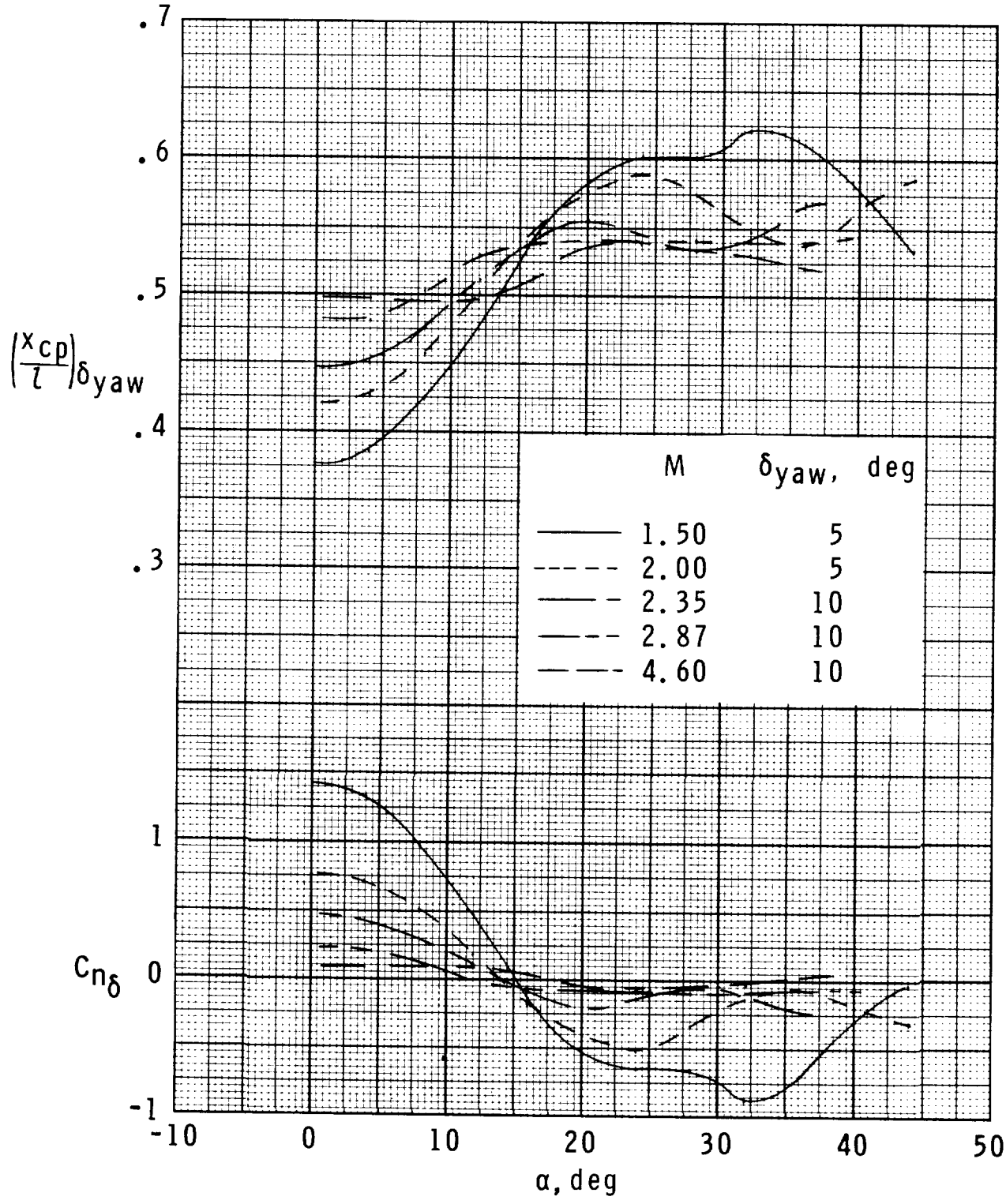

Figure 16.- Wing yaw-control effectiveness and center-of-pressure location. $\phi = 45^\circ$.

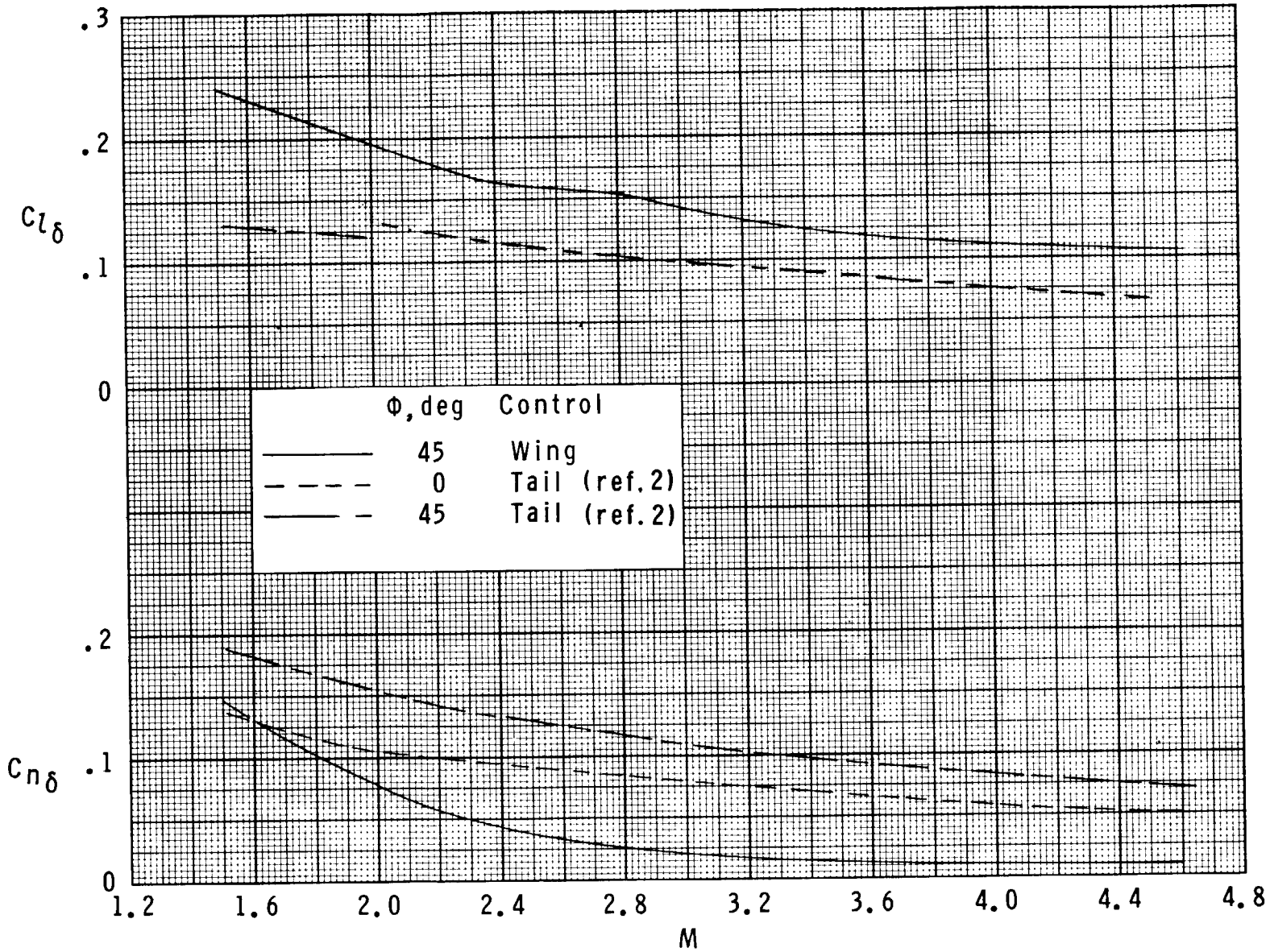

Figure 17.- Summary of lateral- and directional-control characteristics for wing- and tail-control configurations. $\phi = 45^\circ$.

1. Report No.	2. Government Accession No.	3. Recipient's Catalog No.
NASA TP-1078		

4. Title and Subtitle	5. Report Date
SUPERSONIC AERODYNAMIC CHARACTERISTICS OF A SPARROW III TYPE MISSILE MODEL WITH WING CONTROLS AND COMPARISON WITH EXISTING TAIL-CONTROL RESULTS	November 1977
	6. Performing Organization Code
7. Author(s)	8. Performing Organization Report No.
William J. Monta	L-11715
9. Performing Organization Name and Address	10. Work Unit No.
NASA Langley Research Center Hampton, VA 23665	505-11-22-01
	11. Contract or Grant No.
12. Sponsoring Agency Name and Address	13. Type of Report and Period Covered
National Aeronautics and Space Administration Washington, DC 20546	Technical Paper
	14. Sponsoring Agency Code

15. Supplementary Notes

16. Abstract

An experimental investigation has been conducted on a model of a wing-control version of the Sparrow III type missile to determine the static aerodynamic characteristics over an angle-of-attack range from 0° to 40° for Mach numbers from 1.50 to 4.60. Comparisons were made of the characteristics of the wing-control configuration with those of the previously reported tail-control configuration of NASA TM X-2666.

17. Key Words (Suggested by Author(s))	18. Distribution Statement
Sparrow III missile Supersonic aerodynamic characteristics Static stability and control Cruciform missile	Unclassified - Unlimited Subject Category 02

19. Security Classif. (of this report)	20. Security Classif. (of this page)	21. No. of Pages	22. Price*
Unclassified	Unclassified	81	$5.00

* For sale by the National Technical Information Service, Springfield, Virginia 22161

NASA-Langley, 1977